

OPTIMISATION OF PUNCH PRESSURE IN CONTAINERLESS BACKWARD WARM EXTRUSION OF Al-Zn-Mg ALLOYS

Thesis

Submitted in partial fulfilment of the requirements for the award of the degree of

DOCTOR OF PHILOSOPHY

by

RIJESH M



**DEPARTMENT OF METALLURGICAL AND MATERIALS
ENGINEERING
NATIONAL INSTITUTE OF TECHNOLOGY KARNATAKA,
SURATHKAL, SRINIVASNAGAR, MANGALORE - 575025**

October 2014

DECLARATION

I hereby *declare* that the Research Thesis entitled “**Optimisation of Punch Pressure in Containerless Backward Warm Extrusion of Al-Zn-Mg alloys**” which is being submitted to the **National Institute of Technology Karnataka, Surathkal** in partial fulfilment of the requirements for the award of the Degree of **Doctor of Philosophy** in Metallurgical and Materials Engineering is a bonafide report of the research work carried out by me. The material contained in this **Research Thesis** has not been submitted to any University or Institution for the award of any degree.

RIJESH M

Register No. **MT06F03**

Department of Metallurgical and Materials Engineering
National Institute of Technology Karnataka, Surathkal

Place: NITK Surathkal, Srinivasnagar

Date:

C E R T I F I C A T E

This is to certify that the Research Thesis entitled “**Optimisation of Punch Pressure in Containerless Backward Warm Extrusion of Al-Zn-Mg alloys**” submitted by **Rijesh M** (Register Number: **MT06F03**) as the record of the research work carried out by him, is accepted as the **Research Thesis** submission in partial fulfilment of the requirements for the award of degree of **Doctor of Philosophy**.

Dr. A.O. Surendranathan

Research Guide

Professor and Ex-Head

Dept. of Metallurgical and Materials Engineering,

NITK, Surathkal.

Chairman – DRPC

(Signature with Date and Seal)

ACKNOWLEDGEMENT

This thesis has been possible with the guidance and the help of several individuals who in one way or another contributed and extended their valuable assistance in the preparation and completion of this study.

First and foremost, my utmost gratitude to my research guide Prof. A. O. Surendranathan for the continuous support, patience, motivation and enthusiasm. I am very much thankful to him for picking me up as a student at the critical stage of my Ph.D. His guidance helped me in all the time of research and writing of this thesis.

I am also extremely indebted to my former guide Dr. K. Srinivasan for providing necessary infrastructure and resources to accomplish my research work. His immense knowledge, support, and guidance are greatly appreciated. His unflinching courage and conviction will always inspire me, and I hope to continue to work with his noble thoughts.

Prof. Jagannath Nayak, Head, Department of Metallurgical and Materials Engineering, is one of the best teachers that I have had in my life. He introduced me to phase diagrams and his teachings inspired me to work on metals and alloys. I am indebted to him for his continuous encouragement and support.

My heartfelt thanks are due to Prof. K. Narayan Prabhu, Former Head, Department of Metallurgical and Materials Engineering, for allowing me to use the facilities in the department. I take this opportunity to sincerely acknowledge him for providing financial assistance in the form of lectureship which buttressed me to perform my work comfortably.

I gratefully acknowledge Prof. K. R. Udupa for his understanding, encouragement and personal attention which have provided good and smooth basis for my Ph.D. tenure. His support, guidance, advice throughout the research project, as well as his painstaking effort in proof reading the drafts, is greatly appreciated.

I thank my RPAC members, Prof. Gangadharan and Prof. Dwarakish for their helpful suggestions, encouragement, insightful comments, and hard questions during my progress report presentations.

I thank Dr. Udaya Bhat, whose useful suggestions and comments have helped me a lot. I also like to extend my gratitude to Dr. Ravishankar K.S for his support provided during the research work.

Most of the results described in this thesis have been obtained with a close collaboration with strength of materials lab NITK. I owe a great deal of appreciation and gratitude to Prof. Laxman Nandagiri for permitting me to use the laboratory facilities at the time of my experimentation. Mr Seetharam and Mr Srinkant F B deserve my sincere expression of thanks for providing me experimental hands-on-training on UTM.

I thank my fellow labmates in Metal Forming Group: James Valder, for the stimulating discussions, for the sleepless nights we were working together before deadlines, and for all the fun we have had in the last few years. I thank my research colleague Dr Geethalakshmi with whom I started this work and many rounds of discussions on my project with her helped me a lot. I also wish to thank Naveen, Sreesudha, Shahabuddin and Suresh Reddy, M. Tech. students for their support and cooperation during the project work. Basavaraj who enlightened me the first glance of FEM deserves a special mention here.

My special thanks to Mr. Sundar Shettigar for melting and pouring, Mr. Baburao Shettigar for metallography, Mr Vasanth Kumar for procurement of materials, Mr. Satish for turning of samples, Mr. Dinesh and Mr. Yashwanth K.S for helping in experimental work, Mr. Lokesh Naik, Mr Ramachandra, and Mr.Giriyappa Devadiga of the department for their constant support and assistance throughout my research work.

I express my thanks to Ms. Rashmi Banjan for her help in taking the SEM images of my specimens and Mrs Vinaya Shettigar for her help during the project work. Mrs. Sharmila Dinesh deserves a special mention because of her help and suggestions in formatting the thesis and for being a great friend from the day of my graduation.

I would also like to thank some people from early days of my research tenure. Dr Rita Kumari, Dr Ravindra Kotian, Dr Satyapal Hegde, Dr Rajath Hegde and Dr Raghavendra Hebbar were among those who kept me going at the beginning.

My warm appreciation is due to all the Ph.D. students and senior research fellows of the department. Ramesh, Hemanth, Satyanarayan, Vijeesh, Naveen Babu and Shantharam deserve special mention here.

I expand my thanks to Vinod and Vijayalakshmi who shared their residence with me during my stay in Mangalore, and extended brotherly love towards me.

I have no suitable word that can fully describe the everlasting love of my parents. I remember the constant support of my mother when I encountered difficulties in finishing my thesis, especially when I almost wanted to give up on my thesis. She has helped me financially, morally and spiritually.

My sister Rheeja M and brother in law Lt Cdr Rajesh E R, has been my constant reminder that I could do better than what I think I can. Thank you for the support, love and prayers.

I would also like to extend huge, warm thanks to my wife Dr Deepthi RV. My daughter Gayathri who was born before this thesis was completed deserves lots of love and appreciation for cheering me up with her beautiful smile.

Above all, I thank God, for giving me the intellect to understand the complexity of metal forming, and giving me strength to complete this research.

My only regret is that I am not able to share the completion of this thesis with my father.

This thesis is dedicated to my family.

Rijesh M

ABSTRACT

Open-die warm extrusion is an advanced forming technology which can not only reduce the machining time and material waste but also improves the properties of the products. Container wall – billet friction is eliminated in containerless extrusion, which leads to a large reduction in the total force required for extrusion. It is suitable for Al-Zn-Mg alloys, which is difficult to extrude compared to other aluminum alloys. The high specific strength of Al-Zn-Mg alloys and the lower punch pressure for containerless extrusion promises to be a vital combination, which needs to be further explored upon, hence present investigation was to determine theoretically and experimentally the effect of containerless backward extrusion of Al-Zn-Mg alloys namely Al-5Zn-1Mg, Al-10Zn-1Mg, Al-15Zn-1Mg for different geometries under a lubrication condition. Theoretical analysis was carried out using elementary plasticity theory – Dipper model and experimental analysis by conducting containerless backward extrusion experiments. Friction was minimized by lubricating the billets with graphite powder. Experiments were carried out using a 40 T universal testing machine with ram velocity of 3.3×10^{-4} m/s. The effect of specimen geometry on the extrusion pressure at various temperatures after containerless backward extrusion were investigated and presented. Finally, an optimum ratio of lengths to diameters of billets was determined by finite element analysis software called LS. Dyna: Levermore Software Dynamic Non Linear Analysis.

Flow and frictional properties of Al-Zn-Mg were determined at different temperatures from 303 K to 673 K by compression and ring compression tests. Force-stroke data were generated at temperatures 303 K to 673 K for strains 0.1, 0.15, 0.2, 0.29, 0.37 and 0.45 for conventional backward extrusion and containerless backward extrusion for theoretical analysis whereas experimentation was restricted only to containerless backward extrusion. During experimentation force stroke data were generated at temperatures 303 K to 623 K for the same strains. Variation of theoretical punch pressure against extrusion strain at selected temperatures was studied.

From the results of flow stress and frictional analysis of Al-Zn-Mg alloys it was found that the flow stress and friction for forming all the three chosen Al-Zn-Mg alloys were least between 373 K and 573 K. From the theoretical investigation it was found that containerless backward extrusion requires less than half of the force compared to conventional container extrusion and the optimum warm extrusion temperature for Al-5Zn-1Mg and Al-15Zn-1Mg is 373 K and for Al-10Zn-1Mg is 473 K. From the experimental investigation it was found that optimum warm extrusion temperature for Al-5Zn-1Mg is 423 K and for Al-10Zn-1Mg and Al-15Zn-1Mg is 523 K which is in accordance with theoretical analysis. From the experimental investigation it is also found that initial height h_o , of billet, should be as small as possible to make upsetting difficult and diameter (d_o) of the billet should be large in comparison to punch diameter (d_p) to make extrusion strain smaller and extrusion process easier. From the finite element analysis it was found that for a billet of h_o/d_o ratio of 0.5 shows an absence of lateral displacement of material, which is a characteristic of containerless backward extrusion. In the present study dynamic strain aging was observed to occur in the temperature range of 573-673K. The domain where dynamic strain ageing exists must be considered when selecting operating conditions like working temperature and extrusion strain.

Keywords: Container, Extrusion, Friction, Punch pressure, Temperature, Theoretical, Flow properties, Warm working

CONTENTS

List of figures	vi
List of tables	xii
Nomenclature	xiv
1 Introduction	1
1.1 Scope of the present work	4
1.2 Objectives	4
1.3 Structure of the thesis	5
2 Review of Literature	6
2.1 Extrusion	6
2.2 Classification of extrusion based on temperature	8
2.2.1 Cold extrusion	8
2.2.2 Hot extrusion	10
2.2.3 Warm extrusion	11
2.3 Backward extrusion	12
2.3.1 Extrusion pressure	13
2.3.2 Deformation/Flow pattern in backward extrusion	14
2.3.3 Material flow	15
2.3.4 Forces	16
2.3.5 Stresses	17
2.4 Containerless backward extrusion	18
2.4.1 Advantages and disadvantages of containerless backward extrusion	21
2.5 Flow stress determination in metal forming	22
2.5.1 Axisymmetric compression test	23
2.6 Friction and lubrication	27

2.6.1	Ring compression test	29
2.7	Aluminium - Zinc –Magnesium alloys	30
2.7.1	Al-Zn-Mg System	33
2.8	Stress analysis based on the elementary plasticity theory	36
2.9	Simulation of the metal forming processes	39
2.9.1	Concept of FEM	39
2.9.2	Steps involved in the finite element analysis of a typical problem	39
2.9.3	Advantages and limitations of FEM	40
2.9.4	The general purpose FEM packages	41
2.9.5	General purpose programs	41
2.9.6	Engineering application of FEM	42
3	Experimental Procedures	44
3.1	Material	44
3.1.1	Alloys	44
3.1.2	Alloy preparation	44
3.1.2.1	Melting	44
3.1.2.2	Pouring	45
3.2	Sample preparation	45
3.3	Characterization	45
3.3.1	Chemical composition	45
3.3.2	Microstructural analysis	51
3.3.3	Hardness measurement	51
3.4	Axisymmetric compression testing	52
3.4.1	Flow stress determination	52
3.5	Ring compression test	53
3.6	Containerless backward extrusion	56
3.6.1	Design of punch and base plate	56
3.6.2	Die materials	56

3.6.3	Die assembly	56
3.6.4	Preparation of billet specimens	60
3.6.5	Testing	60
4	Results	62
4.1	Microstructural characteristics	62
4.2	Vickers hardness values	65
4.3	Axisymmetric compression test	66
4.4	Ring compression test	76
4.5	Stress analysis of backward extrusion in Al-Zn-Mg alloys with and without container based on the elementary plasticity theory - “Dipper model”	78
4.5.1	Extrusion strains for billets extruded with a punch of 15 mm diameter	78
4.5.2	Force-stroke diagram of backward extrusion with and without a container	79
4.5.3	Theoretical punch pressure for various extrusion strain and temperatures at punch depth of 15 mm for backward extrusion with and without a container	79
4.6	Stress analysis of containerless backward extrusion of Al-Zn-Mg Alloys based on the experimentation	80
4.6.1	Force-Stroke diagram of containerless backward extrusion	80
4.6.2	Punch pressure for various extrusion strain and temperatures for containerless backward extrusion	100
5	Discussions	115
5.1	Microstructural analysis	115
5.2	Vickers hardness	118
5.3	Effect of temperature on yield strength	119

5.4	Effect of zinc content on yield strength	120
5.5	Effect of temperature on strength coefficient and strain hardening exponent	120
5.6	Effect of zinc content on strength coefficient and strain hardening exponent	123
5.7	Effect of temperature on friction factor	124
5.8	Effect of zinc content on friction factor	124
5.9	Effect of lubrication on friction factor	125
5.10	Stress analysis of backward extrusion in Al-Zn-Mg alloys with and without container based on “Dipper Model”	126
5.10.1	The force-stroke diagram	126
5.10.2	Theoretical punch pressure analysis	127
5.11	Stress analysis of backward extrusion in Al-Zn-Mg alloys with and without container based on experimentation	127
5.11.1	The force-stroke diagram	127
5.11.2	Experimental analysis of punch pressure	129
6	Finite Element Analysis of Containerless Backward Extrusion of Al-Zn-Mg Alloys	133
6.1	Problem statement	133
6.2	Problem description	133
6.3	Detailed steps of the finite element analysis	133
6.3.1	Pre-processing	134
6.3.2	Model generation	134
6.3.3	Solving	135
6.3.4	Material model 64: strain rate sensitive power-law plasticity	136
6.4	Contact algorithm	137
6.4.1	Tetrahedron element with 12 degrees-of-freedom	138

6.4.2	Fully integrated tetrahedron element with 24 degrees-of-freedom	138
6.4.3	Post processing	139
6.5	Finite element formulation of the problem	139
6.5.1	Assumptions made in finite element formulation of the problem	139
6.5.2	Pre-processing	140
6.5.3	Solving	140
6.5.4	Post-processing	140
6.5.5	Steps involved for running the program	141
6.5.6	Steps involved for applying load	142
6.5.7	Steps involved for assigning material properties	142
6.5.8	Steps involved in setting the time	143
6.6	Simulation procedure	143
6.7	Results and discussion	143
7	Conclusions	147
	References	149
	Appendix I	164
	Appendix II	166
	Appendix III	167
	List of publication	168
	Bio-data	170

LIST OF FIGURES

Fig. No	Caption	Page No
2.1	Direct extrusion process	7
2.2	Property changes due to cold working and annealing	9
2.3	Backward extrusion	12
2.4	Extrusion pressure vs. ram travel	13
2.5	Flow pattern of the billet during the extrusion process	14
2.6	Forces acting in the backward can extrusion	16
2.7	Punch force-travel diagram for backward can extrusion	17
2.8	Streamline field for backward can extrusion	17
2.9	Backward extrusion with a container	20
2.10	Containerless backward extrusion	20
2.11	Undeformed regions (shaded) due to friction at ends of a compression specimen	24
2.12	Load – deformation curves for compression tests with different values of D_0/h_0	24
2.13	Al-Zn phase diagram	31
2.14	Al-Mg-Zn liquidus projection	34
2.15	Al-Mg-Zn solvus projection	35
2.16	Backward can extrusion process as a double upsetting process	36
3.1	The dimensions of mold cavity used to produce billets of diameter (a) 50 mm (b) 40 mm (c) 35 and 30 mm (d) 27 and 25 mm	47
3.2	Schematic diagram of compression testing sample	47
3.3	Schematic diagram of ring compression testing sample	48

3.4	Schematic diagram of cylindrical billet samples with diameters (a) 50 mm (b) 40 mm (c) 35 mm (d) 30 mm (e) 27 mm and (f) 25 mm for containerless backward extrusion experiments	51
3.5	Photograph of compression test assembly	53
3.6	Photographs of ring compression test assembly	54
3.7	Ring compression test specimen (a) before compression (b) after compression with low friction and (c) after compression with high friction	54
3.8	Types of ring deformations after compression	55
3.9	Calibration chart to determine friction factor (m)	55
3.10	Schematic diagram of punch used for containerless backward extrusion	57
3.11	Schematic diagram of base plate	57
3.12	Heat treatment cycle of AISI M2 HSS for attaining a hardness of 61/62 R_c	58
3.13	(a) Schematic diagram and (b) photograph of containerless backward extrusion die assembly	59
3.14	Photograph of the universal testing machine used for containerless backward extrusion	60
3.15	Photograph of a billet with 40 mm diameter and 50 mm height before and after machining	61
4.1	Low magnification scanning electron micrograph of as-cast and homogenized (a) Al-5Zn-1Mg (b) Al-10Zn-1Mg (c) Al-15Zn-1Mg alloys indicating microstructures that consist mainly α -Al phase with ($\alpha+\tau$) eutectic in inter dendritic regions	63

4.2	Higher magnification scanning electron micrograph of as-cast and homogenized (a) Al-5Zn-1Mg (b) Al-10Zn-1Mg (c) Al-15Zn-1Mg alloys which contains many precipitate phases along the grain boundary	65
4.3	Force – Stroke diagram of (a) Al-5Zn -1Mg (b) Al-10Zn-1Mg (c) Al-15Zn-1Mg during axisymmetric compression testing at various temperatures	68
4.4	Engg. stress – Engg. strain diagram of (a) Al-5Zn -1Mg (b) Al-10Zn-1Mg (c) Al-15Zn-1Mg during axisymmetric compression testing at various temperatures	70
4.5	Log-log plot of true stress - true strain diagram of (a) Al-5Zn -1Mg (b) Al-10Zn-1Mg (c) Al-15Zn-1Mg during axisymmetric compression testing at various temperatures	71
4.6	Effect of temperature on yield stress of Al-Zn-Mg alloys	73
4.7	Effect of temperature on strength coefficient of Al-Zn-Mg alloys	73
4.8	Effect of temperature on strain hardening exponent of Al-Zn-Mg alloys	74
4.9	Effect of Zn content on yield stress of Al-Zn-Mg alloys in the temperature range of 303 – 673 K	74
4.10	Effect of Zn content on strength coefficient of Al-Zn-Mg alloys in the temperature range of 303 – 673 K	75
4.11	Effect of Zn content on strain hardening exponent of Al-Zn-Mg alloys in the temperature range of 303–673 K	75
4.12	Effect of temperature on friction factor of Al-Zn-Mg alloys	77
4.13	Effect of Zn content on friction factor of Al-Zn-Mg alloys in the temperature range of 303 – 673 K	77

4.14	Force – stroke diagram of (a) backward extrusion with a container and (b) containerless backward extrusion of Al-5Zn-1Mg for various strains at room temperature	81
4.15	Force – stroke diagram of (a) backward extrusion with a container and (b) containerless backward extrusion of Al-10Zn-1Mg for various strains at room temperature	82
4.16	Force – stroke diagram of (a) backward extrusion with a container and (b) containerless backward extrusion of Al-15Zn-1Mg for various strains at room temperature	83
4.17	Force – stroke diagram of (a) backward extrusion with a container and (b) containerless backward extrusion of Al-5Zn-1Mg at various temperatures for 0.1 strains	84
4.18	Force – stroke diagram of (a) backward extrusion with a container and (b) containerless backward extrusion of Al-10Zn-1Mg at various temperatures for 0.1 strains	85
4.19	Force – stroke diagram of (a) backward extrusion with a container and (b) containerless backward extrusion of Al-15Zn-1Mg at various temperatures for 0.1 strains	86
4.20	Variation of punch pressure against extrusion strain at various temperatures for punch depth 15 mm for (a) backward extrusion with a container and (b) containerless backward extrusion of Al-5Zn-1Mg.	93
4.21	Variation of punch pressure against extrusion strain at various temperatures for the punch depth of 15 mm for (a) backward extrusion with a container and (b) containerless backward extrusion of Al-10Zn-1Mg.	94
4.22	Variation of punch pressure against extrusion strain at various temperatures for punch depth 15 mm for (a) backward extrusion with a container and (b) containerless backward extrusion of Al-15Zn-1Mg.	95

4.23	Variation of punch pressure with extrusion strain for the punch depth of 15 mm for backward extrusion with and without container for (a) Al-5Zn-1Mg at 373 K (b) Al-10Zn-1Mg at 473 K and (c) Al-15Zn-1Mg at 373 K	97
4.24	Variation of punch pressure against extrusion strain at the punch depth of 15 mm for containerless backward extrusion of Al-Zn-Mg alloys at (a) 303 K (b) 373 K and (c) 473 K	99
4.25	Force-Stroke diagram of containerless backward extrusion of (a) Al-5Zn-1Mg (b) Al-10Zn-1Mg and (c) Al-15Zn-1Mg at room temperature for various extrusion strains	102
4.26	Force-Stroke diagram of containerless backward extrusion of (a) Al-5Zn-1Mg (b) Al-10Zn-1Mg and (c) Al-15Zn-1Mg at 423 K for various extrusion strains	104
4.27	Force-Stroke diagram of containerless backward extrusion of (a) Al-5Zn-1Mg (b) Al-10Zn-1Mg and (c) Al-15Zn-1Mg at 523 K for various extrusion strains	106
4.28	Force-Stroke diagram of containerless backward extrusion of (a) Al-5Zn-1Mg (b) Al-10Zn-1Mg and (c) Al-15Zn-1Mg at 623 K for various extrusion strains	108
4.29	Variation of punch pressure against temperatures for (a) punch depth of 10mm at 0.1 strains and (b) Punch depth of 5mm at 0.15 strains for Al-Zn-Mg alloys	112
4.30	Variation of punch pressure against temperatures for a punch depth of 5mm for Al-Zn-Mg alloys at (a) 0.2 and (b) 0.29 strains	113
4.31	Variation of punch pressure against temperatures for a punch depth of 3mm for Al-Zn-Mg alloys at (a) 0.37 and (b) 0.45 strains	114

5.1	Scanning electron micrograph of Al- 12 wt. % Zn-6 wt. % Mg alloy indicated microstructure that consists mainly by α -Al phase with ($\alpha+\tau$) eutectic in interdendritic regions	116
5.2	Microstructure of as cast Al-Zn-Mg (a) 40 X (b) Precipitate phases along the grain boundaries before solution treatment, 200X	117
5.3	X-Ray diffraction analysis of Al-Zn-Mg alloys	117
5.4	Structure of graphite. (The individual sheets consist of closely packed atoms, separated by a relatively large distance from neighboring sheets)	125
6.1	Stress and displacement distribution for Al-5Zn-1Mg billets of 100 mm diameter and 50 mm height during containerless backward extrusion at room temperature	144
6.2	Stress and displacement distribution for Al-10Zn-1Mg billets of 100 mm diameter and 50 mm height during containerless backward extrusion at room temperature	145
6.3	Stress and displacement distribution for Al-10Zn-1Mg billets of 100 mm diameter and 50 mm height during containerless backward extrusion at room temperature	145
6.4	Stress and displacement distribution for Al-10Zn-1Mg billets of 40 mm diameter and 50 mm height during containerless backward extrusion at room temperature	146

LIST OF TABLES

Table No	Caption	Page No
3.1	Alloys and their nominal composition used for the study	44
3.2	Bulk chemical analysis of Al-Zn-Mg alloys using an Optical Emission Spectrometry	46
3.3	Chemical analysis of AISI M2 HSS used for making the punch and base plate	58
4.1	Vickers hardness data of Al-Zn-Mg alloys in the as-cast and homogenized condition	65
4.2	Flow properties of Al-Zn-Mg alloys	72
4.3	Frictional properties of Al-Zn-Mg alloys	76
4.4	Extrusion strains for billets of diameter 25-50 mm extruded with a punch of 15mm diameter	78
4.5	Variation of theoretical punch pressure with respect to extrusion strain at various temperatures for backward extrusion with a container of Al-5Zn-1Mg	87
4.6	Variation of theoretical punch pressure with respect to extrusion strain at various temperatures for backward extrusion with a container of Al-10Zn-1Mg	88
4.7	Variation of theoretical punch pressure with respect to extrusion strain at various temperatures for backward extrusion with a container of Al-15Zn-1Mg	89
4.8	Variation of theoretical punch pressure with respect to extrusion strain at various temperatures for containerless backward extrusion of Al-5Zn-1Mg	90
4.9	Variation of theoretical punch pressure with respect to extrusion strain at various temperatures for containerless backward extrusion of Al-10Zn-1Mg	91

4.10	Variation of theoretical punch pressure with respect to extrusion strain at various temperatures for containerless backward extrusion of Al-15Zn-1Mg	92
4.11	Punch pressure at various temperatures for a punch depth of 10mm for Al-Zn-Mg alloys at 0.1 strains	109
4.12	Punch pressure at various temperatures for a punch depth of 5mm for Al-Zn-Mg alloys at 0.15 strains	109
4.13	Punch pressure at various temperatures for a punch depth of 5mm for Al-Zn-Mg alloys at 0.2 strains	110
4.14	Punch pressure at various temperatures for a punch depth of 5mm for Al-Zn-Mg alloys at 0.29 strains	110
4.15	Punch pressure at various temperatures for a punch depth of 3mm for Al-Zn-Mg alloys at 0.37 strains	111
4.16	Punch pressure at various temperatures for a punch depth of 3mm for Al-Zn-Mg alloys at 0.45 strains	111

NOMENCLATURE

ABBREVIATIONS

AISI	:	American Iron and Steel Institute
ALPID	:	Analysis of Large Plastic Incremental Deformation
APFIM	:	Atom Probe Field Ion Microscopy
CAD	:	Computer-aided Design
DSA	:	Dynamic Strain Ageing
FEM	:	Finite Element Method
FEA	:	Finite Element Analysis
GP	:	Guinier Preston
HSS	:	High-Speed Steel
LMP	:	Low Melting Point
NEM	:	Natural Element Method
OD	:	Outer Diameter
ID	:	Inner Diameter
PFZ	:	Precipitate Free Zone
SCC	:	Stress Corrosion Cracking
SEM	:	Scanning Electron Microscope
XRD	:	X-Ray Diffraction

SYMBOLS

p	:	Forming stress or Pressure
σ_o	:	The flow resistance of the material for the appropriate stress state
σ_{fm}	:	Mean flow Stress
K	:	Strength Coefficient
ε	:	Strain

n	:	Strain hardening exponent
d_p	:	Punch diameter
$d_o = 2r_o$:	Diameter of billet
r_o	:	Radius of billet
s	:	$\frac{1}{2}(d_o - d_p)$
b	:	Undeformed depth
m	:	Friction factor
A_o	:	Initial area of billet
A_f	:	Final area of billet
h_o	:	Initial height
h_f	:	Final height of billet
$P_{p_{ext}}$:	Theoretical punch pressure for extrusion
$P_{p_{up}}$:	Theoretical punch pressure for upsetting.
ρ	:	Density
τ	:	Interfacial shear strength
σ_y	:	Yield stress
σ_{SS}	:	Strength of the material from solutes
σ_P	:	Strength of the material from precipitates
σ_{Disl}	:	Strength of the material from dislocations
σ_{GB}	:	Strength of the material from grain boundaries
M	:	Taylor factor for tensile deformation
c_{Zn}	:	Concentrations of Zn
c_{Mg}	:	Concentrations of Mg

CHAPTER 1

INTRODUCTION

Extrusion is one of the important metal forming processes. It is a well-known forming method in which a punch applies pressure to the samples, causing the work-piece to flow in the required direction. The relative motion between the punch and the die is obtained attaching either one to the stationary bed and the other to the reciprocating ram (Davis J. R, 2007). The extrusion process can either be cold, warm or hot. During warm extrusion the work-piece or preform enters the extrusion die at a temperature below the temperature range for recrystallization and above room temperature. Extrusion involves indirect, direct or combined indirect and direct displacement of metal by plastic flow under pressure.

Containerless or open die extrusion is mostly used metal forming process for manufacturing of preform or near net shape of many industrial parts used in many different applications. A billet is extruded without a container or with a large clearance between the container and the billet. Since extrusion is done in the absence of a container against conventional extrusion, it is also called as free extrusion. Container wall – billet friction is eliminated in containerless extrusion, which leads to a large reduction in the total force required for extrusion. Surface quality is expected to be better due to absence of friction. As there is no container, the billet is not supported and hence there may be chances of bulging during backward extrusion if height to diameter ratio is high. Therefore containerless backward extrusion is recommended only for producing short components.

Principal applications of containerless extrusion include parts for aerospace industries, automobile industries and aircraft industries (Çan Y et al., 2002). It is an advanced manufacturing process for electro motor shaft production in high efficiency and in mass production (Shuang-jie Zhan et al., 2010).

Aluminum and its alloys are the most commonly extruded metals. The control of extruded aluminum alloy grain structures is being driven by many applications,

particularly those with in the defence industry. Aluminum provides the characteristics of good strength-to-weight ratio, machinability, corrosion resistance, attractive appearance, high thermal conductivity and high electrical conductivity. Aluminum and its alloys encompass a wide range of chemical composition and thus a wide range of hardness. Many recovery and precipitation processes in aluminum alloys can occur at relatively low temperatures, such as 423 to 523 K.

Approximately, all of the aluminum alloys can be cold extruded. Aluminum alloys are well adapted to extrusion. Aluminum and its alloys can be successfully extruded with graphite, grease or high-viscosity oil as lubricants. For slugs of less extrudable aluminum alloys, for maximum extrusion severity surface preparation may be necessary for retention of lubricant. Extensive research studies, involving the effects of die geometry, loading rates, extrusion speeds and ratios of lengths to diameters of billet on the extrusion pressure of cold extrusion process have been undertaken, while research findings have been fairly restricted to containerless backward extrusion for warm and hot extrusion processes.

Open-die warm extrusion is an advanced forming technology which can not only reduce the machining time and material waste but also improves the properties of the products (Li Jun, 1997) and is suitable for Al-Zn-Mg alloys, which is difficult to extrude compared to other aluminum alloys . It is primarily available for axial symmetry parts in shape and easy to realize automated production. Because of the industrial importance, the containerless extrusions have been investigated by many researchers. Some important aspects of the open-die extrusion have been undertaken by Srinivasan K and Venugopal P (1990, 1993, 1997, 1999, 2004, 2007, and 2008). They have done extensive studies on the containerless extrusion of Ti-6Al-4V and commercial purity titanium. Fukui and Seino (1960) have studied the relation between the working pressures and extruded height in the cold containerless extrusion applying E. Siebel's equation originally proposed for compression. Takahashi and Fukuda (1987 and 1988) have studied the process limitations for open die forward extrusion of rod and the effect of structures and skin pass reduction of area on process limitations for cold open die forward extrusion of high carbon steel rod. Cannizaro

(1992) has performed a detailed analysis of the open die forward extrusion by means of numerical FEM simulations and experimental tests in order to determine the limits of the maximum possible reduction in area depending on the ratio between the supported and unsupported billet lengths and frictional condition. Huang and Fu (2001) have studied the bulging problem in the cold open die extrusion of a spline shaft and concluded that by adding a guiding length at the die entrance expansion, bulging can be restricted and the extrusion can be accomplished successfully. Forward extrusion of clover sections from lead billet has been investigated and a good agreement has been established between the measured and the predicted loads (Altinbalik T and Ayer O, 2008). Maccarani et al. (1991) have studied the effect of orifice angle and fillet radius of upper die on the deforming body. For the cylindrical orifices and specimens, it has been shown that the fillet radius has no influence on the compression forces, but the friction had significant effect (15-20%) on extrusion forces. The lubrication characteristics of several tool materials and lubrications were investigated by Nishimura et al. (1995) using injection upsetting combined with backward extrusion. Ishikawa et al. (2006) studied the effect of extrusion conditions on metal flow and microstructures of aluminum alloys. In their investigation, behavior of extrusion billet skin and microstructure of products was indispensable to maintain qualities of extrusions. Lee et al. (2002) studied a non-steady three dimensional finite element analysis of the flat die hot extrusion process with a developed finite element program. Flat and conical dies of H, T, L, elliptical and two-hole sections was designed on the basis of upper bound technique by Kumar S and Vijay, P (2007) for cold and hot extrusion of aluminum and lead alloy.

The research information available on containerless extrusion have shown that under the optimal conditions, the force required for extrusion is very less compared to conventional extrusion. More over the containerless extrusion has been proved to be a very economical process for producing components of short length, its applicability as a large scale production process is not yet established due to lack of study on diverse materials. Even though aluminium alloys are considered to be excellent candidates for conventional extrusion, no research effort has been done to explore the possibility of containerless backward extrusion of aluminium alloys.

The high specific strength of Al-Zn-Mg alloys and the lower punch pressure for containerless extrusion promises to be a vital combination, which needs to be further explored upon, hence present investigation was to determine theoretically and experimentally the effect of containerless backward extrusion of Al-Zn-Mg alloys for different geometries under a lubrication condition. The effect of specimen geometry on the extrusion pressure at various temperatures after containerless backward extrusion were investigated and presented. Finally, an optimum ratio of lengths to diameters of billets was determined by finite element analysis software called LS. Dyna: Livermore Software Dynamic Non Linear Analysis.

1.1 SCOPE OF THE PRESENT WORK

The scope for the present work was to carry out containerless backward extrusion of Al-Zn-Mg alloys and analyze the stress required for deformation at various temperatures and strains to determine the optimum punch pressure for extrusion.

1.2 OBJECTIVES

The objectives of the present research work were as follows:

- i) To determine the flow properties of Al-Zn-Mg alloys by an axysymmetric compression test and frictional properties by a ring compression test in the temperature range of 303 – 673 K
- ii) To study the effect of punch pressure with respect to extrusion strain at various temperatures during containerless backward extrusion of Al-Zn-Mg alloys by elementary plasticity theory (Dipper model)
- iii) To determine the punch pressure, optimum temperature and limiting h_0/d_0 for containerless backward extrusion of Al-Zn-Mg alloys after experimentation
- iv) To simulate the metal flow and generate the grid deformation pattern for containerless backward extrusion of Al-Zn-Mg alloys for optimizing containerless backward extrusion based on finite element methods.

1.3 STRUCTURE OF THE THESIS

The thesis is presented in different chapters. A brief chapter wise description of the thesis is as follows:

Chapter 1 gives an introduction to the research problem undertaken with a brief mention about the current status of research work existing in the relevant field along with some remarks on the gaps existing in the current knowledge of containerless extrusion. It also includes the scope and objectives of the research work undertaken and organization of thesis with a chapter wise description of the contents of the thesis.

Literature background related to the research is detailed in chapter 2. A brief introduction to extrusion with emphasis on containerless backward extrusion, along with a detailed account of flow stress, friction, Al-Zn-Mg system, elementary plasticity theory- Dipper model and simulation of metal forming processes is presented.

Chapter 3 describes testing methods to determine flow and frictional properties at various temperatures for the chosen alloys. Experimental set-ups and procedure for containerless backward extrusion are also presented in the same chapter.

Results of flow and frictional properties at various temperatures along with theoretical and experimental analysis of containerless backward extrusion for the chosen alloys are presented in Chapter 4.

A detailed interpretation and analysis of results were carried out and the related discussion is presented in Chapter 5

Detailed account of the finite element formulation of containerless backward extrusion, solving and analysis of the results using the grid formation of the deformed Al-Zn-Mg billets is discussed in Chapter 6

The conclusion drawn based on the discussions and FEM simulation are listed in Chapter 7.

CHAPTER 2

REVIEW OF LITERATURE

Metal forming, with its thousands of years of history, is one of the oldest and most important materials processing technologies. Metal forming processes have become increasingly important in almost all manufacturing industries. The major industries employing metal forming processes extensively are the following:

- (i) Aerospace
- (ii) Steel plants and Non-ferrous metal plants
- (iii) Automobile
- (iv) Nuclear and Thermal Power plants

While these industries involve forming processes for manufacturing of large components, forming processes are also employed for making of small pins, screws, foils, wires and washers.

2.1 EXTRUSION

Extrusion as an industrial process was invented around 1800 A.D. in England, during the industrial revolution when the country was leading the world in technological innovations. The invention consisted of the first hydraulic press for extruding lead pipes. An important step forward was made in Germany around in 1890 A.D., when the first horizontal extrusion press was built for extruding metals with higher melting points than lead. The feature that made this possible was the use of a dummy block that separated the ram from the work billet (Kalpakjian, 1992).

Extrusion is a plastic deformation process in which material is forced to flow through one or more die orifices to produce the products of desired configuration. Extrusion is the process by which a block of metal is reduced in cross section by forcing it through a die orifice under high pressure. In general, extrusion is used to produce cylindrical bars or hollow tubes, but shapes of irregular cross-sections may be produced from the more readily extrudable metals like aluminum. Extrusion is an indirect-compression process. Indirect-compressive forces are developed by the reaction of the work piece

(billet) with the container and the die as shown in Fig. 2.1. These forces reach high values as the reaction of the billet with the container results in high compressive stresses that are effective in reducing the cracking of the billet material during primary breakdown from the billet. Extrusion is the best method of breaking down the cast structure of the billet because the billet is subjected to compressive forces only (Laue and Stenger, 1976). This is an important reason for the increased utilization of extrusion in the working of metals difficult to form, like stainless steels, nickel-based alloys and other high-temperature materials (Saha, 2008)

Extrusion can be a hot-working process which, like forging, rolling, etc., uses the good deformability of heated metallic materials for shaping them. The most important aspect of the process is that it enables considerable changes of shape to be achieved in a single operation and provides a means of dealing with metals and alloys whose physical structure renders them unsuitable for shaping by other methods. Besides, with extrusion it is possible to form complex sections that cannot be produced in other ways. Finally, extrusion also offers economic advantages in that the dies are relatively inexpensive and are interchangeable, so that one extrusion machine can be used for the production of a wide variety of sections.

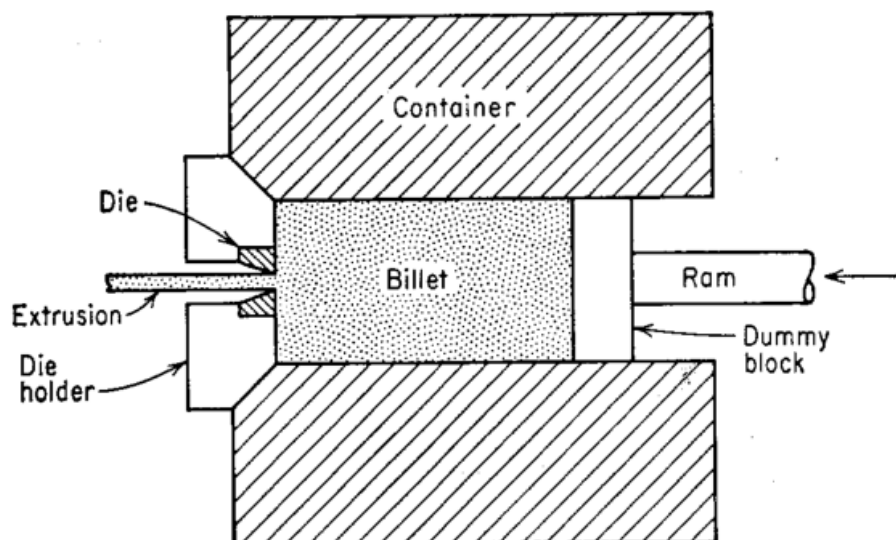


Fig.2.1 Direct extrusion process.

A metal billet heated to the appropriate temperature is fed into the cylindrical container of the extrusion press and is forced by the action of a ram through a hardened steel die whose orifice has the desired shape to produce the solid or hollow section. The metal emerges from the die as a continuous bar, which is cut to the required lengths. Extrusion products are therefore essentially “linear” in character, in the sense that shaping is confined to the cross section only. The process is therefore eminently suitable for the production of bar-like and tubular objects.

Most metals and alloys can be shaped by extrusion. At first the process was confined to nonferrous metals and has now in fact largely superseded other methods for the shaping of such metals. Cable sheathing, lead pipe and aluminum alloy structural sections are typical of such extrusion products. The extrusion of steel presented difficulties because of the heavy wear on the dies and the high working temperatures and stresses. However, these difficulties have been overcome, and extrusion is used, for example, in the production of stainless steel tubes.

For making tubular sections, a mandrel is arranged in the die orifice, and during extrusion the metal flows through the annular space so formed. Hollow billets are used for tubes, or solid billets are first pierced in the extrusion operation. Extrusion machines are generally hydraulic presses with capacities ranging from about 500 tons to about 7500 tons. Graphite grease is commonly used for lubrication between metal and tools.

2.2 CLASSIFICATION OF EXTRUSION BASED ON TEMPERATURE

Depending on the working temperature, the extrusion processes are classified as cold extrusion, hot extrusion and warm or semi hot extrusion processes.

2.2.1 Cold Extrusion

Cold extrusion is defined as the process of plastically deforming a metal or an alloy under the conditions of temperature and strain rate that the strain hardening or work hardening is not relieved. Normally cold extrusion is carried out at the temperature which is below the recrystallization temperature of metals or alloys. During cold extrusion, the strength of the metals increases with increasing amount of cold working

as shown in the Fig. 2.2. If the cold working exceeds certain limit, the metal will fracture. To avoid this problem, the metal must be annealed before further cold working. During annealing process the formability of the metal is restored. The annealing or the softening process is normally called as interstage annealing. By controlling the annealing process variables, the original property suitable for cold forming operation can be obtained in the annealing process as shown in the Fig. 2.2.

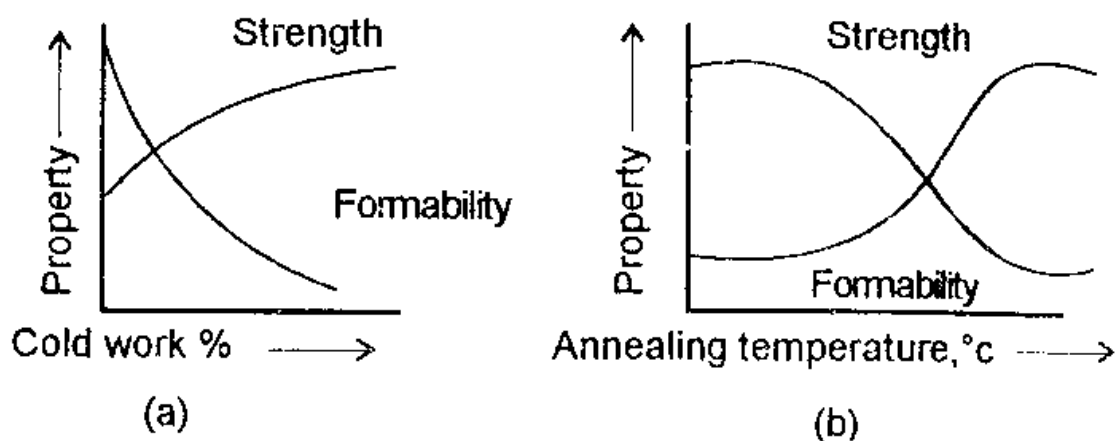


Fig. 2.2 Property changes due to cold working and annealing.

The advantages of cold working are that no scaling and oxidation occurs because the deformation occurs at low temperatures, hence, there is less wastage of material. The surface finish obtained is excellent and very good dimensional tolerances can be achieved and as a result in many cases reduced or no machining allowance is required. Automation is possible because of low working temperature and thin gauge wires or sheets can be produced by cold working. The strength of the finished products can be controlled within certain limits because of work hardening, by controlling the amount of cold work as per requirements.

The disadvantages are that as the strength of the metal is very high at low temperatures, large forces are required for deformation, calling for higher capacity machines which are costly. The formability is poor at lower temperatures. Hence cold working requires several stages (Rowe, 1977) with intermediate annealing, which increases cost. Cold working introduces severe stresses in the metal which invariably

calls for stress relieving or other annealing treatment and this again increases cost. The tooling must be specially designed because of very high forces involved in the process. The punches and dies used in cold extrusion are subjected to severe working conditions and are made of wear-resistant tool steels, e.g., high-alloy chromium steels.

In cold extrusion, which is used for the manufacture of special sections and hollow articles, the material is generally made to flow in the cold condition by the application of high pressure. The high pressures force the material through a cavity enclosed between a punch and a die. Cold extrusion can be used with any material that possesses adequate cold workability, e.g., tin, zinc, copper and its alloys, aluminium and its alloys. Indeed it is for these metals that the process is more widely adopted. Low-carbon soft annealed steel can also be cold extruded (Tiernan et al., 2005).

2.2.2 Hot Extrusion

Hot extrusion is defined as the process of plastically deforming a metal or an alloy under such conditions of temperature and strain rate such that recovery and recrystallization occur during or immediately after deformation. In other words, in hot working no work hardening occurs in the metal. It is noted that when forces are applied on the metal, the microstructure elongates in the direction of the maximum strain. Since the temperature is very high which depend on the material being extruded, nuclei of new grains are formed. This grows with time so that ultimately a fine grained-equiaxed recrystallised structure is obtained. The size of the grains obtained depends upon the amount of reduction and the temperature of working. Larger the amount of reduction, the finer will be the grains.

The advantages of hot working are that because of high temperature the strength of the metal is low and therefore low tonnage equipment is sufficient. This is generally greater than 60% of the absolute melting temperature of the metal. The number of stages required for forming is reduced and so intermediate annealing is avoided because of high ductility/formability at high temperatures. Since no work hardening takes place large deformation can be obtained by a single pass. Stress relieving is not required as high temperatures are involved.

The rapid diffusion at high temperatures reduces chemical inhomogeneties. Blow holes and porosities are eliminated by welding action at high temperatures.

The disadvantages of the hot forming processes are that high temperature heating facilities are required which increases the investment cost for machinery and its upkeep (Oberg et al., 2000). Due to high temperatures, surface reactions between the metal and the furnace atmosphere give problems, particularly in the case of reactive metals like titanium and these calls for inert atmospheres. Material losses are possible due to scaling and oxidation. Poor dimensional tolerance and surface finish are obtained and thin gauge sheets and wires cannot be produced. Automation is difficult. Surface decarburization which occurs in the case of steels reduces the strength, hardness and wear property on the surface. Due to non-uniform deformations, the microstructure and properties of hot worked metals are generally not uniform over the cross-section. This requires an additional normalizing heat treatment.

The hot extrusion process is used to produce metal products of constant cross section, such as bars, solid and hollow sections, tubes, wires, and strips, from materials that cannot be formed by cold extrusion (Frank and Jay, 2005).

2.2.3 Warm Extrusion

Warm extrusion or semi hot extrusion is defined as a process of plastically deforming a metal or an alloy under such conditions of temperature and strain rate such that the drawbacks of both cold working and hot working are eliminated and their advantages are combined together.

The selection of the working temperature for warm working is based on the following factors:

- (i) Yield or flow strength of the material.
- (ii) Ductility or formability of the material.
- (iii) Dimensional tolerance.
- (iv) Scaling and oxidation losses.

If the formability or the reduction of number of forming stages is the main aim, then higher warm working temperature can be selected for forming operation. For other factors, the lower warm working temperature can be employed for forming operation

(Narayanasamy, 2000). It is usually used to achieve the proper balance of required forces, ductility and final extrusion properties (Avitzur, 1987).

2.3 BACKWARD EXTRUSION

In backward extrusion, the billet remains stationary relative to the container wall while the die is pushed into the billet by a ram (Charles et al., 1984). The die at the front end of the hollow stem moves relative to the container but there is no relative displacement between the billet and the container. The schematic sketch of backward extrusion is shown in Fig. 2.3 (George, 1988). The lengths of the billet used in backward extrusion are limited only by the column strengths of the ram. Since the billet is not forced to move relative to the container this process is characterized by the absence of friction between the billet and the container walls and as a result the ram force is therefore lower than the forward extrusion. Limitations of backward extrusion are imposed by the lower rigidity of the hollow ram and the difficulty in supporting the extruded product as it exits the die. Impurities and defects on the surface of the billet affect the surface of the extrusion. These defects ruin the piece if it needs to be anodized or the aesthetics are important. In order to get around this the billets may be wire brushed, machined or chemically cleaned before being used (Drozda et al., 1984). This process isn't as versatile as direct extrusions because the cross-sectional area is limited by the maximum size of the stem.

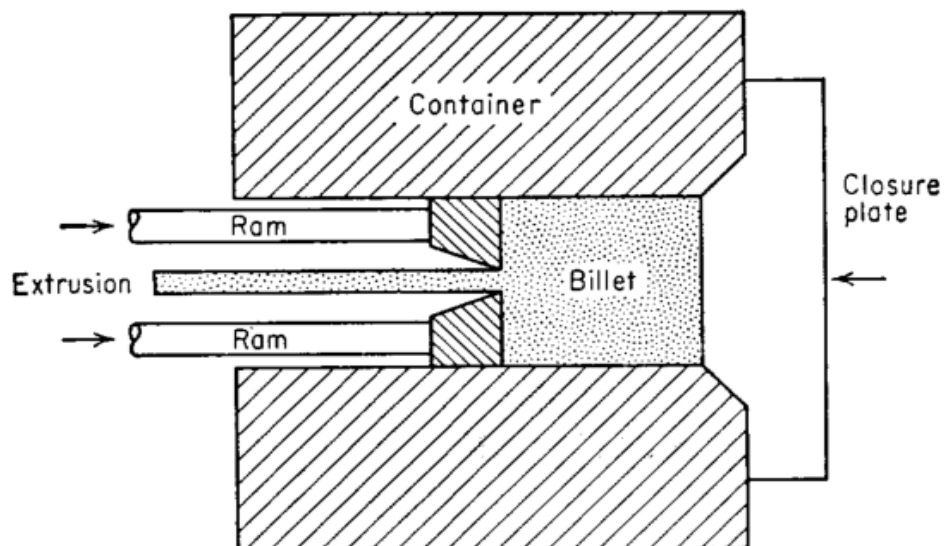


Fig. 2.3 Backward extrusion.

2.3.1 Extrusion Pressure

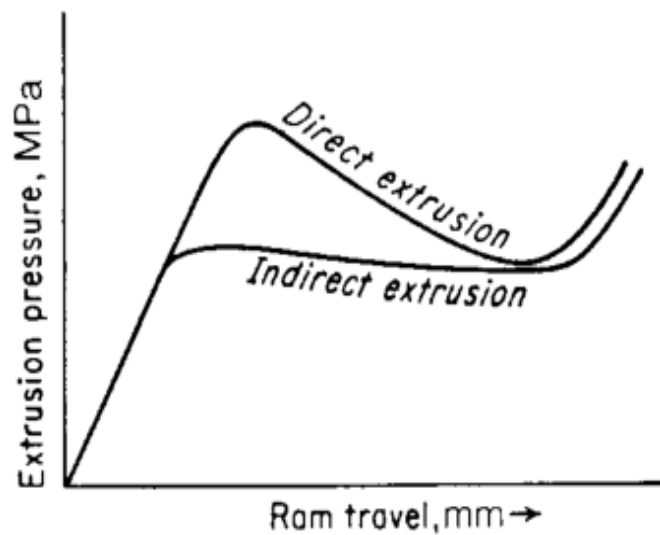


Fig. 2.4 Extrusion pressure vs. ram travel.

In the above Fig. 2.4 (George, 1988), the extrusion pressure is plotted against the ram travel for both the backward and forward extrusion. Extrusion pressure is the extrusion force divided by the cross-sectional area of the billet. The rapid rise in pressure during the initial ram travel is due to the initial compression of the billet to fill the extrusion container. The metal begins to flow through the die at the maximum value of pressure, called the breakthrough pressure (George, 1988). As a result of metal motion through a die, a friction force appears opposite to that motion, so the coefficient of friction has an important effect in the extrusion process. Therefore, extrusion pressure must be a function of friction force (Jabbar, 2010). The breakthrough pressure needed with backward extrusion is significantly lower than forward extrusion because of the absence of friction between the billet and the container walls. After the breakthrough pressure, as the billet extrudes through the die, the pressure requirements to maintain the flow progressively remain essentially constant throughout the extrusion stroke. Near the end of the stroke, as the unextruded butt thickness becomes thinner, the force necessary rises significantly, as is also the case with forward extrusion.

2.3.2 Deformation/Flow Pattern in Backward Extrusion

The pressure required to produce an extrusion is dependent on the way the metal flows in a container and extrusion die and this is largely determined by the conditions of lubrication. Certain defects which occur in extrusion are directly related to the way the metal deforms during extrusion. The Fig. 2.5 (George, 1988) below shows the characteristic types of deformation in extrusion for different cases.

Thus the two factors that greatly influence metal flow in extrusion are the frictional conditions at the billet-container-die interfaces and thermal gradients in the billet.

Using the natural element method (NEM) for simulation of metal forming processes Javanmard et al. (2011) suggests that non steady-state metal forming problems such as backward extrusion involve high mesh distortion with large material deformation and boundary motion, non-linear material behavior, and continuous changes in boundary conditions.

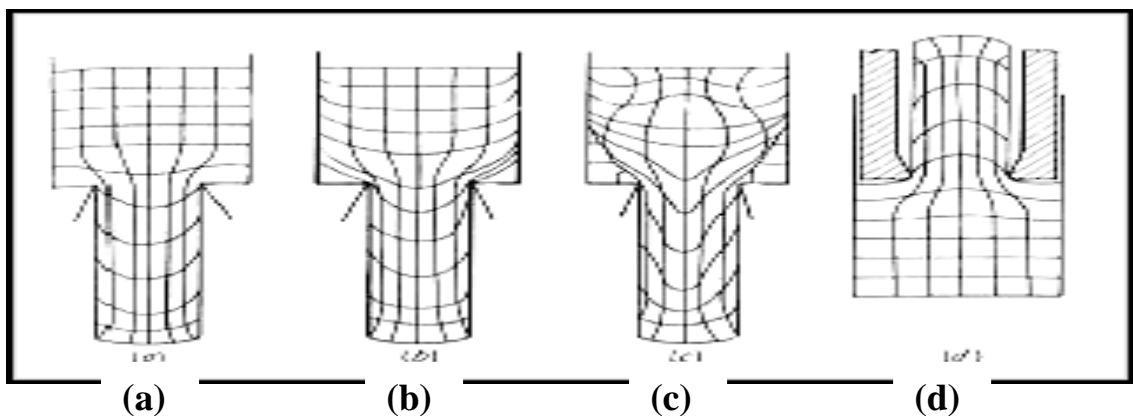


Fig. 2.5 Flow pattern of the billet during the extrusion process.

Fig. a - A nearly homogeneous deformation is shown and is typical of low container friction with lubricated billet.

Fig. b - The deformation of the billet is relatively uniform until close to the die entrance. It represents a case of increased container-wall friction, producing a dead zone of stagnant metal which undergoes little deformation.

Essentially pure deformation of the billet takes place at the center and extensive shear deformation along the side of the container walls. The latter requires an expenditure of energy called as redundant work.

Fig. c - It represents the case for high friction at container-billet interface where the flow is concentrated toward the center and an internal shear plane develops due to the cold container. When sticking friction prevails, between the billet surface and the container, the metal will separate internally along a shear zone and a thin skin will be left in the container and a new metal surface is obtained.

Fig. d - This is the case of backward extrusion, where a homogeneous deformation is obtained because of the absence of the container-wall friction and a well lubricated billet (Narayanasamy, 2000).

2.3.3 Material Flow

The billet with diameter d_o and height h_o is slid into the die, using the small clearance between die and billet. When the punch starts to penetrate into the billet, the material is axially upset and increases in diameter corresponding to the inner die diameter d_D . Once the conical face of the hot punch is entirely inside the billet, the material fills the die cavity completely so that it has full contact with the tool surfaces. Further penetration of the punch into the billet forces the material to flow through the orifice formed by the die and the punch, in the opposite direction of the punch movement, first along the die wall and later outside of the die.

The material coming through the orifice formed by the punch wall and the die wall undergoes no strain after this point. The remaining volume between the punch and the die bottom is only partly in the deformation zone. Depending upon the geometrical and the friction conditions, a dome-shaped rigid plastic zone is formed in this region. This zone is also affected by the can bottom thickness and the reduction in area (Lange, 1985). The die geometry directly influences material flow, and therefore it affects the distribution of the effective strain and flow stress in deformation zone. At forward and backward extrusion, at the same displacement a large die angle increases

the volume of metal undergoing shear deformation and results in an increase in shear deformation load, on the other hand, the ratio of reduction decreases, which result in a decrease in die friction load (Bashir and Mustafa, 2012).

2.3.4 Forces

The Fig. 2.6 (Lange, 1985) shows the various forces acting in the backward can extrusion process. The punch force F_P and the force on the bottom F_B can be measured easily. The variation of the punch force F_P as a function of the deformation is shown in the Fig. 2.7 (Lange, 1985). The force increases rapidly to its maximum and then reduces slowly to its final value. The first portion is characterized by the elastic deflection of the tooling-workpiece system and the increasing influence of strain hardening and the second is characterized by the decrease in volume of the material participating in the deformation process (Lange, 1985). In recent years many researchers have focused on the investigation of various forming parameters to this process in order to reduce forming force and to improve formability and forming accuracy (Branimir et al., 2008).

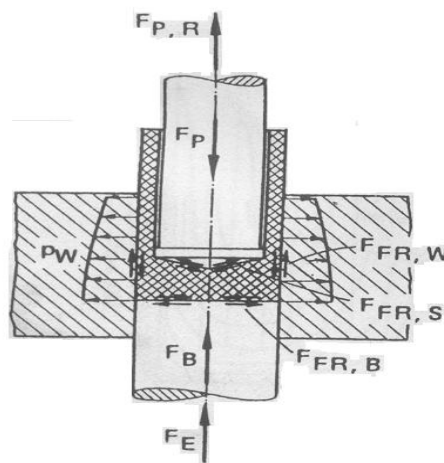


Fig. 2.6 Forces acting in the backward can extrusion

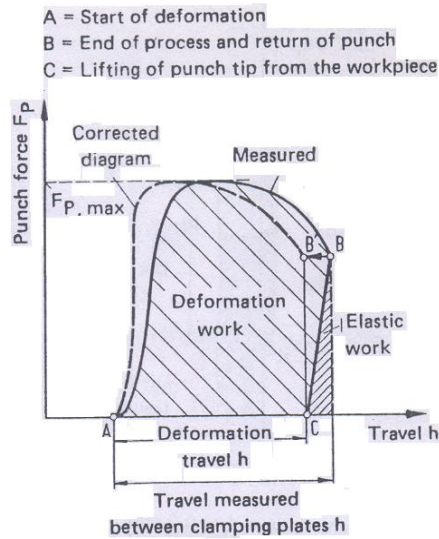


Fig. 2.7 Punch force-travel diagram for backward can extrusion.

2.3.5 Stresses

Stresses can be determined from the strain rates by approximate methods which are complicated. Schmitt (1968) has calculated the trajectory of the principle shear stress (slip line field) for pieces with rotational symmetry and has shown that the axis of symmetry (z-axis) is intersected at an angle of 45° by the trajectories of the principle shear stresses. Based on this, the principle normal stress should act along the axis. In the imaginary vertical extension of the punch edge, the trajectory of the principle shear stresses is also vertical. Shearing takes place along this edge. This aspect is assumed in analyzing the backward can extrusion process for force calculations. Tri-axial state of stress exists in the deformation zone and a very high local stresses also acts on the tools. A streamline field for backward can extrusion is shown in Fig. 2.8 (Lange, 1985).

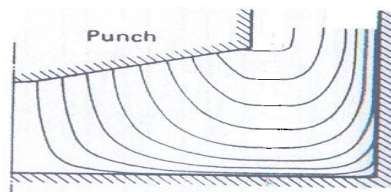


Fig. 2.8 Streamline field for backward can extrusion.

2.4 CONTAINERLESS BACKWARD EXTRUSION

In backward can extrusion, the shape of the workpiece is formed by the gap between the punch and the die. The metal is nonstationary throughout the deformation process. The can extrusion of soft materials like aluminium and tin belongs to the oldest applications of the process for mass production and it has been in use since 1800 A.D. Combinations of backward and forward can extrusion processes with other deformation processes are also widely used. The important parameters in these processes are material selection, change of material properties, surface treatment and lubrication, and selection of machines.

In cold forming of axi- symmetric backward extrusion, the quality of the components is improved by selecting a suitable loading for pressing the die against the plastic metal. The contact pressure is decided by the type of contact by the punch, like a flat base or with some kind of radius at the edge which is either pre existing or generated by wear. The complexity of this problem is the contact pressure between an elastic face with sliding friction and the surface of plastic metal (Ban Bakir Alamer, 2013). In this process workpiece material flows both in axial and radial direction fulfilling the opening in the die. It has been concluded that geometry of the die has a substantial influence on material flow and thus on component geometry, whilst friction has little (Miroslav Plančak et al., 2012)

Containerless extrusion is carried out without using a container so that the billet is free to move in all directions. As a result, the friction between the workpiece and the container is absent. The force required to carry out the extrusion is also lower compared to other processes. It is basically a low strain process i.e., when the punch forces its way through the workpiece, the amount of workpiece displaced is in small amount. At higher strains, initial upsetting predominates the extrusion, requiring very low punch forces to carryout the process. It can be of two types, forward (Avitzur, 1968, Binder and Lange, 1980, Srinivasan and Venugopal, 1993, Avitzur, 1983, Haarschiedt and Lange, 1983) or backward. Not many investigations are there on backward containerless extrusion. Containerless piercing of cup is reported in

literature (Lange, 1985, Schmitt et al., 1965, Samuel et al., 1996). In this process there is lateral displacement of material. Initial and final heights of cup are equal, only the outer diameter of cup is more than the initial diameter of the cylindrical billet. In containerless backward extrusion there is no lateral displacement of material or outer diameter of cup is equal to the initial diameter of cylindrical billet and final height of cup is more than the initial height of billet. This is possible as long as extrusion pressure is less than yield stress of billet material. Once it crosses yield stress it becomes piercing process. If punch pressure for extrusion ($P_{p_{ext}}$) is less than punch pressure for upsetting ($P_{p_{up}}$), containerless backward extrusion dominates; if $P_{p_{ext}}$ is greater than $P_{p_{up}}$ containerless piercing of cup dominates and if $P_{p_{ext}}$ equals $P_{p_{up}}$ a combination of above two will take place.

In comparison with deep drawing, it has techno-economic advantages in spite of considerable investments in tooling if deep drawing would be conducted in more steps (Barisic et al., 2002). For backward extrusion, it can be said that due to its material savings, different distributions of stresses in relation to similar process, and increasingly reduced machining, it has become one of the most promising manufacturing process (Barisic et al., 2004). It is known that frictional conditions at the interface of the die/workpiece could affect metal flow, total deformation load, final properties of the product, and cause energy losses or premature die wear. The effect of friction between the work piece and the forming tools (dies) is complex and results in the appearance of surface shears. Thus friction directly affects the planes of principal stresses and is therefore, considered to be a major variable in metal forming processes where the work piece undergoes large plastic deformation (Sofuoglu and Gedikli, 2002). In the case of backward extrusion with a container which is shown in Fig. 2.9, material has a strong tendency to stick to the container wall and nonuniform flow occurs, thus increasing the total deformation load.

One of the significant trends in the research and application of containerless backward extrusion is the increase of the workpiece complexity. This can be achieved by combining of the mentioned basic extrusion processes which, in most cases, leads to complex material flow around the base of the punch. As a result, wider spectrum of

component geometries can be obtained by varying the dimensions of punch. A theoretical analysis of so called “non-conventional” types of extrusion is carried out by Miroslav Plančák et al. (2012).

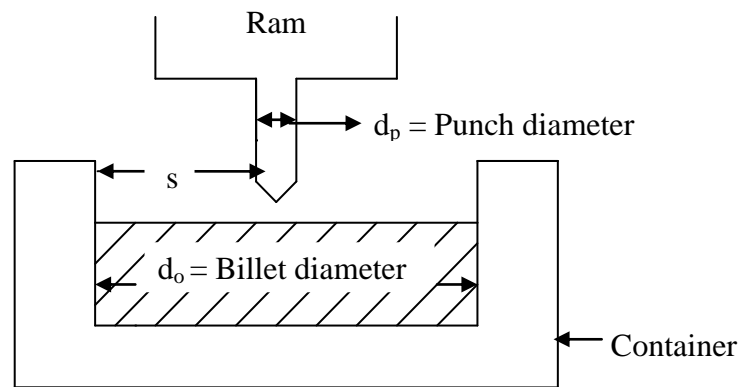


Fig. 2.9 Backward extrusion with a container

Containerless backward extrusion as shown in Fig. 2.10 is characterized by the absence of friction between the billet surface and container since extrusion is carried out in the absence of a container. The load required therefore is decreased (Kurt Laue and Helmut Stenger, 1981)

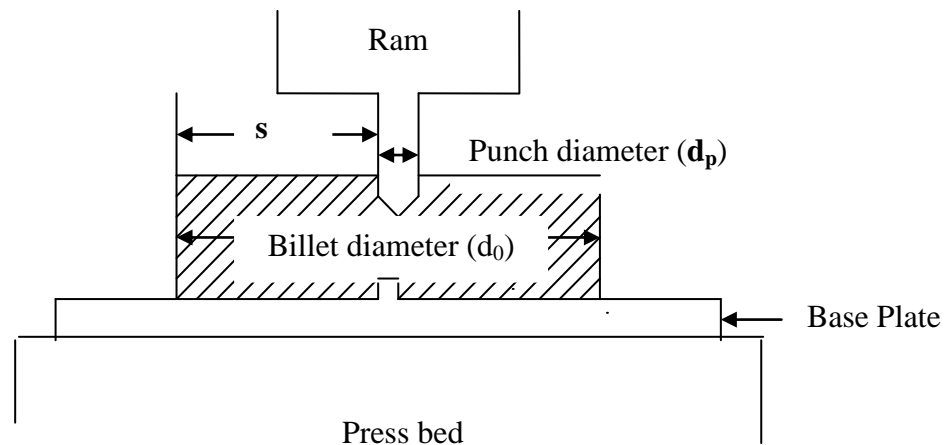


Fig. 2.10 Containerless backward extrusion

2.4.1 Advantages and Disadvantages of Containerless Backward Extrusion

The advantages of containerless backward extrusion are partly related to the lower load needed and partly to the more uniform flow pattern developed because of the absence of relative motion between the billet and the container – no heat is generated by friction (Charles et al., 1984) .

The main advantages are

- (i) A 25 to 30% reduction in load compared with direct extrusion
- (ii) The resultant higher extrusion load available can be used either to extrude smaller cross sections or to decrease the billet temperature, permitting the use of higher speeds
- (iii) The extrusion pressure is not a function of billet length because there is no relative displacement of the billet centre relative to the peripheral region. The billet length is therefore not limited by the load required for this displacement but only by the length and stability of the punch
- (iv) No heat is produced by friction between the billet and the container, and consequently no temperature increase occurs at the billet surface towards the end of extrusion therefore, there are fewer tendencies for the surfaces and edges to crack and significantly higher extrusion speeds can be used.
- (v) The service life of tooling is increased , because of the almost total absence of friction
- (vi) There is more uniform deformation of the complete billet cross section with no tendency to form an extrusion defect or coarse-grained peripheral zone
- (vii) Impurities on the billet surface do not finish up inside the extrusions

The disadvantage of containerless backward extrusion is that impurities or defects on metal surface affect the surface of the extrusion; therefore machined billets have to be used in many cases. In addition, the cross sectional area and length of billet while extrusion is limited by the size of the punch.

2.5 FLOW STRESS DETERMINATION IN METAL FORMING

The various expressions that are developed to describe the forming stress, or pressure, in a particular metal working process invariably consists of three terms as given below:

$$p = \sigma_o g(f)h(c) \quad (2.1)$$

where,

σ_o = the flow resistance of the material for the appropriate stress state, i.e., uniaxial, plane strain, etc. It is a function of strain, temperature, and strain rate.

$g(f)$ = an expression for the friction at the tool-workpiece interface.

$h(c)$ = a function of the geometry of the tooling and the geometry of the deformation.

This term may or may not include a contribution from redundant deformation. It is obvious from the above relationship that if we are to make accurate predictions of forming loads and stresses, we need accurate values of flow resistance (flow stress). The experimental problems in measuring the flow curve under metal forming conditions are more severe than those in the usual stress-strain test determined for structural or mechanical design applications. Since metal forming processes involve large strains, it is desirable to measure the flow curve out to a true strain of 2.0 to 4.0. In addition, many of these processes involve high strain rates ($\dot{\epsilon} \approx 100 \text{ s}^{-1}$), which may not be obtained easily with ordinary test facilities. Further, many metal working processes are carried out at elevated temperatures where the flow stress is strongly strain rate sensitive but nearly independent of strain. Thus, tests for determining flow stress must be carried out under controlled conditions of temperature and constant true-strain rate (McQueen and Jonas, 1971).

The true stress- true strain curve determined from the tension test is of limited usefulness because necking limits uniform deformation to true strains less than 0.5. This is particularly severe in hot working, where the low rate of strain hardening allows necking to occur at ($\epsilon \approx 0.1$). The formation of a necked region in the tension specimen introduces a complex stress state and locally raises the strain rate. The compression of a short cylinder between anvils is a much better test for measuring the

flow stress in metalworking applications (Altan et al., 1983). There is no problem with necking and the tests can be carried out to strains in excess of 2.0 if the material is ductile. However, the friction between the specimen and anvils can lead to difficulties unless it is controlled.

2.5.1 Axisymmetric Compression Test

In the homogeneous upset test a cylinder of diameter D_0 and initial height h_0 would be compressed in height to h and spread out in diameter to D . According to the law of constancy of volume

$$D_0^2 h_0 = D^2 h \quad (2.2)$$

During deformation, as the metal spreads over the compression anvils to increase its diameter, frictional forces will oppose the outward flow of the metal. This frictional resistance occurs in that part of the specimen in contact with the anvils while the metal at specimen mid height can flow outward undisturbed. This leads to a barreled specimen profile, and internally a region of undeformed metal is created near the anvil surfaces as shown in Fig. 2.11 (George, 1988). As these cone shaped zones approach and overlap, they cause an increase in force for a given increment of deformation and the load deformation curve bends upward as shown in Fig. 2.12 (George, 1988). For a fixed diameter, a shorter specimen will require a greater axial force to produce the same percentage reduction in height because of the relatively larger undeformed region (Fig. 2.11). Thus one way to minimize the barreling and non uniform deformation is to use a low value of D_0/h_0 . However there is a practical limit of $D_0/h_0 \approx 0.5$, for below this value specimen buckles instead of barreling. The true flow stress in compression without friction can be obtained (Cooke and Larke, 1945) by plotting load vs D_0/h_0 for several values of reduction and extrapolating each curve to $D_0/h_0 = 0$.

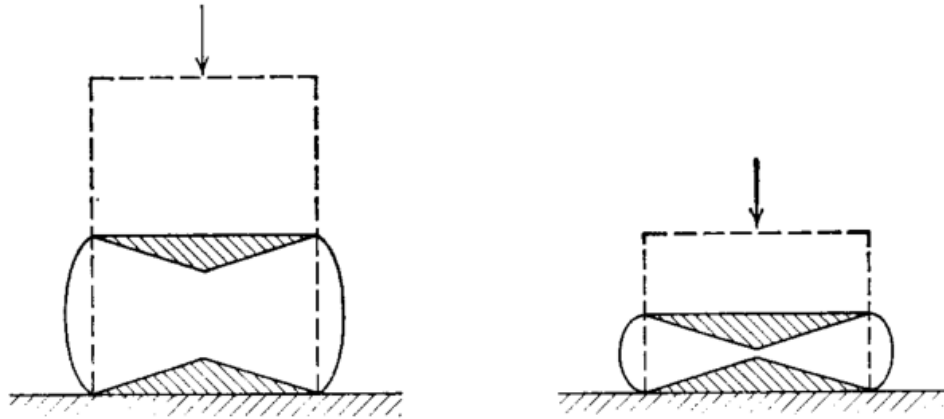


Fig. 2.11 Undeformed regions (shaded) due to friction at ends of a compression specimen.

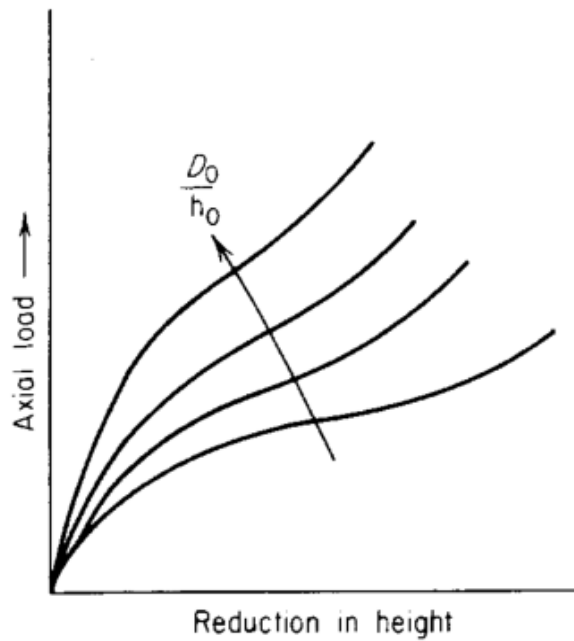


Fig. 2.12 Load – deformation curves for compression tests with different values of D_0/h_0 .

In the absence of efficient lubrication, the compression test is complicated by the fact that friction at the platens restricts the metal flow at the ends of the specimen and imparts non-homogeneous deformation in the specimen as compression proceeds (Chakraborty, 1988). The friction at the specimen-platen interface can be minimized (Van Rooyen and Backofen, 1960, Pearsall and Backofen, 1963) by using smooth,

hardened platens, grooving the ends of the specimen to retain lubricant, and carrying out the test in increments so that the lubricant can be replaced at the intervals (Hsu, 1969) . Solids, such as graphite and molybdenum disulfide are layered lattice compounds which are effective lubricants. When friction is not present the uniaxial compressive force required to produce yielding is

$$P = \sigma_0 A \quad (2.3)$$

The true compressive stress p produced by this force P is

$$p = 4P / \pi D^2 \quad (2.4)$$

and using the constancy of volume relationship

$$p = 4Ph / \pi D_0^2 h_0 \quad (2.5)$$

where D_0 and h_0 are the initial diameter and height and h is the height of the cylindrical sample at any instant during compression. The true compressive strain is given by

$$\epsilon_c = \ln(h_0/h) \quad (2.6)$$

During the forming process, the mechanical properties and metal flows are essentially influenced by strength coefficient, strain hardening, strain rate, temperature, prior deformation, deformation velocity, tool-workpiece interface friction, tool temperature and materials used for making tool. The flow behaviour of many materials are expressed by power law equation

$$\sigma = K \epsilon^n \quad (2.7)$$

where σ is the flow stress, K is the strength coefficient and n is the strain hardening exponent. In metal forming, the power law equation has always been a significant basis for analyzing plastic deformation. The strength coefficient and strain hardening

exponent are the two major and indispensable parameters of power law equation. Metals with high strength coefficient require higher capacity machines for forming. A strain hardening exponent is a measure of resistance to plastic flow while metal is deformed. A metal with high strain hardening exponent but a low strength coefficient will achieve a high strength after a large plastic deformation (Campbell, 2008).

Several attempts have been made in the past to ascertain the flow behaviour in homogeneous uniaxial compression tests (Hsu and Young, 1967). Aluko and Adeyemi (1998) have analyzed true stress versus true strain curves and shapes of the deformed workpiece to study the barreling effect. Rao et al., (1999) investigated the flow properties of commercial purity aluminium using compression test at different temperatures. Woodward (1977) attempted to obtain the flow stress in compression by varying the h/d ratio using upper bound method.

The stress strain curve and the flow properties are strongly dependant on the temperature at which the test is carried out. In general, strength decreases and ductility increases as the temperature rises. Thermally activated processes assist deformation and reduce strength at elevated temperatures. The temperature dependence of flow stress at constant strain and strain rate can generally be represented by

$$\sigma = C_2 e^{Q/RT} \left| \epsilon, \dot{\epsilon}_0 \right. \quad (2.8)$$

Where Q is the activation energy for plastic flow

R is the universal gas constant

T is the temperature at which test was carried out

If equation 2.8 is obeyed, a plot of $\ln \sigma$ versus $1/T$ will yield a straight line of which the slope will be equal to Q/R . Hence the activation energy for plastic flow can be determined.

The present study has been carried out to understand the behaviour of Al-Zn-Mg alloys at various temperatures between room temperature 303K and 673K, by means of axysymmetric compression test.

The mechanical properties obtained at various temperatures were used as material constants for Dipper model modified for containerless backward extrusion.

2.6 FRICTION AND LUBRICATION

Friction is unavoidable in many metal-forming processes. Whenever a die is in contact with the metal to be formed, a relative motion, and resistance (friction) to this motion arises. Friction, in spite of being an independent parameter, is not measured directly, whereas independent parameters such as reduction and die angle can be measured directly. Still, in many metal-forming processes, the effect of friction is given equal importance to measurable independent parameters (Betzalel Avitzur, 1992). Friction has significant effects on both the workpiece and process variables such as deformation load, metal flow and surface quality, and internal structure of the product in metal forming processes. Therefore, the interface friction has to be optimized (Hassan et al., 2001). For effective friction control, effects of lubrication must be investigated. There are several methods developed for quantitative evaluation of friction at the die/workpiece interface in metal forming processes. The most accepted one is to define a coefficient of friction, μ , the Coloumb law of friction, or the friction factor m , a value varies from zero for frictionless interface to one for sticking friction.

$$\mu = (\tau / \sigma) \quad (2.9)$$

where τ is shear stress at the interface and σ is normal stress at the interface. This is valid when there is sliding. When there is sticking,

$$\mu = (\tau_y / \sigma_y) \quad (2.10)$$

where τ_y and σ_y are yield stresses in shear and normal case. When there is perfect sliding $\mu=0$. When there is perfect sticking it is equal to 0.5 if Tresca criteria are adopted and 0.577 when Von Mises- criteria are used. To avoid such inconvenience, instead of friction coefficient, friction factor ' m ' is used.

$$m = (\tau/\tau_y) \quad (2.11)$$

where τ is interfacial shear strength and τ_y is yield stress in shear. When there is perfect sliding $m=0$ and when there is perfect sticking $m=1$ in both Tresca and Von Mises-criteria. m is independent of normal stress at the interface while μ depends on it. μ is inversely related to normal stress at the interface which is contrary to reality. More over m is easy to measure by a simple ring compression test and also easy to handle in mathematical equations (Srinivasan, 2005).

Solid lubricants are thin films composed of a single solid or a combination of solids introduced between two rubbing surfaces for the purpose of reducing friction and wear. Applications or operations involving severe temperatures, pressures, and environments, which preclude the use of organic fluids, have promoted the development of solid lubricants. Many common solid lubricants, such as graphite and molybdenum disulfide are layered lattice compounds that shear easily along preferred planes of their structure. Molybdenum disulfide shows relatively low coefficient of friction because of the weak van der Waals forces between sulfur bonds. It also oxidizes at approximately 672 K in air, and the oxides can be abrasive. The low friction associated with graphite depends on intercalation with gases, liquids, or other substances. For example, the presence of absorbed water in graphite imparts good lubricating qualities. Thus, pure graphite has deficiencies as a lubricant except when used in an environment containing contaminants such as gases and water vapour. With proper additives, graphite can be effective up to 922 K (John Rumierz, 1992).

Graphite and MoS_2 exhibit low friction because of their layered structures. The former consisting of carbon atom arranged in hexagonal lattice while in the later each sulfur centre is pyramidal to three Mo centers. Each layer contains strong bonds that make it resistant to breakup and thereby enable it to carry substantial load. Because of the weak van der Waals interactions between the layers, they slide readily over one another. Direct microscopic observations of the dynamics of solid lubrication show that sliding is accompanied by severe ductile shear of the solid lubricant film (Sloney, 1978). Thus a solid lubricant must have low shear strength for a low friction factor.

2.6.1 Ring Compression Test

During plastic deformation of materials, working pressure or forming forces are not only influenced by material properties, but also by contact frictional conditions. It represents the reliable and most widely applied indirect method for estimation of contact friction in bulk forming processes (Altan et al., 2004). The change of inner diameter at compression of the ring realistically represents the condition of tool and material contact.

Originally, it was conceived as the qualitative method for comparing the lubrication conditions of the various lubricants to the contact friction in cold extrusion process (Kunogi, 1954). The application and development of this method has been the subject of many investigations. The method consists of monitoring the changes of inner diameter of the ring which is compressed, because the changes are considered to be the representatives of the level of sensitivity to active contact friction. Graphic dependence between height strain and inner diameter strain, at various influences of friction, gives calibration curves for reading the value of friction factor. Male and Cockroft (1964) established the calibration curves by experimental method, assuming friction in inter-contact of ring and tool. The initial dimensions of the ring in the following ratios of measures – outer diameter: inner diameter: thickness (OD: ID: thickness) in the ratio 6:3:2, were adopted as standard dimensions in ring compression test method.

In the ring compression test, when a flat ring specimen is compressed between two flat platens, increasing friction results in an inward flow of the material, while decreasing friction results in an outward flow of it (Shahriairi et al., 2010). For a given percentage of height reduction during compression tests, the corresponding measurement of the internal diameter of the test specimen provides a quantitative knowledge of the magnitude of the prevailing friction factor at die-workpiece interface. At the total frictionless extreme, the ring would deform under compression radially outward similar to a solid disk, and this would be reflected in the resulting reduction in height and increase in inner diameter. However as the interfacial friction

increases, the inner radius eventually decreases as inner surface barrels inwards, and the friction factor approaches unity for perfectly “sticky” surfaces.

Male (1966) carried out a study in order to obtain variations in the friction factor of metals during compressive deformations at room temperature. His results showed that the friction factor tended to increase with an increasing deformation rate under dry conditions as well as with solid lubricants. He further showed that friction factor changes with temperature (Male 1973).

As the temperature is increased, he observed that friction factor may or may not increase which is dependent on the material of the ring. Jain and Bramely (1968) have made a detailed investigation of the relationship between friction factor and forging speed using ring compression test at a constant temperature of 1393 K. Pohlandt et al. (2004) has found a radical anisotropy during ring compression. Realistic values of radical anisotropy may cause an apparent friction factor and the assumption of isotropy may cause errors in the calculation of friction.

The present study has also been carried out to understand the frictional behaviour of Al-Zn-Mg alloys at various temperatures between room temperature 303K and 673K, by means of ring compression test with graphite as a lubricant. The friction factors “m” obtained at various temperatures were used as material constants for Dipper model modified for containerless backward extrusion.

2.7 ALUMINIUM - ZINC –MAGNESIUM ALLOYS

Among the light metals, although aluminum itself is soft and low in strength, it can be made stronger by giving proper combination of suitable alloying elements (Dennis, 1961). The properly treated aluminum alloy may possess strength level about thirty times that of pure aluminum. In terms of specific strength (the ratio of strength to density) a properly treated aluminum alloy is about three times that of normal low carbon steels (Donald, 1994). The binary Al-Zn system shown in Fig. 2.13 (Murray, 1983) has a favorable solubility (sloping solvus line) and zones and intermediate precipitate characteristics. The Al-Zn alloys fulfill a significant fraction of industry’s demand for the development of lightweight materials having high strength and

toughness characteristics (Emad M. Ahmed, 2014). But it is not a good age hardening system at room temperature; because the zinc atom is too mobile and the coarse equilibrium precipitate (Zn) forms at quite low temperatures by continuous and discontinuous precipitation.

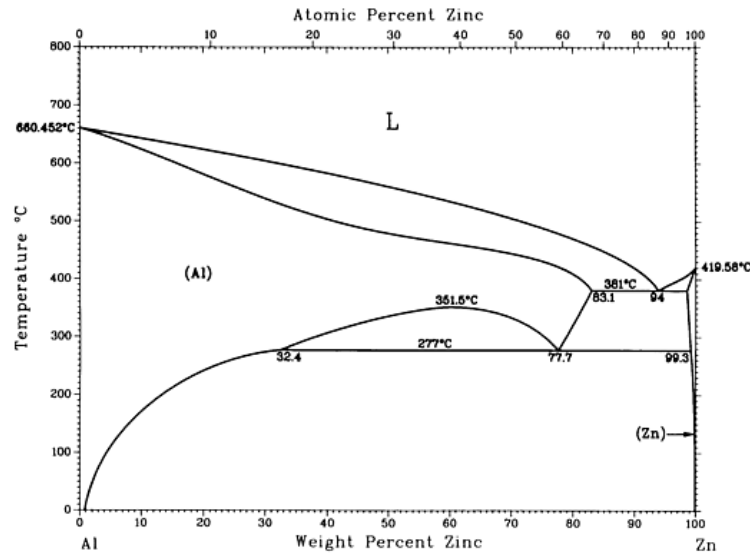


Fig. 2.13 Al-Zn phase diagram

On the other hand by adding Mg to Al-Zn alloys one obtains a good age hardening ternary alloy system in which zones and intermediate precipitates are formed leading towards the stable $MgZn_2$ compound. In this ternary system occurs the strongest and hardest aluminium alloy among all the alloys in the aluminium family. The Al-Zn-Mg alloy has gathered a wide acceptance in fabrication of light weight structures where a high strength to weight ratio is an important criteria for application. They are important aerospace alloys. Fabrications of various structures like bridge girders, road and railway transport systems etc are possible with this alloy. Forming of such alloys becomes important to produce useful shapes at low forces and surface finish (Varun Bhat et al., 2007).

These alloys differ from the other weldable aluminium alloys in that they age-harden significantly at room temperature. Moreover, the strength properties developed are relatively insensitive to cooling from higher temperatures and possess a wide range of temperature for solution treatment. Thus there is a considerable recovery of strength

after welding. The tensile strength of about 320 MPa are obtained without further heat treatment. The alloys containing copper (Al-Zn-Mg-Cu) attain the highest strength of all aluminium alloys, exceeding low carbon steel. They are widely used for aeronautical applications, especially in aeroplane wing structures (Marlaud et al., 2010), but the extrudability is very poor and the alloys are not weldable under normal conditions. Yield strengths may be as much as double compared to welded components made from the more commonly used Al-Mg and Al-Mg-Si alloys. At a lower strength, alloys containing 4.5 % Zn and 1 % Mg can be welded without losing their heat treated strength. This is possible because they age at room temperature in about one month after welding and the weld develops strength equal to that of a parent metal. Having heat treated strength of about 280 MPa and 15-20 % elongation; they are good alloys for on-site construction works.

The alloys can be used as both castings and wrought products, but because of the poor castability, the bulk is in the form of wrought products. Over the years, new alloys have been developed with increasing total solute content and varying ratios between the three main alloying elements (Zn, Mg and Cu), in order to reach very high levels of strength (Warner, 2006). High Zn: Mg produces the best strengths and response to heat treatment, together with the highest susceptibility to various types of corrosion (stress corrosion cracking, intergranular corrosion, exfoliating corrosion, etc.) (Varley, 1970, Zhao and Frankel, 2006, 2007 and Kuntz et al., 1997). The improvement in the resistance to stress corrosion cracking (SCC) has come through the control of both composition and heat treatment procedures. Thus they often need to be used in an over-aged state for better corrosion resistance at the cost of a somewhat lower strength (e.g. T7651 temper as compared to T651 peak-aged temper). With respect to composition, both tensile strength and susceptibility to cracking increase as the Zn+Mg content increases and it is necessary to seek a compromise while selecting an alloy for a particular application. Generally the Zn+Mg content should be less than 6% in order for a weldable alloy to have a satisfactory resistance to cracking, although the additional controls may be required. The maximum resistance to stress corrosion cracking occurs if this ratio is between 2.7 and 2.9. Small amount of copper and more particularly, silver have been shown to increase the

resistance to SCC but the addition of silver is considered too great a cost penalty for this range of alloys. Many compositions are now available, which contain zinc and magnesium together with smaller amounts of one or more of chromium, manganese and zirconium. These elements are mainly added to control the grain structure during fabrication and heat treatment (Polmear, 1995). Although very hard, the basic alloy is plagued by grain boundary weakness due to precipitate-free regions.

2.7.1 Al-Zn-Mg System

Compositions within Al-Zn-Mg system form important classes of heat treatable alloys and in the quaternary system with copper, yield highest strengths known for commercial aluminium alloys. In almost all cases, zinc is the major alloying addition. Age-hardening 7000 series alloys are based on precipitation in the Al-Zn-Mg system, in the composition range (wt. %) 3–7% zinc and 0.8–3% magnesium. Due to the high strength that is attained in the hardened state, the alloys are used in aerospace and automotive applications for highly stressed components, such as automobile bumpers. It may be formed in the annealed condition and subsequently heat treated. 7075 aluminum alloy offers good machinability when machined using single-point or multi spindle carbide tools on screw machines (Watkins and Kondic, 1963). The anodizing response rating for 7075 alloy is good using commercially available methods. The alloy can be both hard and clear-coat anodized.

These alloys form precipitates following the classical sequence leading from the solid solution to Guinier-Preston (GP) zones (at room temperature up to 393 K approximately), followed by the metastable precipitate η' and by the equilibrium phase η (Lendvai, 1996). More complicated sequences including vacancy rich clusters and several types of GP zones have been identified (Waterloo et al., 2000, Berg et al., 2001, Li et al., 2008) but are mostly important in alloys where little room temperature ageing is given before the artificial ageing begins. The equilibrium phase η has the hexagonal structure $MgZn_2$ ($a = 0.5221\text{nm}$, $c = 0.8567\text{nm}$) (Friauf, 1927, Laves et al., 1935, Komura, 1980). The widest applications of these alloys are in the aircraft industry where fracture-critical design concepts have provided the impetus for high toughness alloy development (Kutz, 2006).

The characteristics of ternary aluminium-zinc-magnesium alloys are influenced by the high solid solubility of both zinc and magnesium is shown in Fig. 2.14 and Fig. 2.15(Willey, 1973). In the ternary system, matrix compositions for invariant reactions are at such high zinc and magnesium levels that non-equilibrium melting is rarely encountered. For commercial compositions, solvus temperatures are generally low in comparison to those in other heat treatable alloy systems (Hatch, 1985).

In the solid state, aluminium can be in equilibrium with Mg_5Al_8 , $Mg_3Al_3Zn_2$, $MgZn_2$, $MgZn_{11}$, $ZnAl$ and Zn . Four ternary aluminium-zinc-magnesium alloy groups can be distinguished (Mondolfo, 1976).

- (i) Alloys in which Mg_5Al_8 predominates. These alloys have a Mg:Zn ratio of 6:1 or higher
- (ii) Alloys in which $Mg_3Al_3Zn_2$ predominates. These alloys represent a wide range of compositions, from a Mg:Zn ratio of 6:1 to 3:7
- (iii) Alloys in which $MgZn_2$ is the precipitating phase atleast at the lower temperatures. The exact range of these alloys is not ascertained
- (iv) In alloys with Mg:Zn ratio is less than 1:10, $MgZn_{11}$ should be the precipitating phase

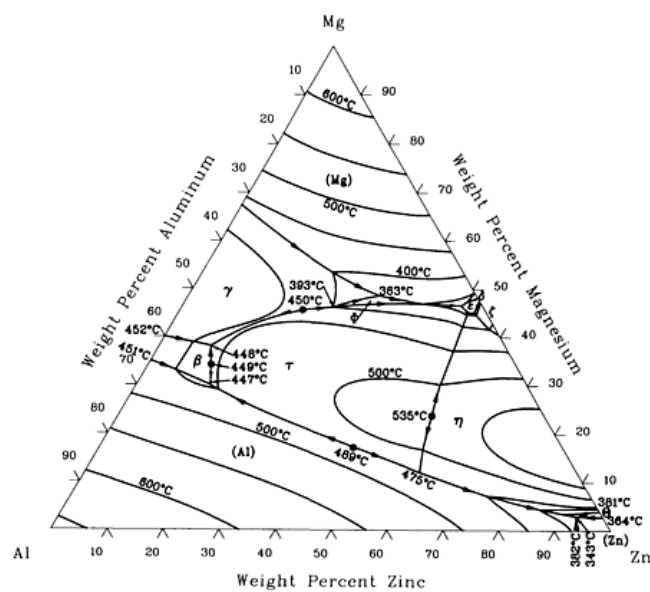


Fig. 2.14 Al-Mg-Zn liquidus projection

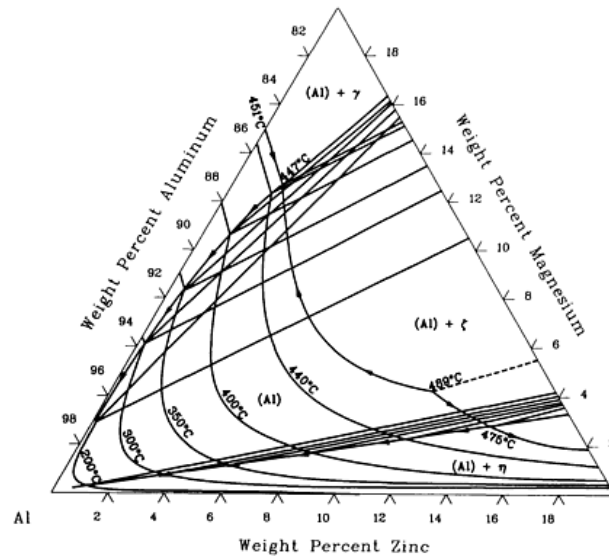


Fig. 2.15 Al-Mg-Zn solvus projection

The limits given for the ranges are only approximate and refer to the free magnesium and zinc, not necessarily total. The alloys in range 1 behave approximately as the binary aluminium-zinc alloys. The group of alloys in which Mg_2Zn_{11} should be the precipitating phase, require zinc content well above 30% and do not have properties that will make them commercially attractive since they tend to enhance the stress corrosion susceptibility. At high zinc contents, Mg_2Zn_{11} transforms to $MgZn_2$ in a four phase reaction at 638 K (Kammer, 1999). The third group of alloys in which $MgZn_2$ is the precipitating phase have been proved the most suitable for commercial purposes and are the most investigated ones. In many of these alloys $MgZn_2$ precipitates at lower temperatures and ternary $Mg_3Al_3Zn_2$ precipitates at higher temperatures. According to the phase diagram of the Al-Zn-Mg system the presence of zinc and magnesium in it at a (Mg/Zn) ratio of the alloys chosen for the study may make it susceptible to precipitate $MgZn_2$.

Even though a number of papers have investigated the composition of precipitates in various 7000 series Al alloys, no systematic study on stress analysis of containerless backward extrusion of Al-Zn-Mg alloys as a function of alloy composition is available.

The following equation is used for computing the coefficient of friction (Lange, 1985).

$$\mu = \frac{1}{2}(\mu_1 + 0.5) \quad (2.12)$$

The frictional forces are calculated based on an average cylinder with radius $(d_1+d_2)/2$

The force equilibrium on a ring element in zone 2 gives

$$\left[-\sigma_{z,2} + \left(\sigma_{z,2} + d\sigma_{z,2} \right) \right] \frac{\pi}{4} (d_0^2 - d_i^2) = 2\mu\sigma_{f,2} dz \frac{d_i + s}{2} 2\pi \quad (2.13)$$

$$d\sigma_{z,2}s = 2\mu\sigma_{f,2}dz \quad (2.14)$$

Integrating with boundary condition $\sigma_{z,2} = 0$ at $z = b$, we have

$$\sigma_{z,2} = -\frac{2\mu\sigma_{f,2}}{s} (b - z) \quad (2.15)$$

The average normal stress can be calculated for the area $A_2 = 2[(d_i + s)/2] \pi b$ as

$$\sigma_{z,2,m} = -\mu\sigma_{f,2} \frac{b}{s} \quad (2.16)$$

According to the Tresca flow conditions,

$$\sigma_{r,2,m} = \sigma_{z,2,m} - \sigma_{f,2} = -\sigma_{f,2} \left(1 + \mu \frac{b}{s} \right) \quad (2.17)$$

For zone 1 – axial upsetting – the force equilibrium equation on the ring element is

$$\left[-\sigma_{r,1} + \left(\sigma_{r,1} + d\sigma_{r,1} \right) \right] \pi r b = 2\mu_1 \sigma_{f,1} \pi r dr \quad (2.18)$$

$$d\sigma_{r,1} b = 2\mu_1 \sigma_{f,1} dr \quad (2.19)$$

Using the boundary condition $\sigma_{r,1} = \sigma_{r,2,m}$ for $r = d_1/2$ (transposition of the average radial pressure from zone 2 to zone 1), we have

$$\sigma_{r,1} = -\frac{\mu_1 \sigma_{f,1}}{b} \left(\frac{d_i}{2} - r \right) + \sigma_{r,2,m} \quad (2.20)$$

The average radial stress over the area $\pi d_1^2/4$ is given by

$$\sigma_{r,1,m} = -\frac{1}{3} \mu_1 \sigma_{f,1} \frac{d_i}{b} + \sigma_{r,2,m} \quad (2.21)$$

Substituting for $\sigma_{r,2,m}$, we obtain the average radial stress as

$$\sigma_{r,m} = \sigma_{r,1,m} + \sigma_{r,2,m} = -\frac{1}{3} \mu_1 \sigma_{f,1} \frac{d_i}{b} - \sigma_{f,2} \left(1 + \mu \frac{b}{s} \right) \quad (2.22)$$

Applying the Tresca flow condition, the axial stress on the punch is

$$\sigma_{z,m} = \sigma_{r,m} - \sigma_{f,1} \quad (2.23)$$

$$\sigma_{z,m} = -\sigma_{f,1} \left(1 + \frac{1}{3} \mu_1 \frac{d_i}{b} \right) - \sigma_{f,2} \left(1 + \mu \frac{b}{s} \right) = P_p \quad (2.24)$$

In the present study of containerless backward extrusion, the second term contained in the backward extrusion (which accounts for radial upsetting) can be ignored by assuming that in this low strain process, material to material shearing in this second zone (in the vicinity of punch corner face) is negligible.

Therefore the punch pressure for containerless backward extrusion is,

$$P_p = \sigma_{fm} \left(1 + \frac{1}{3} \mu \frac{d_i}{b} \right) \quad (2.25)$$

2.9 SIMULATION OF THE METAL FORMING PROCESSES

The finite element method (FEM) is a numerical method, used for the accurate solution of complex engineering problem. It was first developed in 1956 for the analysis of aircraft structural problem. Thereafter within decades, the potential of the method for the solution of different types of applied science and engineering problem were recognized. Over the years, the finite element technique has been so well established that today it is considered to be one of the best methods for solving a wide variety of practical problems and stress analysis efficiently.

2.9.1 Concept of FEM

In the finite element analysis, the continuum is divided into a finite number of elements, having finite dimensions and reducing the continuum having infinite degrees of freedom to finite degree of freedom. The elements are interconnected at joints, called nodes or nodal points. An important ingredient of the FEA is the behavior of the individual elements. The function ϕ which might represent any of the several physical quantities varies smoothly in an actual structure, within each element ϕ is a smooth function called an interpolating polynomial. The degree of interpolation function depends on the number of nodes in the element and the order of differential equation being solved. The equations over all the elements of collection are connected by the continuity of primary variables.

The boundary conditions are imposed, and then the connected sets of equations are solved.

2.9.2 Steps Involved in the Finite Element Analysis of a Typical Problem

The following are the steps involved:

- 1) Discretisation of a given domain into a collection of prescribed finite elements
 - (i) Construct the nodes and elements
 - (ii) Number the nodes and elements
 - (iii) Generate the geometric properties (e.g. coordinates and cross sectional areas) needed for the problem.

- 2) Derivation of element equations for all typical elements in the mesh.
 - (i) Construct the variational formulation of the given differential equation over the typical element.
 - (ii) Assume that a typical dependent variable is of the form $u = \sum_I u_I \phi_I$ and substitute it into the step 2a to obtain the elemental equations in the form $[K^e]\{u^e\} = \{F^e\}$
 - (iii) Derive element interpolation functions N_I and compute the element matrices

- 3) Assembly of the element equations to obtain the equations of the whole problem
 - (i) Identify the inter element continuity conditions among the primary variables (Relationship between the total degrees of freedom and global degrees of freedom connectivity of elements) by relating the element nodes to global nodes
 - (ii) Identify the equilibrium conditions among the secondary variables.
 - (iii) Assemble the element equations using steps 3a and 3b

- 4) Apply the boundary condition of the problem

- 5) Solution of the assembled equations

- 6) Post processing of the results
 - (i) Complete the gradient of the solution and other desired quantities from the primary degree of freedom. Compute in step 5 mentioned above.

- 7) Represent the result in tabular or graphical form

2.9.3 Advantages and Limitations of FEM

The main advantage of this analysis is those physical problems that were so far intractable and complex for any closed bound solutions can be analyzed by this method. Other advantages are:

- (i) The method can efficiently be applied to irregular geometry.
- (ii) It can take care of any type of boundary.

(iii) Materials anisotropy and non-homogeneity can be treated without much difficulty.

(iv) Any type of loading can be handled.

(v) Though the solution obtained by FEM is at discrete node points, it can be extended to all other locations of the body.

FEM can also be employed for non-engineering applications

The major limitations of FEM are:

(i) Approximations used in the development of element stiffness.

(ii) Aspect ratio may affect the final results

2.9.4 The General Purpose FEM Packages

The rapid advances made in computer hardware and software leads to significant developments in FEA software. Finite element programming has emerged as specialized discipline, which require knowledge and experience in the diverse area such as foundation of mechanics, numerical analysis and computational skills in the area of software technology, programming techniques, data structures, database management and computer graphics (Alton and Gegel, 1983).

The following are the features of FEM

(i) Input: Physical modeling, geometry, material, loading and boundary conditions

(ii) Library: Elements, generation of equilibrium equations

(iii) Assembly and solution: construction and solution of structural system

(iv) Output: Display of predicted displacement, stress, strain, temperature distributions and other desired output parameters.

2.9.5 General Purpose Programs

The following are the main purpose programmes:

(i) ANSYS: Engineering analysis system (developed by Swanson analysis system).

- (ii) SAP: Structural analysis program (developed by E.L.Wilson, university of California, USA).
- (iii) NASTRAN: NASA (US National Aeronautics and space administration) structural analysis NONSAP: Nonlinear structural analysis program
- (iv) ALPID, ELFEN : FEA softwares for metal forming plasticity
- (v) LS Dyna: Livermore Software Dynamic non-linear analysis

2.9.6 Engineering Application of FEM

In particular, the FEM can be systematically programmed to accommodate complex and difficult problems such as non-homogeneous materials, on-linear stress-strain behavior and complicated boundary conditions. The FEM is applied to wide range of boundary value problems in engineering. According to Ansys 9.0 theory manual(1994) , in boundary value problems, a solution is sought in the region of the body, while on the boundaries or edges of the region, values of dependent variables or their derivatives are prescribed (Krishnamoorthy, 1994, William and Robert, 1993).

There are three major types of boundary value problems:

- 1) Equilibrium or steady state problems
- 2) Eigen value problems.
- 3) Propagation or transient problems.

Majority of applications is in solid mechanics. In an equilibrium problem, we need to find the steady state displacement or stress distribution if it is in solid mechanics problem, temperature or heat flux distribution if it is a heat transfer problem and pressure or velocity distribution if it is a fluid mechanics problem.

In Eigen value problem, time will not appear explicitly. They may be considered as extensions of equilibrium problem in which critical values of certain parameters are to be determined in addition to the corresponding steady state configurations. In these problems we have to find the natural frequencies or buckling loads and mode shapes if it is a solid mechanics or structural problem, stability of laminar flow if it is a fluid mechanics problem and resonance characteristics, if it is an electric circuit problem.

Propagation or transient problems are time dependent problems. This type of problem arises, for example, whenever we are interested in finding the response of a body under time varying loads, in the area of solid mechanics and sudden heating or cooling in the field of heat transfer.

FEA can also be employed for non engineering applications, such as in medical researches on the simulation of a particular organ of a human body. For example we can determine the fatigue produced on the valves of the heart due to the pumping action (Surendra, 1985, Zienkiewicz, 1993).

CHAPTER 3

EXPERIMENTAL PROCEDURES

3.1 MATERIAL

3.1.1 Alloys

Three varieties of Al-Zn-Mg alloys, different in composition were selected for the study. Nominal composition of these three alloys are presented in Table 3.1

Table 3.1 Alloys and their nominal composition used for the study

Alloy	Al (Wt. %)	Zn (Wt. %)	Mg (Wt. %)
Al-5Zn-1Mg	94	5	1
Al-10Zn-1Mg	89	10	1
Al-15Zn-1Mg	84	15	1

3.1.2 Alloy Preparation

3.1.2.1 Melting

Melting of the alloy was carried out in electric resistance furnace with automatic temperature controller which had allowed the variation of $\pm 5^\circ$ C. Pure aluminium (99.97 %) pieces were charged into silicon carbide crucible along with appropriate addition of zinc granules. The charge was melted and held at a temperature of 1023 K. The melt was degassed with hexachloroethylene tablets. Magnesium in the pure elemental form was added to the melt just before pouring. In order to avoid the loss by flaring magnesium was packed in aluminium foil with a few pieces of aluminium. The package was immersed into the superheated melt using graphite pusher rod. No flux was used to cover the melt. The melt was mildly stirred; surface dross is skimmed off and immediately poured into the mold. In order to get homogeneous composition, the solidified alloy was remelted and poured into an appropriate mold.

3.1.2.2 Pouring

Alloy melt was poured into a mild steel die. The die was not preheated and mold surfaces were not coated. The dimensions of the mold cavity are presented in Fig.3.1. The cast billets were homogenized at 623 K for 3 hours in the electric resistance furnace.

3.2 Sample Preparation

From the cast cylindrical billets following types of samples were prepared:

- (i) Axisymmetric compression test samples – The schematic diagram of this sample is shown in Fig.3.2. h_o/d_o ratio for the samples were fixed at 1.5 where $h_o = 37.5$ mm and $d_o = 25$ mm.
- (ii) Ring compression test samples – The schematic diagram of this sample is shown in Fig.3.3. The proportion ($d_o: d_i: h_o$) was fixed at 6: 3: 2 where $d_o = 24$ mm, $d_i = 12$ mm and $h_o = 8$ mm respectively.
- (iii) Cylindrical billet samples for containerless backward extrusion experiments – The schematic diagram of these samples are shown in Fig. 3.4.

In the present investigation experiments were carried out in homogenized condition of the sample. It is important to note that they were not precipitation hardened. Alloys will contain two phases viz aluminium substitutional solid solution and $MgZn_2$ [ASM International, 1999]

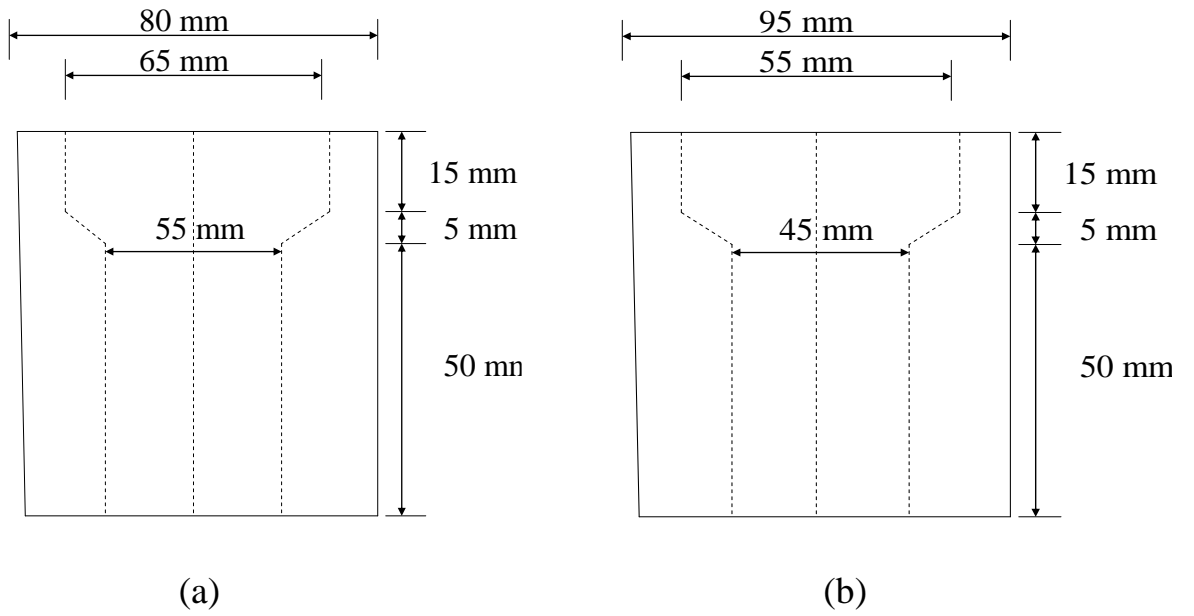
3.3 Characterization

3.3.1 Chemical composition

Samples were taken from top and bottom of each cylindrical cast ingots and chemically analyzed using optical emission spectroscope. The chemical composition of the material is presented in Table 3.2. From the various values presented in Table 3.2 it can be seen that all the ingots meet the specified requirement and can be taken for further investigation.

Table 3.2 Bulk chemical analysis of Al-Zn-Mg alloys using an Optical Emission Spectrometry

Alloy	Si (%)	Fe (%)	Cu (%)	Mn (%)	Mg (%)	Zn (%)	Al (%)
Al-5Zn-1Mg	0.86	0.238	0.016	0.56	1.46	5.72	91.146
Al-10Zn-1Mg	0.69	0.189	0.012	0.53	1.13	10.14	87.309
Al-15Zn-1Mg	0.74	0.228	0.01	0.5	1.42	14.4	82.702



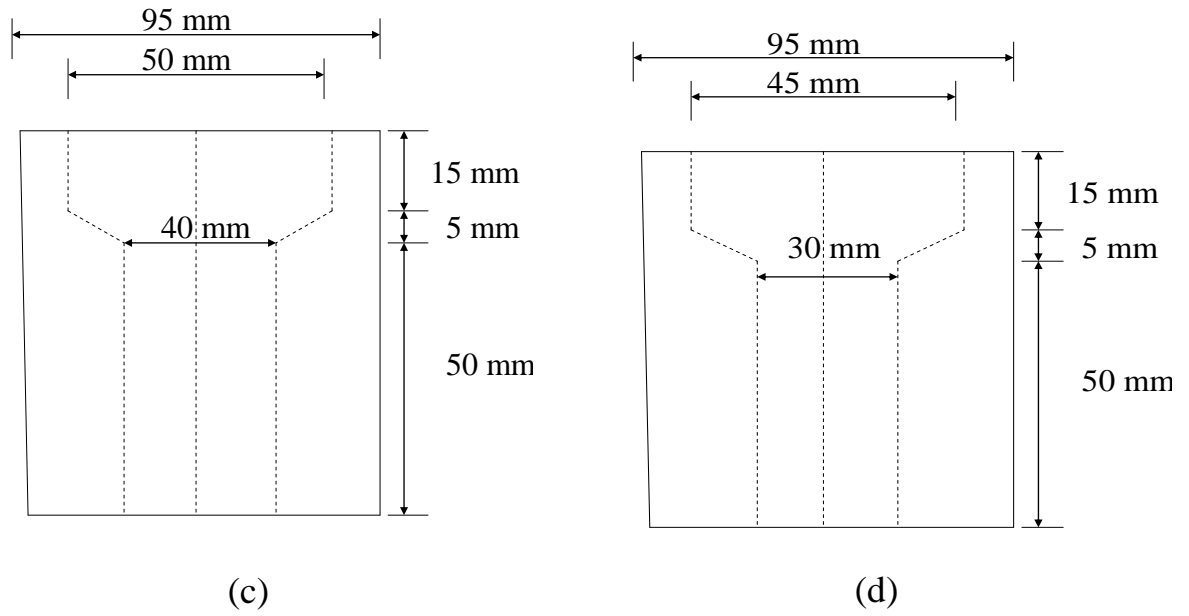


Fig. 3.1 The dimensions of mold cavity used to produce billets of diameter

(a) 50 mm (b) 40 mm (c) 35 and 30 mm (d) 27 and 25 mm.

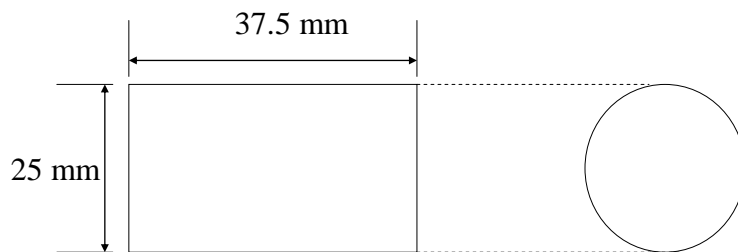


Fig.3.2 Schematic diagram of compression testing sample

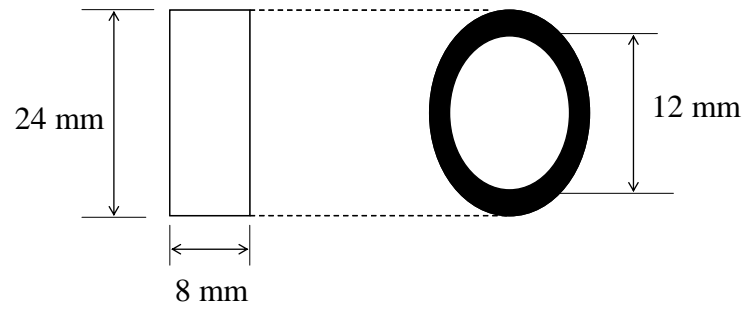
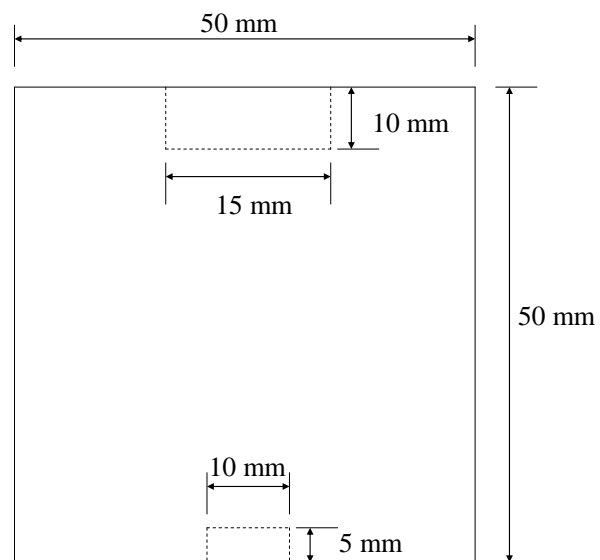
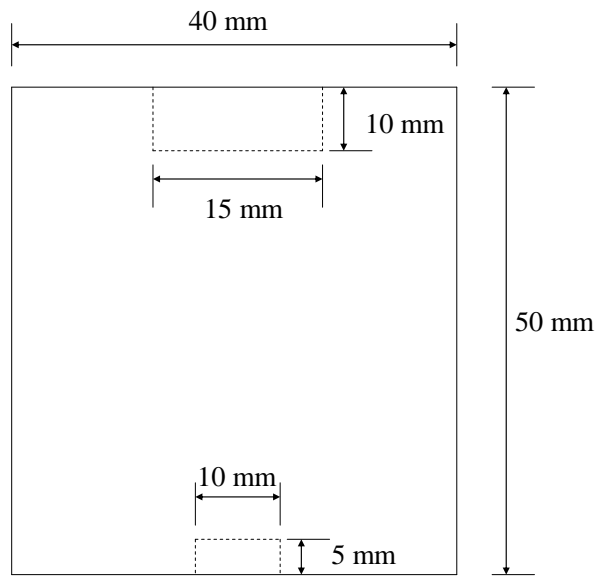


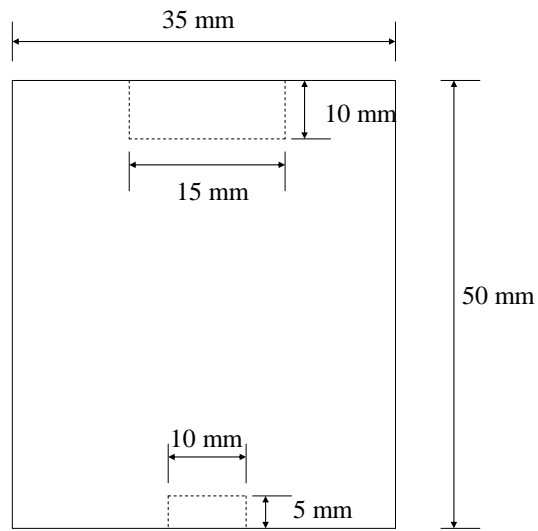
Fig.3.3 Schematic diagram of ring compression testing sample



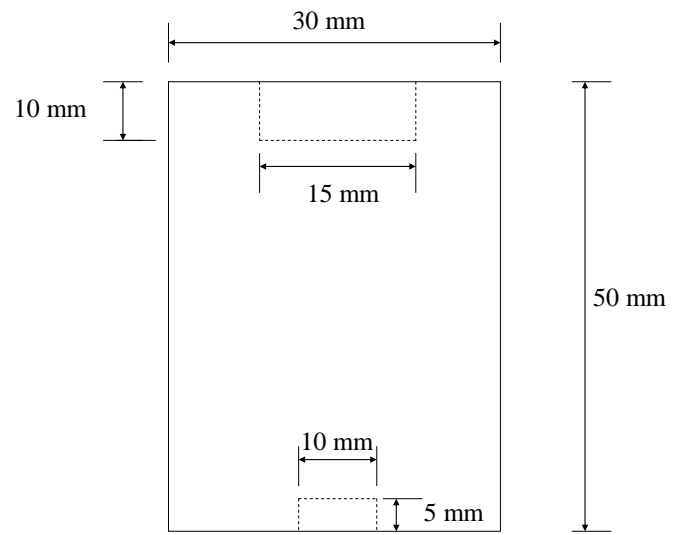
(a)



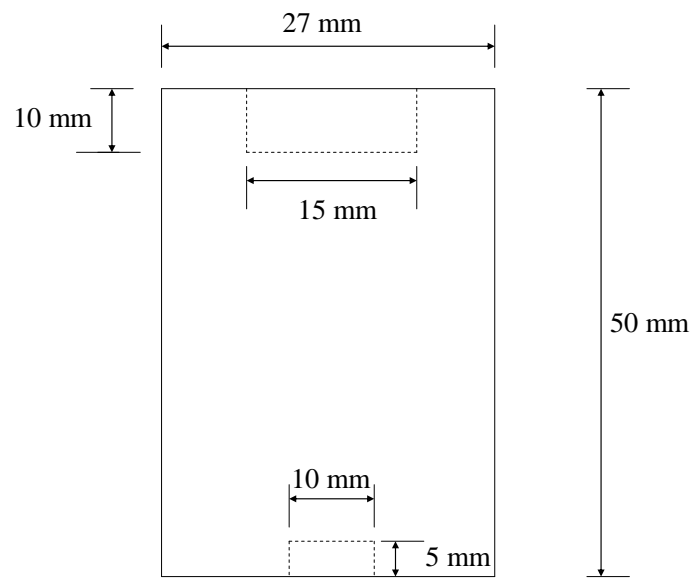
(b)



(c)



(d)



(e)

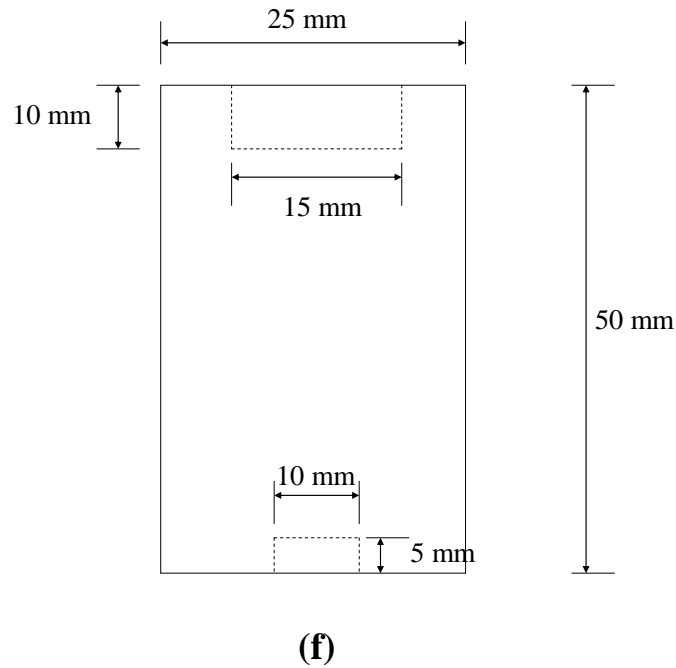


Fig. 3.4 Schematic diagram of cylindrical billet samples with diameters (a) 50 mm (b) 40 mm (c) 35 mm (d) 30 mm (e) 27 mm and (f) 25 mm for containerless backward extrusion experiments

3.3.2 Microstructural analysis

Standard metallographic technique was resorted to polish the sample for microstructural analysis. The polished samples were etched with Keller's reagent* and their microstructures were studied under scanning electron microscope (SEM Jeol 6380)

3.3.3 Hardness measurement

Vickers hardness machine was used to find out the hardness of the material: it was measured on the polished surface of the samples, both in transverse and vertical direction, with 5 Kg load. Average of minimum five readings were taken in each field.

* 5% HNO₃, 5% HCl, 3% HF and 87% H₂O

3.4 Axisymmetric Compression Testing

3.4.1 Flow stress determination

The compression test is carried out using 40 T universal testing machine (Fuel Instruments & Engineers Pvt Ltd. Model – UTN/E40). The photograph of compression test assembly is shown in Fig. 3.5. The test was carried out in the range of temperature of 303 - 673 K in steps of 100 K. Samples were lubricated with graphite powder and heated in an electric resistance furnace. All the heated samples were tested with a constant ram speed of 3.3×10^{-4} m/s. Experiments were carried out in the following steps:

- (i) Extend of compression at different loads were found out for all the categories of the samples at different temperatures
- (ii) From the above experimental data force – stroke diagrams were generated.
- (iii) Force – stroke diagrams were converted to engineering stress - strain curves. Yield strength for the materials at different temperatures was determined by 0.1% offset method.
- (iv) From the stress – strain diagrams true stress – true strain diagrams were derived and plotted on log – log scale.
- (v) Finally these flow curves were fitted into well known Hollomon equation, i.e.

$$\sigma = K\varepsilon^n$$

Where σ = true stress, K = material strength coefficient and n denotes the strain hardening exponent (Zone-Ching Lina et al., 2009). K and n were determined for various temperatures in the range of 303 – 673 K.

- (vi) Using these values plots were drawn which show the variation of K and n with respect to temperature

3.5 Ring Compression Test

Schematic diagram of the sample for ring compression test is shown in Fig.3.3. The test was carried out using 40 T Universal testing machine (Fuel Instruments & Engineers Pvt Ltd. Model – UTN/E40). Fig. 3.6 shows the photographs of ring compression test assembly. Fig. 3.7 shows the schematic diagrams of the cut half of rings before and after carrying out the ring compression test. The deformation of ring specimens for zero friction, low friction, high friction and sticking friction are shown in Fig. 3.8 (Srinivasan, 2005; John Rumierz, 1992; Altan et al., 1983; Schey, 1983; Cockcroft and Latham, 1968; Dieter, 2003). The test is carried out at a constant load of 11000 Kgf and reduction in height ($t - t_0$) and reduction in internal diameter ($d - d_0$) was noted down. Using the calibration chart (Fig.3.9) as developed by Male and Cockcroft (1964-65) friction factor (m) for various temperatures in the range of 303 – 673 K were determined. A plot of the friction factor v/s temperature was developed.



Fig. 3.5 Photograph of compression test assembly

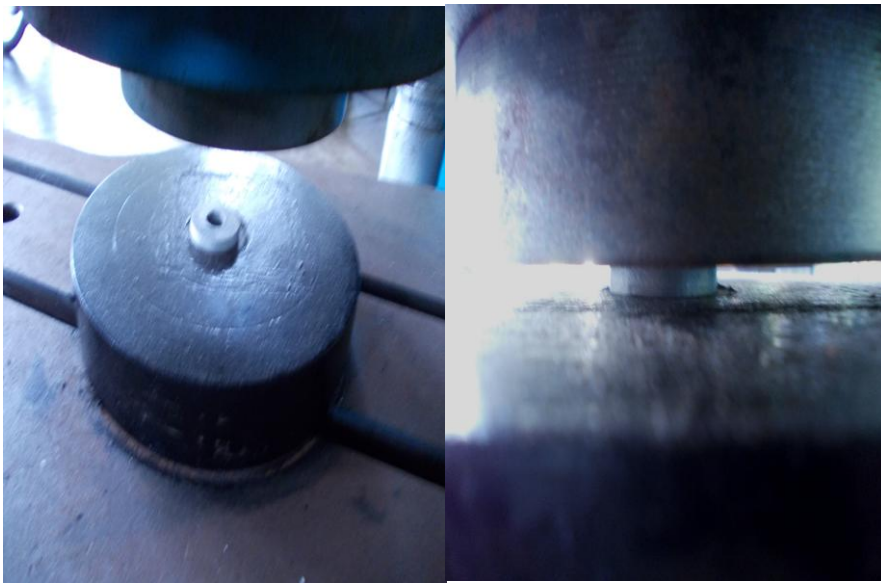


Fig. 3.6 Photographs of ring compression test assembly

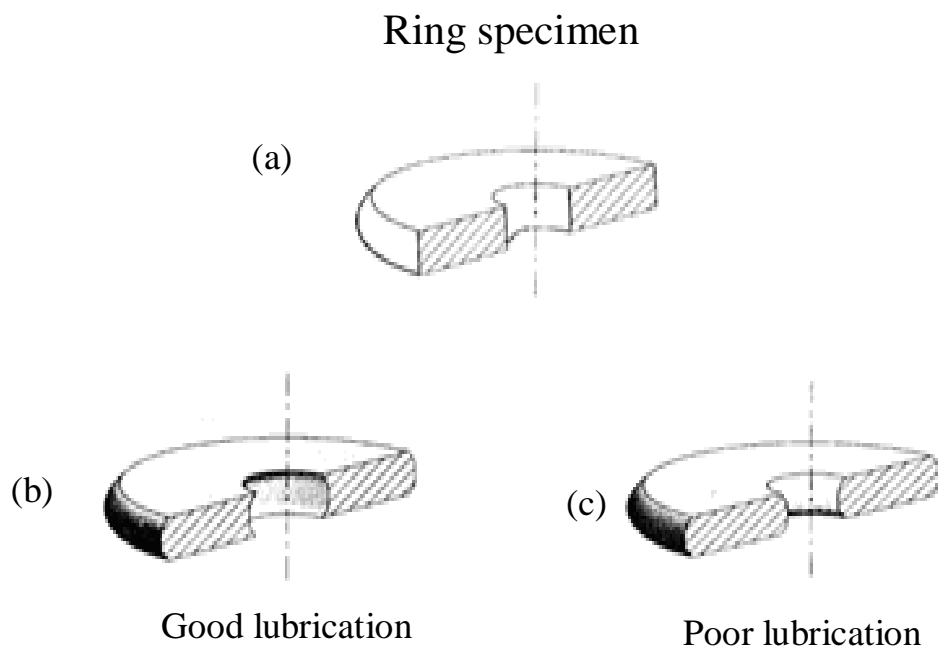


Fig. 3.7 Ring compression test specimen (a) before compression (b) after compression with low friction and (c) after compression with high friction

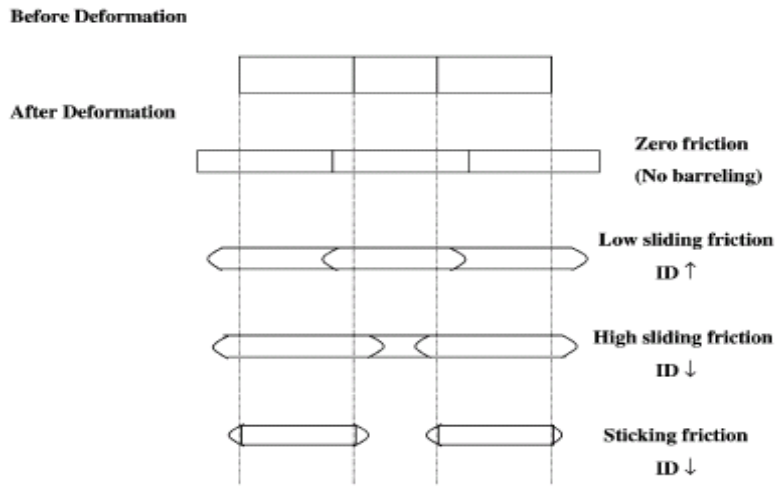


Fig.3.8 Types of ring deformations after compression

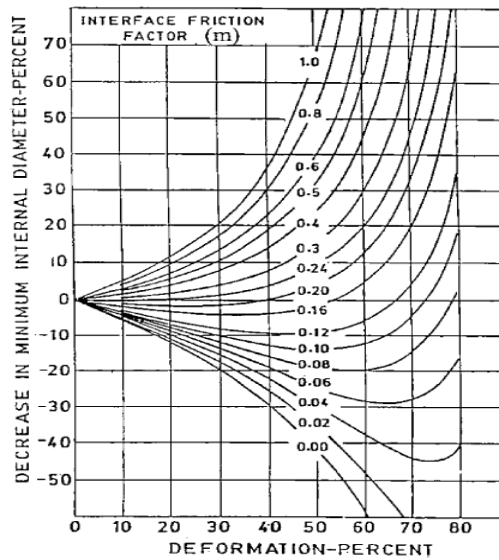


Fig.3.9 Calibration chart to determine friction factor (m)

3.6 Containerless Backward Extrusion

3.6.1 Design of punch and base plate

It is important to design punch and base plate properly. Otherwise, stripping the pallet will be difficult and base plate may slip making it difficult to produce the pallet. The design details of the punch are shown in the schematic diagram presented in the Fig.3.10. It should be noted that a small taper ($\approx 1^\circ$) is provided on the stem. The punch nose is provided with the taper of 45° . While the former helps in withdrawal of the punch the latter helps in the penetration of the punch. Further, it should be noted that the stripper which is necessary in the case where the work piece stick to the punch is not there in the present set up. Fig.3.11 shows the schematic diagram of the base plate which includes a projection (5 mm \times 10 mm \varnothing) at the centre. The projection is necessary to hold the billet from slipping.

3.6.2 Die materials

AISI M2 HSS was used for making the punch and dies. The sample of the material was analyzed using optical emission spectroscopy and its chemical composition is presented in the Table.3.3. The billet was rough machined, close to the dimensions of die and punch and given the appropriate heat treatment. The time – temperature diagram of heat treatment is depicted in Fig. 3.12. The heat treatment in vacuum was carried out by Bhat Metals Research Pvt. Ltd. Bangalore. The final hardness after the heat treatment was determined and found to be $R_C 62$ which is appropriate for present experimental work. Having ensured adequate hardness the final fine machining was carried out to arrive at the correct dimensions of the die and punch.

3.6.3 Die assembly

The die and punches were fitted on to the 40 T universal testing machine, as shown in Fig.3.13. The photograph of the universal testing machine used for present investigation is presented in Fig.3.14. A cylindrical hole of 5 mm depth and 10 mm in diameter was drilled at bottom of each billet sample to fit into the projection of the

base plate. Another cylindrical hole of 10 mm depth and 15 mm diameter is drilled on the top of the billet to guide the punch during the extrusion process.

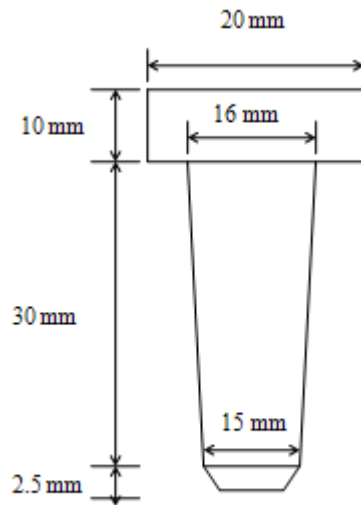


Fig.3.10 Schematic diagram of punch used for containerless backward extrusion

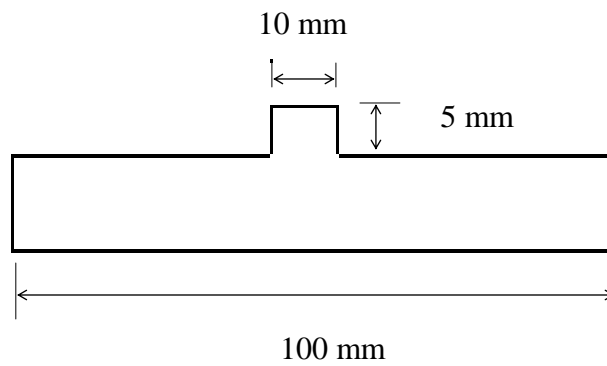


Fig.3.11 Schematic diagram of base plate

Table 3.3 Chemical analysis of AISI M2 HSS used for making the punch and base plate

Alloy	C (%)	Si (%)	Mn (%)	Cr (%)	W (%)	V (%)	Mo (%)
AISI M2 HSS	0.8	0.4	0.4	4.3	6.5	2	5

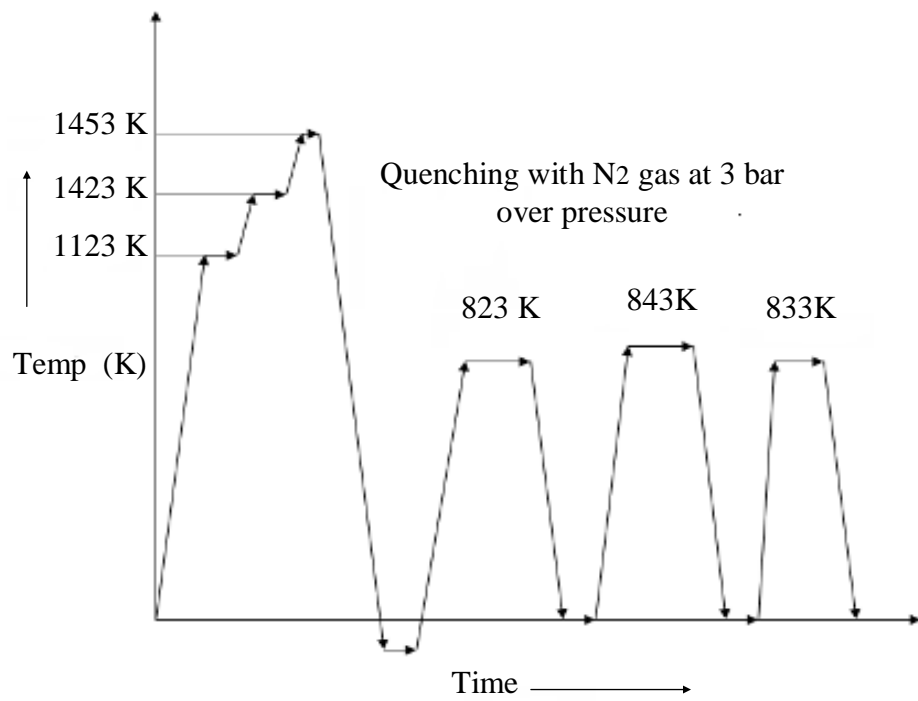
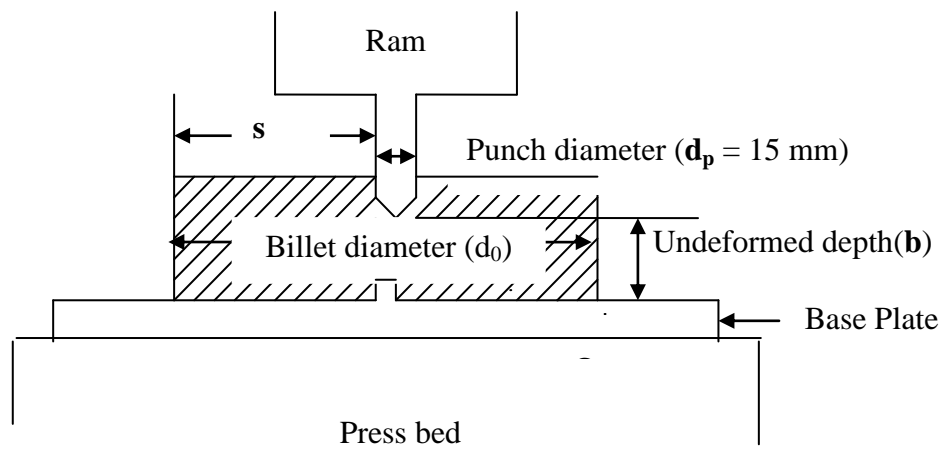


Fig.3.12 Heat treatment cycle of AISI M2 HSS for attaining a hardness of 61/62 R_c



(a)



(b)

Fig.3.13 (a) Schematic diagram and (b) photograph of containerless backward extrusion die assembly



Fig.3.14 Photograph of the universal testing machine used for containerless backward extrusion

3.6.4 Preparation of billet specimens

From the alloy ingots billet samples of various diameters i.e. 25, 27, 30, 35, 40 and 50 mm and height of 50 mm each were machined. The photograph of a billet sample before and after machining is shown in Fig. 3.15.

3.6.5 Testing

The containerless backward extrusion test is carried out using 40 T universal testing machine with ram velocity of 3.3×10^{-4} m/s. These billet samples were coated with graphite and heated to various temperatures from 303 to 623 K in temperature controlled electric resistance furnace. Containerless extrusion is carried out varying the load and measuring the stroke from which force stroke diagrams were generated. Punch pressure or stress is equal to the ratio of punch load to the cross sectional area of the punch.



Fig.3.15 Photograph of a billet with 40 mm diameter and 50 mm height before and after machining

CHAPTER 4

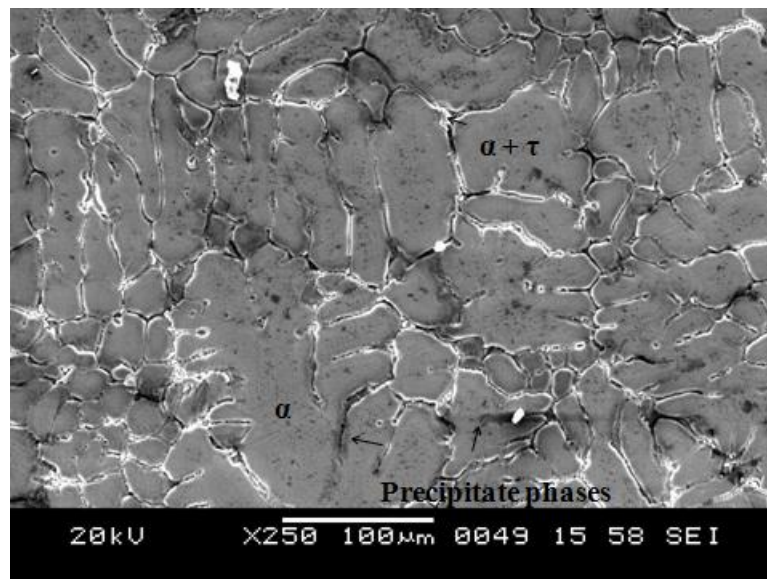
RESULTS

The experimental results are presented in six sections in this chapter.

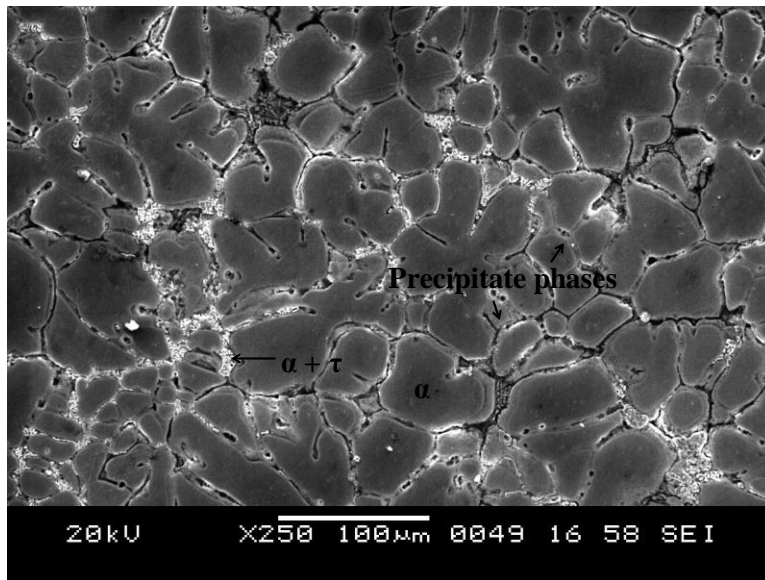
4.1 MICROSTRUCTURAL CHARACTERISTICS

Scanning electron microscopy was utilized to study microstructures and was examined for dendritic morphology and uniformity. After etching, the microstructures of the samples were clearly observed and they are presented in Figs. 4.1 (a to c) and 4.2 (a to c).

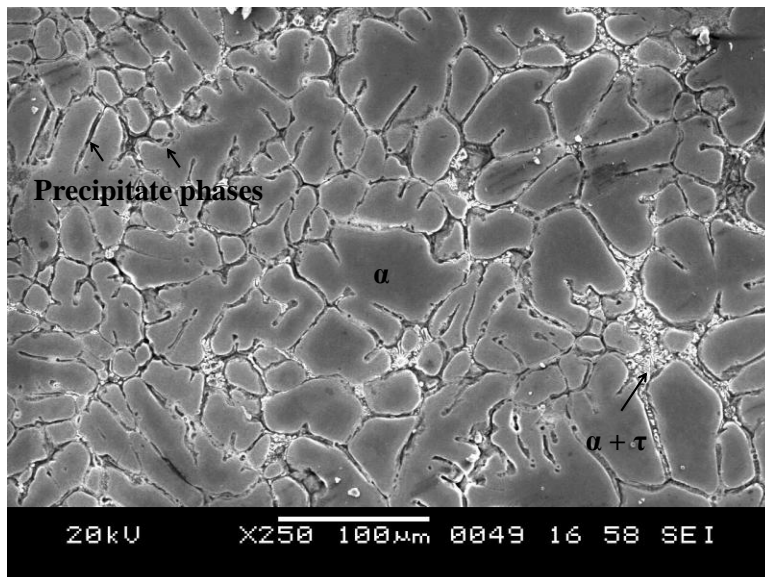
The microstructure of as-cast Al-Zn-Mg alloy after homogenization and before containerless backward extrusion consisted of dendrites of α -Al phase with ($\alpha+\tau$) eutectic in inter dendritic regions. This structure was obtained from the billet which has been cooled in a mould made up of mild steel to obtain equi-axed network structure. The microstructure consists of particles of several intermetallic compounds formed by combinations of the alloying elements in this alloy. Some of these compounds are soluble while others have slight or partial solubility.



(a) Al-5Zn-1Mg



(b) Al-10Zn-1Mg

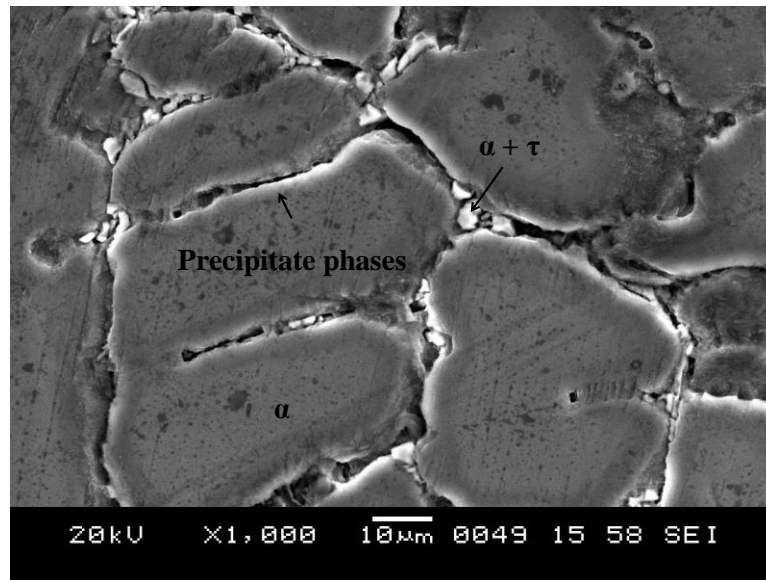


(c) Al-15Zn-1Mg

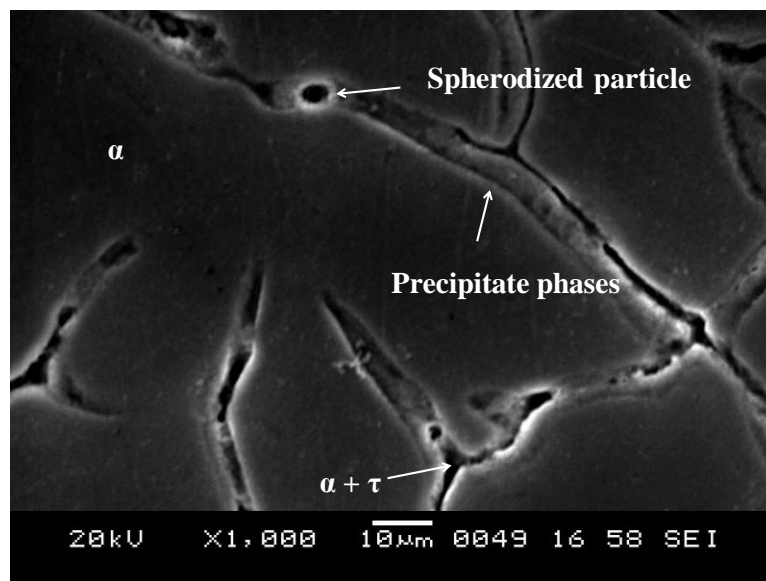
Fig. 4.1 Low magnification scanning electron micrograph of as-cast and homogenized (a) Al-5Zn-1Mg (b) Al-10Zn-1Mg (c) Al-15Zn-1Mg alloys indicating microstructures that consist mainly α -Al phase with ($\alpha + \tau$) eutectic in inter dendritic regions

The fine precipitates distributed were identified as hexagonal $MgZn_2$ η phase by many researchers. It was found to have various orientation relationships to the Al (Zhang et al., 2010).

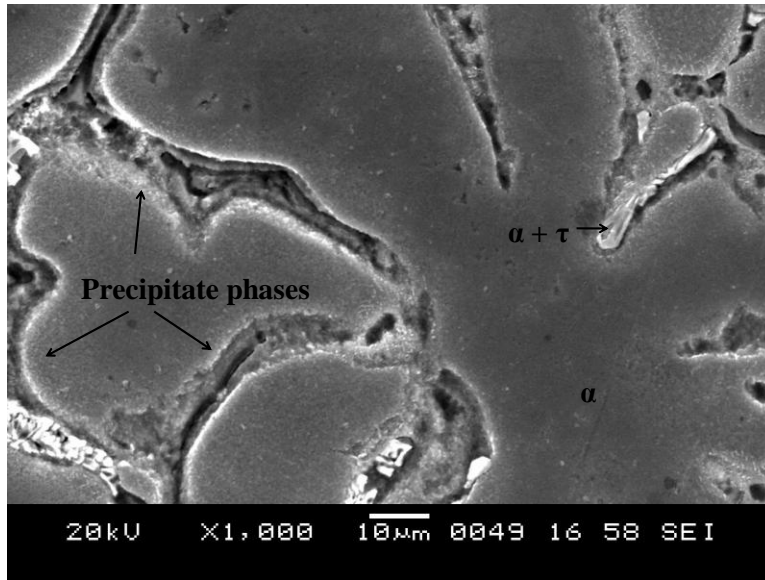
In as-cast condition, this alloy contains precipitate phases along the grain boundaries and near the grain boundary as shown in Fig. 4.2 (a to c) which is in agreement with the work of Alvarez et al. (2005)



(a) Al-5Zn-1Mg



(b) Al-10Zn-1Mg



(c) Al-15Zn-1Mg

Fig. 4.2 Higher magnification scanning electron micrograph of as-cast and homogenized (a) Al-5Zn-1Mg (b) Al-10Zn-1Mg (c) Al-15Zn-1Mg alloys which contains many precipitate phases along the grain boundary

4.2 VICKERS HARDNESS VALUES

Results of Vickers hardness measurement on cast and annealed samples are presented in Table 4.1. From the values presented in the Table it can be observed that hardness of Al-Zn-Mg alloys fall in the range of 150 – 180 VHN. Further, it is noted that hardness of the material increases substantially as Zn content of the alloy increases.

Table 4.1 Vickers hardness data of Al-Zn-Mg alloys in the as-cast and homogenized condition

Alloy	Vickers hardness (VHN)
Al-5Zn-1Mg	152
Al-10Zn-1Mg	170
Al-15Zn-1Mg	179

4.3 AXISYMMETRIC COMPRESSION TEST

Results of the compression test carried out in the temperature range of 303 – 673 K are presented in the form of three profiles:

- (i) Force – Stroke diagrams (Fig. 4.3)
- (ii) Engineering Stress – Engineering Strain diagrams (Fig. 4.4)
- (iii) Log –log plot of True Stress – True Strain diagrams (Fig. 4.5)

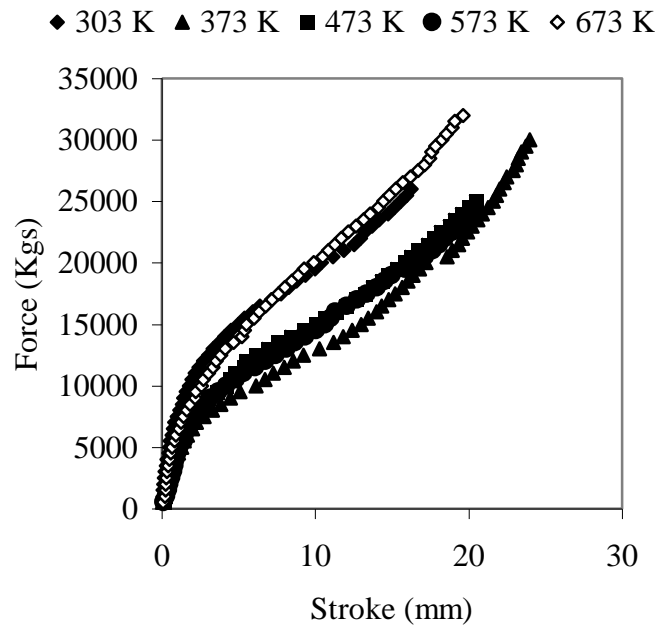
Using above profile following material characteristics was determined:

- (i) Yield strength
- (ii) Strength coefficient and
- (iii) Strain hardening exponent

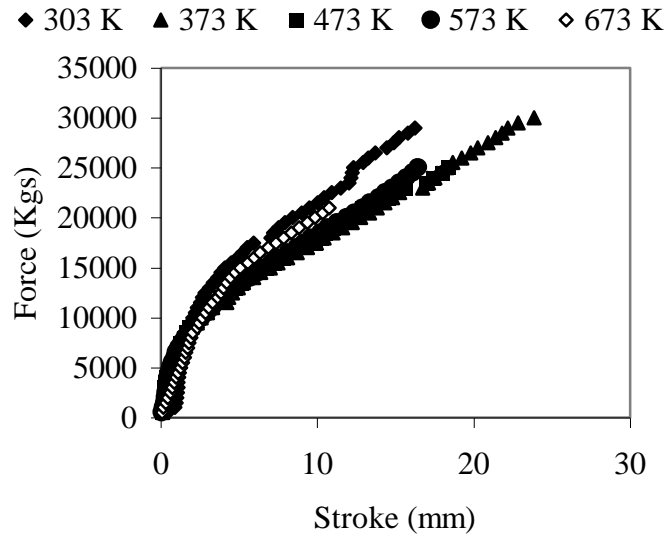
The above characteristics are determined at different temperature levels and their values are presented in Table 4.2. From the values presented in the Table 4.2 different profiles which depict the variation of characteristics viz: yield strength (σ_y), strength coefficient (K) and strain hardening exponent (n) with temperature of compression are presented in Fig. 4.6, 4.7 and 4.8 respectively. Following inferences can be drawn from these profiles:

- (i) Variation of yield strength with temperature shows a complex relation. Yield strength decreases with temperature and increases at intermediate level and decreases once again at higher level.
- (ii) Materials exhibit higher yield strength with Zn content for the corresponding temperature level with exception in one or two cases. This is illustrated by plot of yield strength v/s Zn content in Fig. 4.9
- (iii) The variation of strength coefficient (K) with temperature of compression shows a complex relation. Though K value shows an increasing trend with temperature, considerable amount of fluctuation is seen in the profile

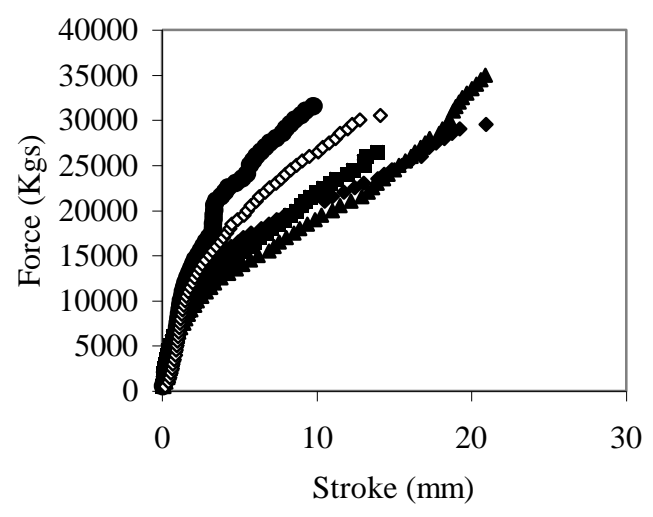
- (iv) Strength coefficient K increases with increasing Zn content of the material at a given temperature, except in one case. This is illustrated by the plot of K v/s Zn content of the material as shown in Fig. 4.10.
- (v) Strain hardening exponent (n) varies with temperature in a complex way. It goes up and down with increasing temperature.
- (vi) Variation of strain hardening exponent (n) with Zn content of the alloy is depicted in Fig. 4.11. Except in one case of temperature of testing, in all the cases profile shows maxima with respect to Zn content. The exceptional case happens to be one which has been tested at the temperature level of 373 K.



(a) Al-5Zn-1Mg

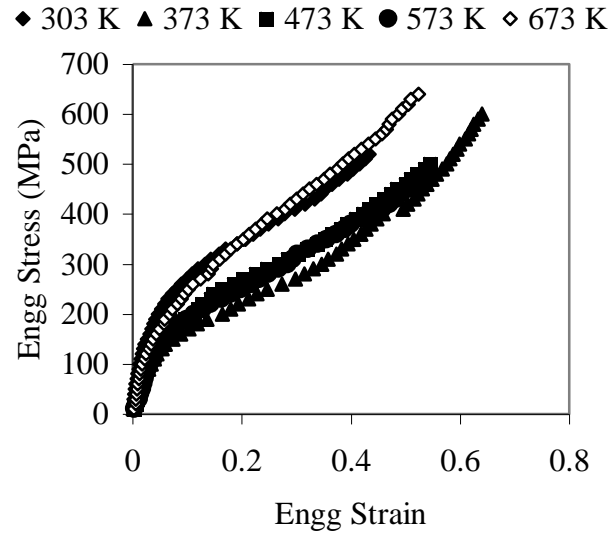


(b) Al-10Zn-1Mg

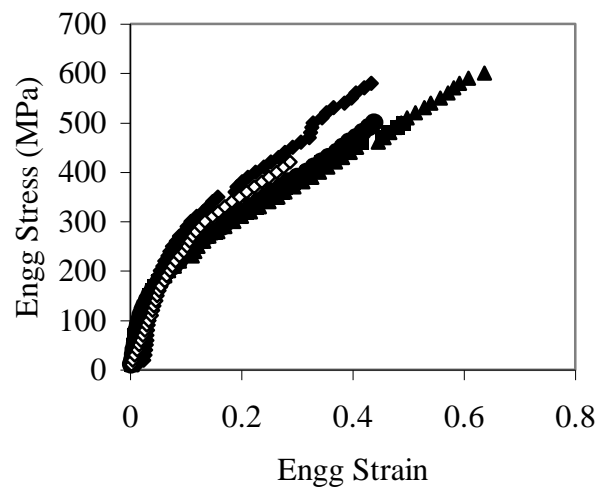


(c) Al-15Zn-1Mg

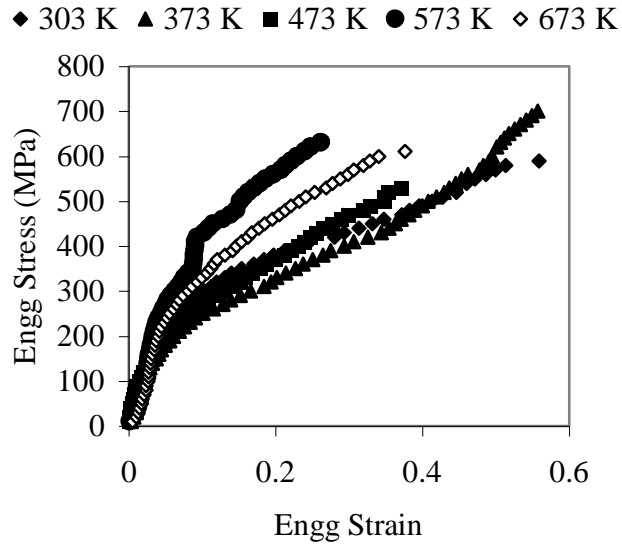
Fig.4.3 Force – Stroke diagram of (a) Al-5Zn -1Mg (b) Al-10Zn-1Mg (c) Al-15Zn-1Mg during axisymmetric compression testing at various temperatures



(a) Al-5Zn-1Mg

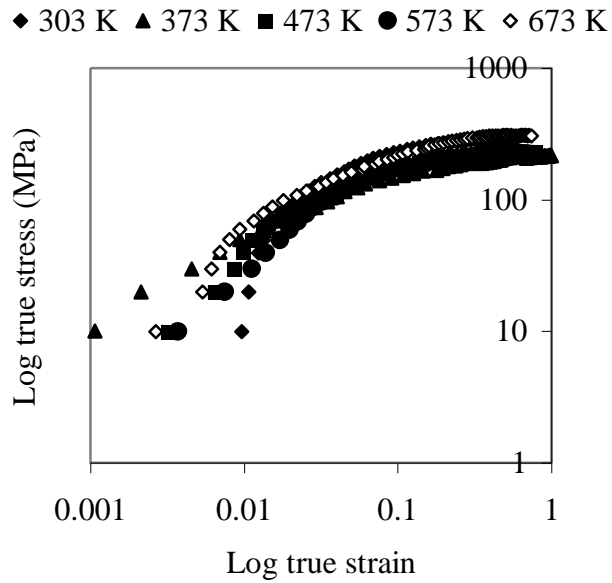


(b) Al-10Zn-1Mg



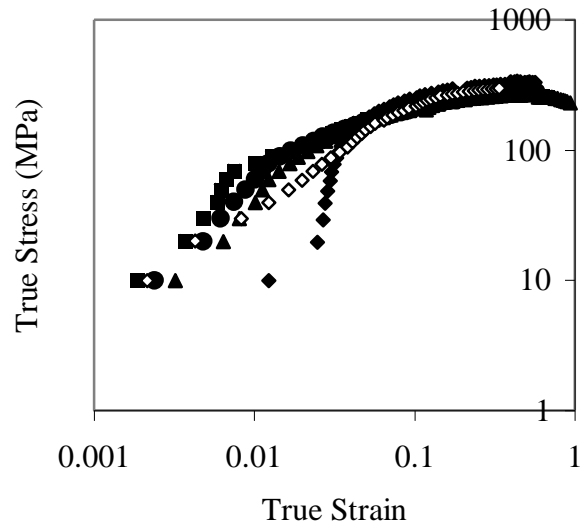
(c) Al-15Zn-1Mg

Fig.4.4 Engg. stress – Engg. strain diagram of (a) Al-5Zn -1Mg (b) Al-10Zn-1Mg (c) Al-15Zn-1Mg during axisymmetric compression testing at various temperatures

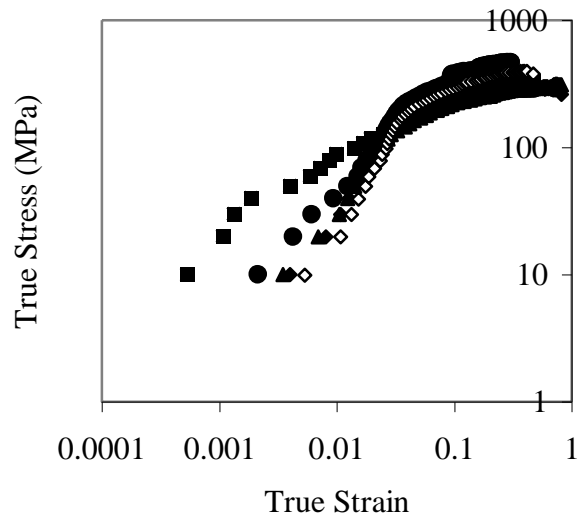


(a) Al-5Zn-1Mg

◆ 303 K ▲ 373 K ■ 473 K ● 573 K ◇ 673 K



(b) Al-10Zn-1Mg



(c) Al-15Zn-1Mg

Fig. 4.5 Log-log plot of true stress - true strain diagram of (a) Al-5Zn -1Mg (b) Al-10Zn-1Mg (c) Al-15Zn-1Mg during axisymmetric compression testing at various temperatures

Table 4.2 Flow properties of Al-Zn-Mg alloys

Alloy	Temperature (K)	Yield Stress (σ_y) (MPa)	Strength Coefficient (K) (MPa)	Strain hardening exponent (n)
Al-5Zn-1Mg	303	150	314.2	0.1
	373	100	232.76	0.16
	473	110	237.46	0.08
	573	140	228.15	0.11
	673	120	314.19	0.1
Al-10Zn-1Mg	303	160	347.23	0.11
	373	140	257.24	0.04
	473	100	314.19	0.15
	573	120	298.87	0.11
	673	180	365.04	0.2
Al-15Zn-1Mg	303	200	314.19	0.05
	373	160	403.43	0.28
	473	100	376.15	0.17
	573	250	492.75	0.11
	673	230	445.86	0.12

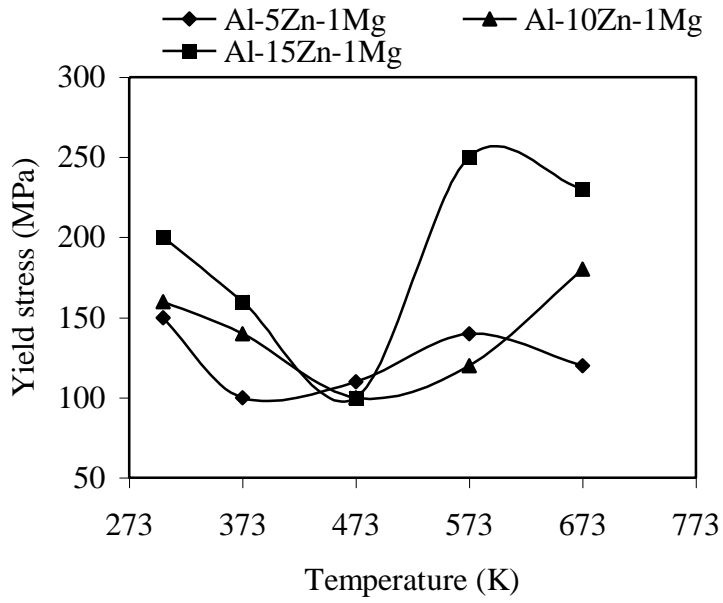


Fig. 4.6 Effect of temperature on yield stress of Al-Zn-Mg alloys

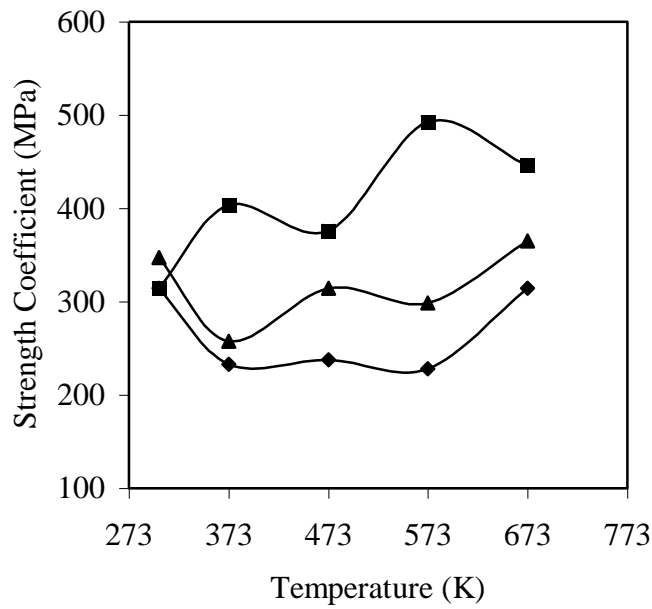


Fig. 4.7 Effect of temperature on strength coefficient of Al-Zn-Mg alloys

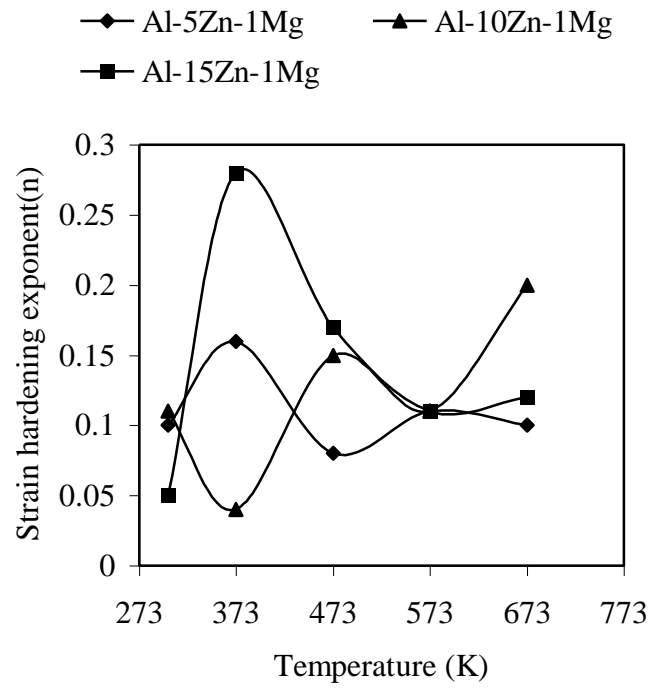


Fig 4.8 Effect of temperature on strain hardening exponent of Al-Zn-Mg alloys

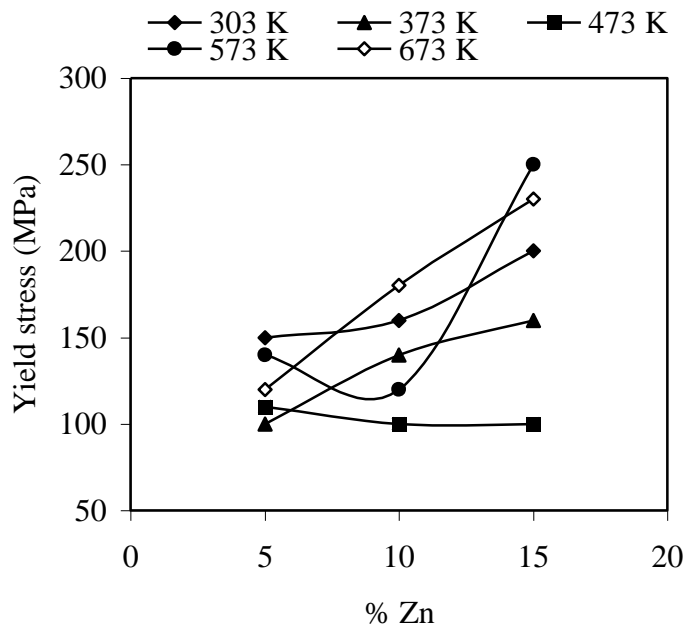


Fig 4.9 Effect of Zn content on yield stress of Al-Zn-Mg alloys in the temperature range of 303 – 673 K

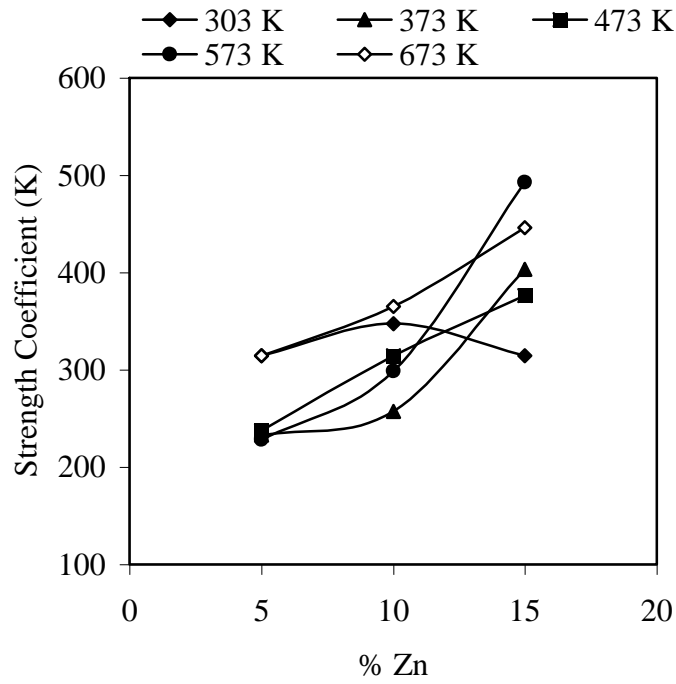


Fig 4.10 Effect of Zn content on strength coefficient of Al-Zn-Mg alloys in the temperature range of 303 – 673 K

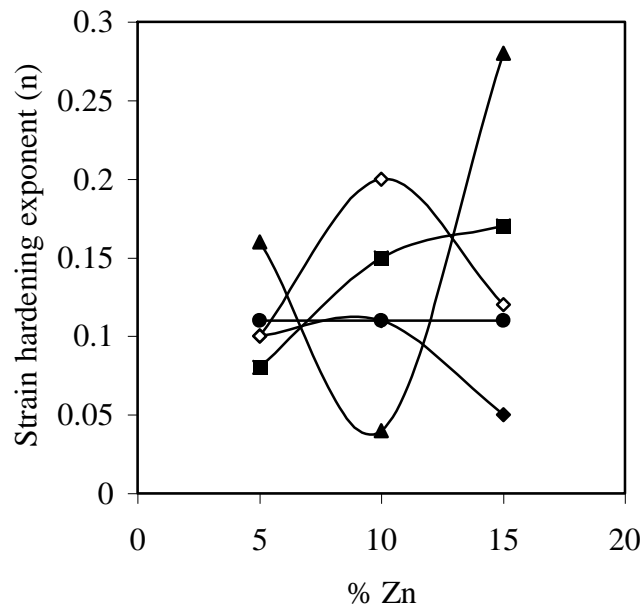


Fig 4.11 Effect of Zn content on strain hardening exponent of Al-Zn-Mg alloys in the temperature range of 303 – 673 K

4.4 RING COMPRESSION TEST

Results of ring compression tests are presented in Table 4.3. The profiles in Fig. 4.12 depict the variation of friction factor (μ) with temperature. It suggests that the relation between friction factor and temperature is a complex one; the former goes up and down with temperature.

The profile in Fig. 4.13 depicts the variation of friction factor (μ) with Zn content of the alloy. It shows that except in one case, for all the other cases of testing temperature, the profiles show maxima with respect to Zn content. The exceptional case happens to be one which has been tested at a temperature level of 473 K.

Table 4.3 Frictional properties of Al-Zn-Mg alloys

Alloy	Temperature (K)	Friction factor (μ)
Al-5Zn-1Mg	303	0.31
	373	0.36
	473	0.37
	573	0.34
	673	0.37
Al-10Zn-1Mg	303	0.36
	373	0.35
	473	0.33
	573	0.39
	673	0.35
Al-15Zn-1Mg	303	0.27
	373	0.3
	473	0.3
	573	0.34
	673	0.36

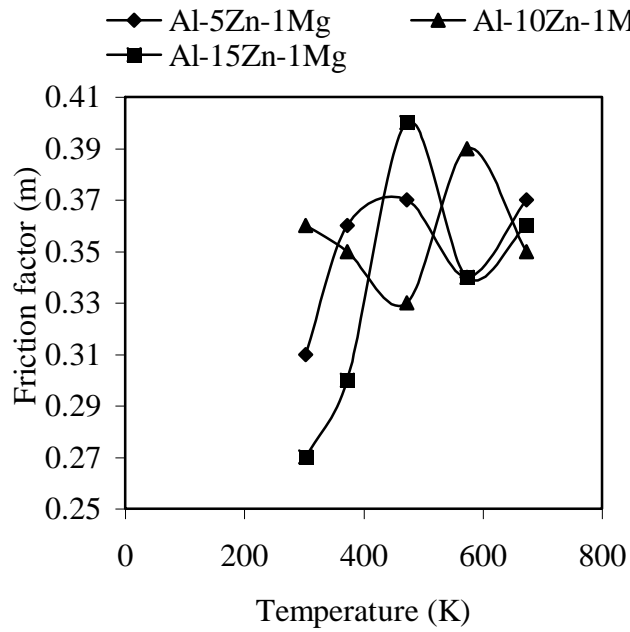


Fig 4.12 Effect of temperature on friction factor of Al-Zn-Mg alloys

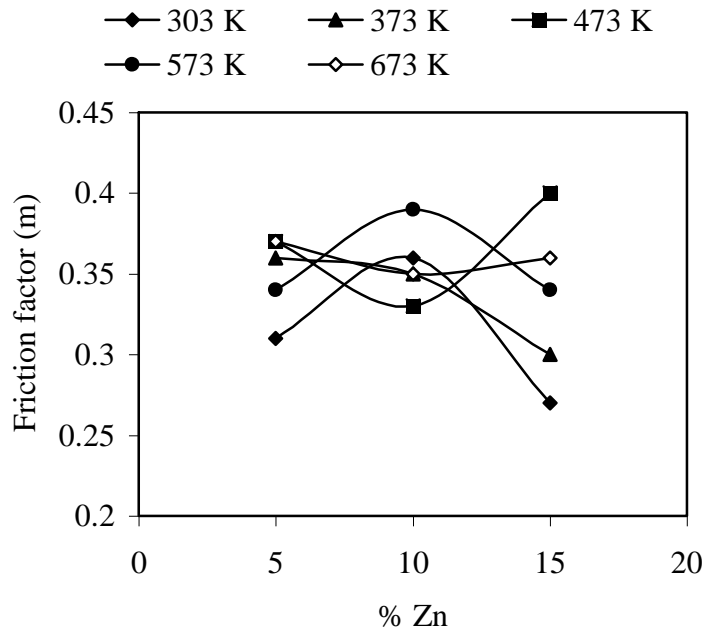


Fig 4.13 Effect of Zn content on friction factor of Al-Zn-Mg alloys in the temperature range of 303 – 673 K

4.5 STRESS ANALYSIS OF BACKWARD EXTRUSION IN Al-Zn-Mg ALLOYS WITH AND WITHOUT CONTAINER BASED ON THE ELEMENTARY PLASTICITY THEORY - “DIPPER MODEL”

4.5.1 Extrusion strains for billets extruded with a punch of 15 mm diameter

Taking the diameter of the punch as 15 mm (fixed) and height of the billet as 50 mm (fixed) backward extrusion with and without container was carried out for different billet diameters i.e. 25mm, 27 mm, 30 mm, 35 mm, 40mm & 50mm.

Extrusion strains calculated for different billet diameters are contained in Table 4.4

Table 4.4 Extrusion strains for billets of diameter 25-50 mm extruded with a punch of 15mm diameter

Diameter of billet (d_o)	Height (h_o)	h_o / d_o	Extrusion strain (ϵ)
25	50	2	0.45
27	50	1.85	0.37
30	50	1.67	0.29
35	50	1.43	0.2
40	50	1.25	0.15
50	50	1	0.1

It is found that as area of cross section of billet decreases extrusion strain increases. In the present study the extrusion strain is maximum for billet of 25 mm diameter & minimum for billet of 50 mm diameter.

Flow and friction properties of selected alloys at temperatures 303 - 673 K are given in Table 4.2 and 4.3. Depth of penetration of the punch on to the billet is fixed as 5mm, 10mm & 15 mm. As the upsetting of the billet is considered as the criterion, the effect of varying all these parameters on the upsetting is studied and the punch

pressure is calculated theoretically by substituting these values in Dipper model equation for backward extrusion with and without container (Equations 2.24 and 2.25).

4.5.2 Force-stroke diagram of backward extrusion with and without a container

Force-Stroke diagram of backward extrusion with and without a container for various strains at room temperature for the three chosen alloys are shown in Fig. 4.14, 4.15 and 4.16 respectively. Further the same data were generated at different temperatures keeping strain constant at 0.1 (Fig. 4.17 to 4.19).

While for backward extrusion with a container, force decreases with stroke; for containerless backward extrusion, force increases with stroke. However force increases as extrusion strain increases for both backward extrusions, i.e. with and without container for Al-Zn-Mg alloys.

At 373 K force is minimum for backward extrusion with and without container for Al-5Zn-1Mg and Al-15Zn-1Mg where as it is 473 K for backward extrusion with container and 673K for backward extrusion without container for Al-10Zn-1Mg.

4.5.3 Theoretical punch pressure for various extrusion strain and temperatures at punch depth of 15 mm for backward extrusion with and without a container

Theoretical punch pressure calculated for different extrusion strain at various temperatures for punch depth 15 mm for backward extrusion with and without a container for all the three alloys are contained in Tables 4.5 to 4.10

Theoretical punch pressure against extrusion strain at various temperatures for punch depth 15 mm for backward extrusion with and without a container for all the three alloys are shown in Figs. 4.20, 4.21 and 4.22 respectively.

Theoretical punch pressure increases with increase in strain at all temperatures. 373 K gives minimum punch pressure for Al-5Zn-1Mg and Al-15Zn-1Mg where as 473 K gives minimum punch pressure for Al-10Zn-1Mg for both backward extrusions.

Theoretical punch pressure against extrusion strain at 373 K for punch depth 15 mm for backward extrusions with and without container for Al-5Zn-1Mg and Al-15Zn-1Mg and that at 473 K for punch depth 15 mm for backward extrusions for Al-10Zn-1Mg are shown in Fig. 4.23.

The above optimum warm working temperatures can be employed for backward extrusions of Al-Zn-Mg alloys with and without container. Theoretical punch pressure for backward extrusion with container is more than twice that for containerless backward extrusion. Rate of change of punch pressure with respect to strain is also more in backward extrusion with a container compared to containerless backward extrusion.

Theoretical punch pressure against extrusion strain for the punch depth of 15 mm for containerless backward extrusions for Al-Zn-Mg alloys for the temperatures of 303, 373 & 473 K are shown in Fig. 4.24.

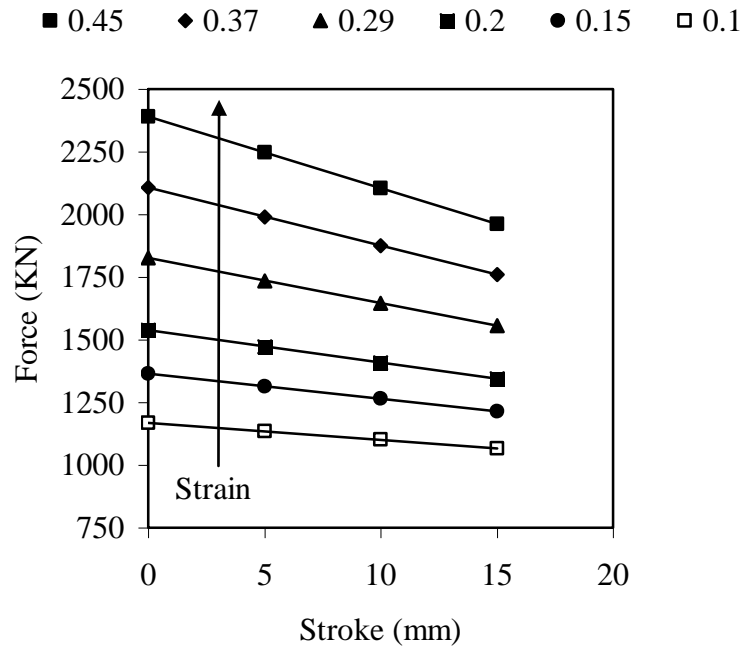
4.6 STRESS ANALYSIS OF CONTAINERLESS BACKWARD EXTRUSION OF Al-Zn-Mg ALLOYS BASED ON THE EXPERIMENTATION

4.6.1 Force-Stroke diagram of containerless backward extrusion

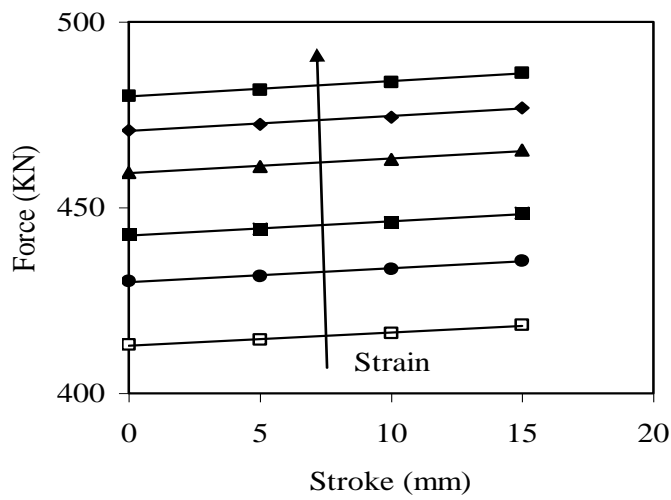
Force-stroke diagrams of containerless backward extrusion for various strains at room temperature for the three chosen alloys are shown in Fig.4.25. Further the same data were generated at different temperatures (Fig.4.26 to 4.28).

For containerless backward extrusion force increases with stroke for all the three chosen alloys at the chosen temperatures

At 423 K force required for deformation is minimum for Al-5Zn-1Mg where as it is 523 K for Al-10Zn-1Mg and Al-15Zn-1Mg.



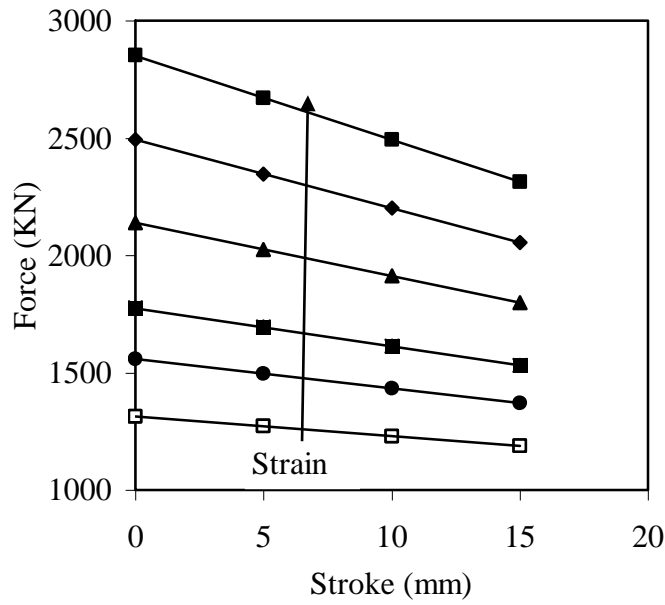
(a) Backward extrusion with a container



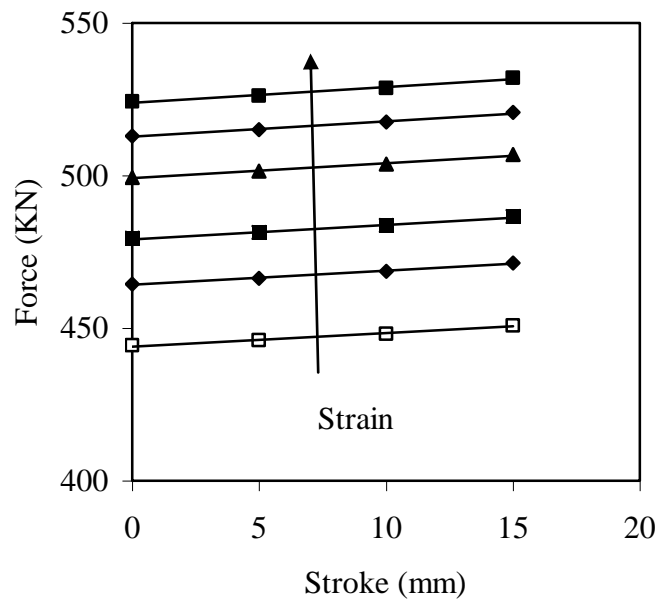
(b) Containerless backward extrusion

Fig. 4.14 Force – stroke diagram of (a) backward extrusion with a container and (b) containerless backward extrusion of Al-5Zn-1Mg for various strains at room temperature

■ 0.45 ◆ 0.37 ▲ 0.29 ■ 0.2 ● 0.15 □ 0.1



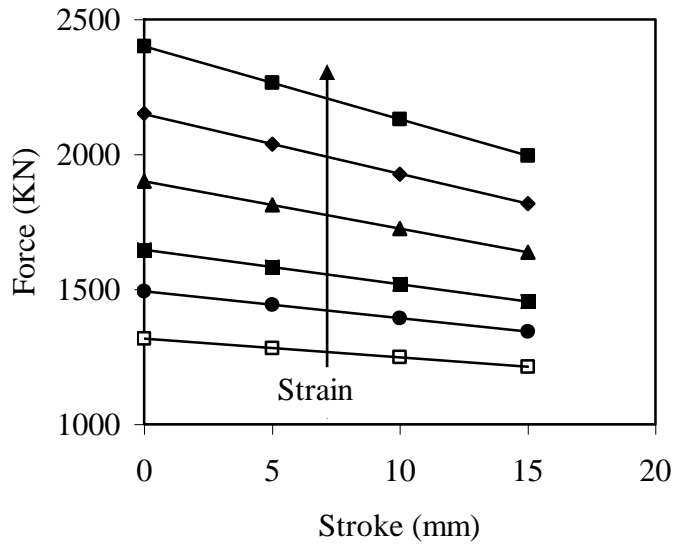
(a) Backward extrusion with a container



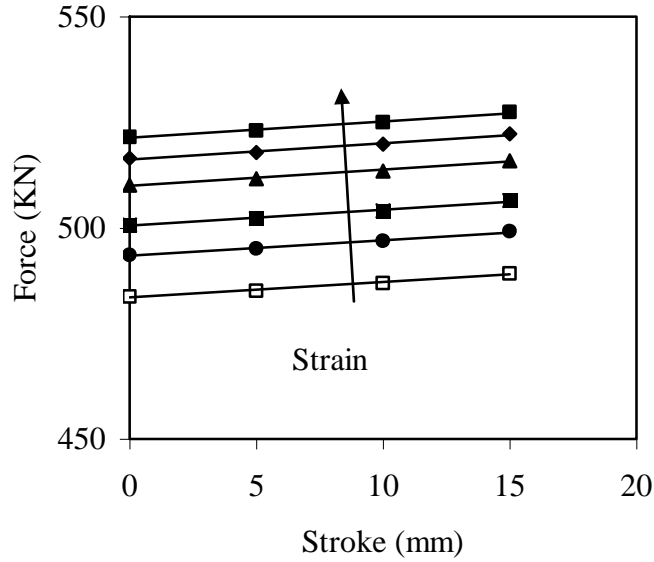
(b) Containerless backward extrusion

Fig. 4.15 Force – stroke diagram of (a) backward extrusion with a container and (b) containerless backward extrusion of Al-10Zn-1Mg for various strains at room temperature

■ 0.45 ♦ 0.37 ▲ 0.29 ■ 0.2 ● 0.15 □ 0.1

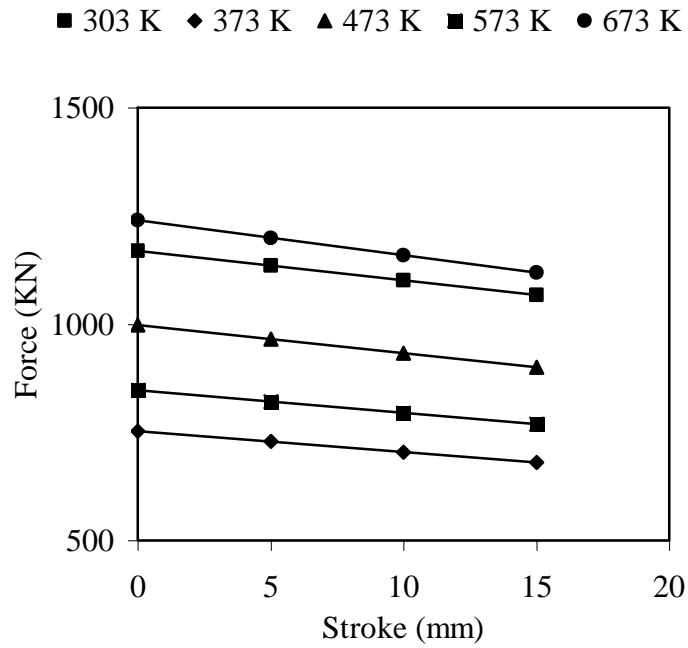


(a) Backward extrusion with a container

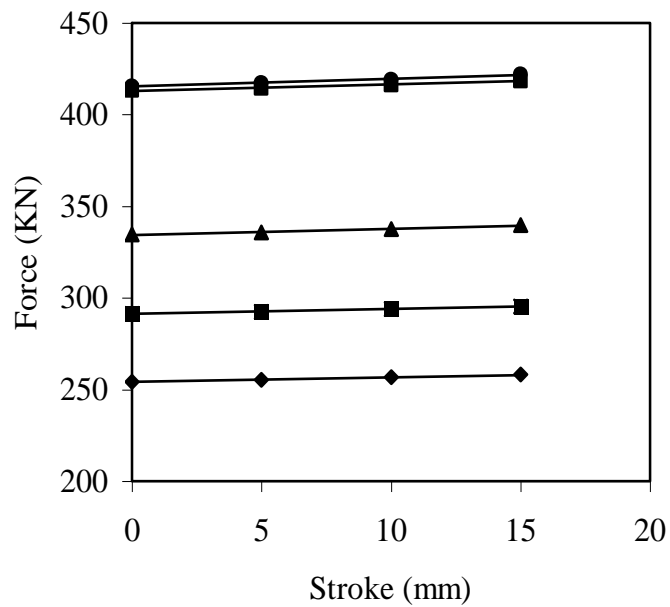


(b) Containerless backward extrusion

Fig. 4.16 Force – stroke diagram of (a) backward extrusion with a container and (b) containerless backward extrusion of Al-15Zn-1Mg for various strains at room temperature

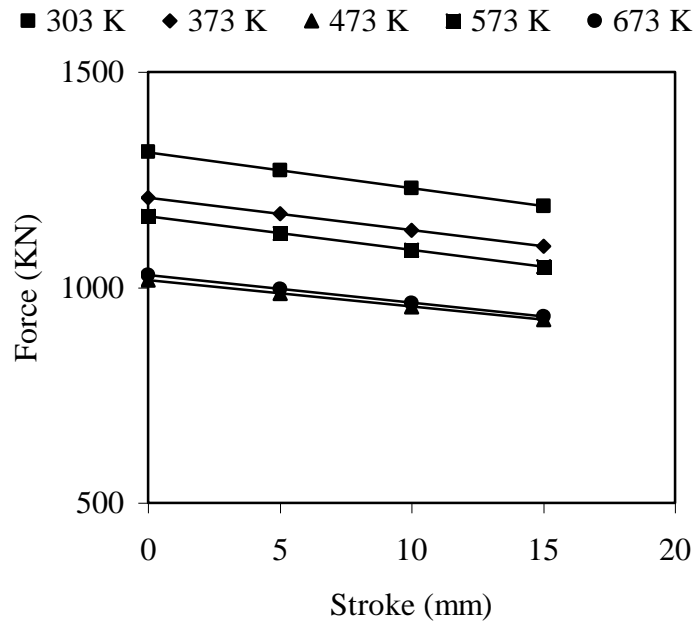


(a) Backward extrusion with a container

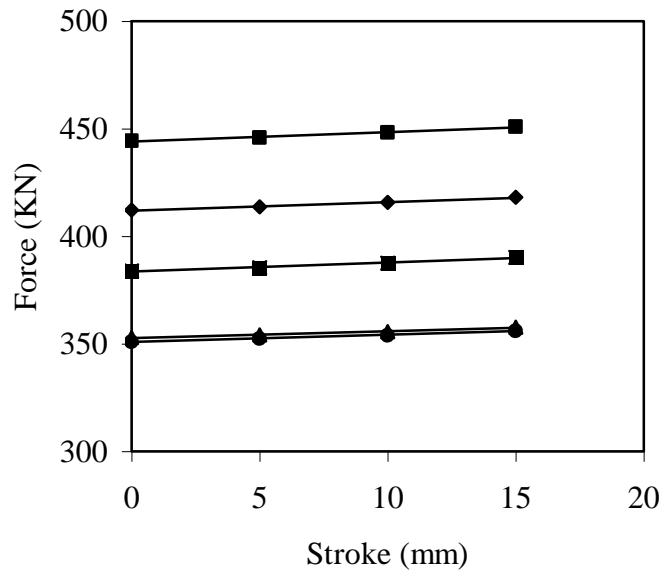


(b) Containerless backward extrusion

Fig. 4.17 Force – stroke diagram of (a) backward extrusion with a container and (b) containerless backward extrusion of Al-5Zn-1Mg at various temperatures for 0.1 strains.

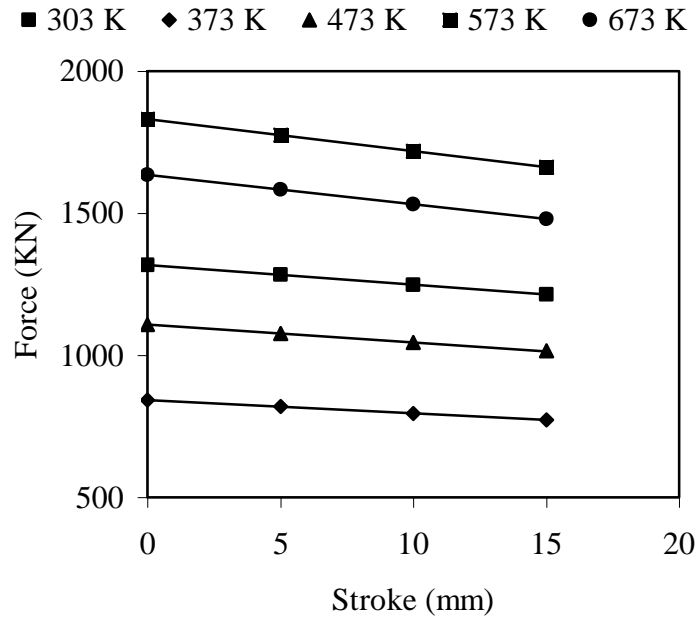


(a) Backward extrusion with a container

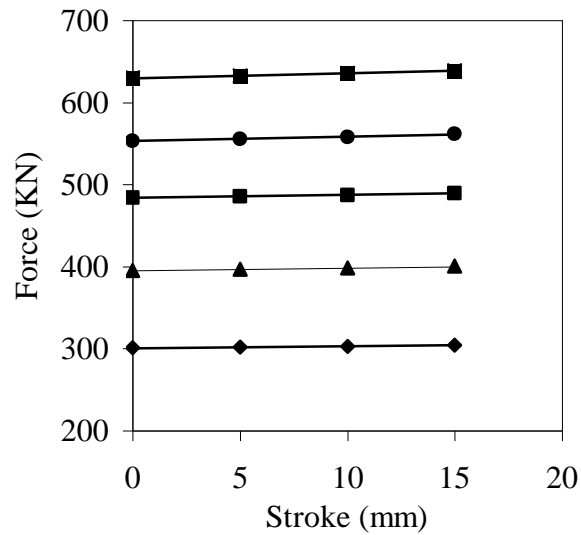


(b) Containerless backward extrusion

Fig. 4.18 Force – stroke diagram of (a) backward extrusion with a container and (b) containerless backward extrusion of Al-10Zn-1Mg at various temperatures for 0.1 strains.



(a) Backward extrusion with a container



(b) Containerless backward extrusion

Fig. 4.19 Force – stroke diagram of (a) backward extrusion with a container and (b) containerless backward extrusion of Al-15Zn-1Mg at various temperatures for 0.1 strains.

Table 4.5 Variation of theoretical punch pressure with respect to extrusion strain at various temperatures for backward extrusion with a container of Al-5Zn-1Mg

Temperature (K)	Extrusion strain	Theoretical Punch pressure at 15 mm punch depth
303	0.45	1110.66
	0.37	995.66
	0.29	880.48
	0.2	760.48
	0.15	687.67
	0.1	604.11
373	0.45	808.1
	0.37	711.23
	0.29	614.83
	0.2	514.14
	0.15	453.64
	0.1	385.12
473	0.45	955.8
	0.37	853.47
	0.29	751.2
	0.2	645.91
	0.15	582.38
	0.1	509.77
573	0.45	833.17
	0.37	742.38
	0.29	651.65
	0.2	557.29
	0.15	500.25
	0.1	435.06
673	0.45	1223.61
	0.37	1088.33
	0.29	953.27
	0.2	813.59
	0.15	729.36
	0.1	633.27

Table 4.6 Variation of theoretical punch pressure with respect to extrusion strain at various temperatures for backward extrusion with a container of Al-10Zn-1Mg

Temperature (K)	Extrusion strain	Theoretical Punch pressure at 15 mm punch depth
303	0.45	1308.92
	0.37	1163.34
	0.29	1017.99
	0.2	867.23
	0.15	776.28
	0.1	672.53
373	0.45	1077.06
	0.37	971.69
	0.29	866.24
	0.2	758.84
	0.15	694.04
	0.1	619.77
473	0.45	1055.4
	0.37	934.3
	0.29	813.47
	0.2	686.79
	0.15	610.33
	0.1	523.29
573	0.45	1180.72
	0.37	1045.71
	0.29	911.1
	0.2	771.93
	0.15	688.2
	0.1	592.94
673	0.45	1166.72
	0.37	1020.12
	0.29	874.65
	0.2	721.99
	0.15	630.63
	0.1	527.77

Table 4.7 Variation of theoretical punch pressure with respect to extrusion strain at various temperatures for backward extrusion with a container of Al-15Zn-1Mg

Temperature (K)	Extrusion strain	Theoretical Punch pressure at 15 mm punch depth
303	0.45	1128.85
	0.37	1028.22
	0.29	927.23
	0.2	823.24
	0.15	760.08
	0.1	687.26
373	0.45	1043.03
	0.37	903.98
	0.29	766.45
	0.2	620.5
	0.15	533.61
	0.1	436.69
473	0.45	1162.38
	0.37	1029.35
	0.29	896.46
	0.2	756.03
	0.15	671.06
	0.1	574.22
573	0.45	1801.53
	0.37	1605.23
	0.29	1409.03
	0.2	1205.01
	0.15	1081.68
	0.1	940.72
673	0.45	1654.07
	0.37	1467.23
	0.29	1280.8
	0.2	1087.07
	0.15	970.26
	0.1	837.18

Table 4.8 Variation of theoretical punch pressure with respect to extrusion strain at various temperatures for containerless backward extrusion of Al-5Zn-1Mg

Temperature (K)	Extrusion strain	Theoretical Punch (MPa) pressure at 15 mm punch depth
303	0.45	275.22
	0.37	269.88
	0.29	263.39
	0.2	253.78
	0.15	246.58
	0.1	236.79
373	0.45	185.86
	0.37	180.13
	0.29	173.25
	0.2	163.25
	0.15	155.9
	0.1	146.11
473	0.45	216.75
	0.37	213.38
	0.29	209.26
	0.2	203.13
	0.15	198.51
	0.1	192.17
573	0.45	197.27
	0.37	193.07
	0.29	187.96
	0.2	180.44
	0.15	174.82
	0.1	167.19
673	0.45	277.48
	0.37	272.1
	0.29	265.55
	0.2	255.86
	0.15	248.61
	0.1	238.73

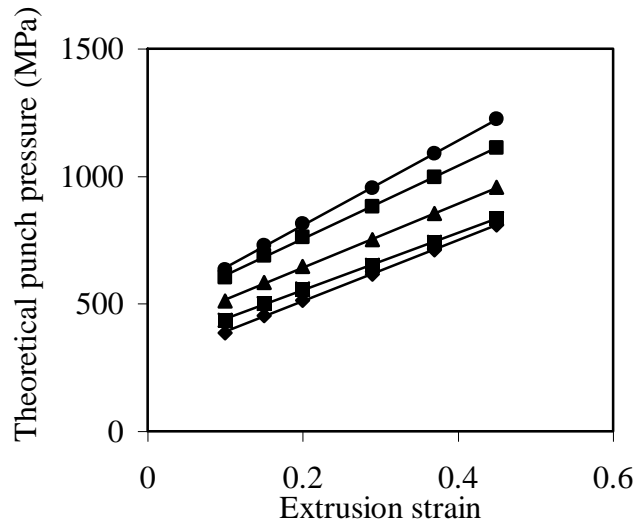
Table 4.9 Variation of theoretical punch pressure with respect to extrusion strain at various temperatures for containerless backward extrusion of Al-10Zn-1Mg

Temperature (K)	Extrusion strain	Theoretical Punch pressure(MPa) at 15 mm punch depth
303	0.45	301.05
	0.37	294.64
	0.29	286.85
	0.20	275.36
	0.15	266.78
	0.10	255.14
373	0.45	251.31
	0.37	249.35
	0.29	246.94
	0.20	243.29
	0.15	240.51
	0.10	236.64
473	0.45	253.64
	0.37	246.30
	0.29	237.46
	0.20	224.59
	0.15	215.11
	0.10	202.41
573	0.45	260.46
	0.37	254.92
	0.29	248.16
	0.20	238.24
	0.15	230.82
	0.10	220.75
673	0.45	272.23
	0.37	261.78
	0.29	249.33
	0.20	231.48
	0.15	218.53
	0.10	201.51

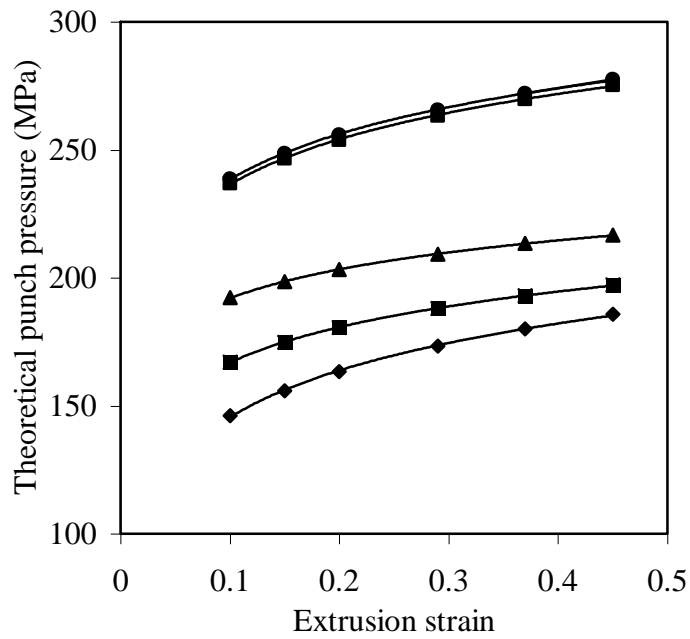
Table 4.10 Variation of theoretical punch pressure with respect to extrusion strain at various temperatures for containerless backward extrusion of Al-15Zn-1Mg

Temperature (K)	Extrusion strain	Theoretical Punch pressure(MPa) at 15 mm punch depth
303	0.45	298.43
	0.37	295.52
	0.29	291.94
	0.20	286.57
	0.15	282.48
	0.10	276.81
373	0.45	262.55
	0.37	248.55
	0.29	232.16
	0.20	209.22
	0.15	193.03
	0.10	172.31
473	0.45	292.6
	0.37	283.02
	0.29	271.54
	0.20	254.92
	0.15	242.75
	0.10	226.58
573	0.45	426.56
	0.37	417.47
	0.29	406.43
	0.20	390.15
	0.15	378
	0.10	361.51
673	0.45	380.44
	0.37	371.6
	0.29	360.9
	0.20	345.16
	0.15	333.45
	0.10	317.61

■ 303 K ◆ 373 K ▲ 473 K ■ 573 K ● 673 K



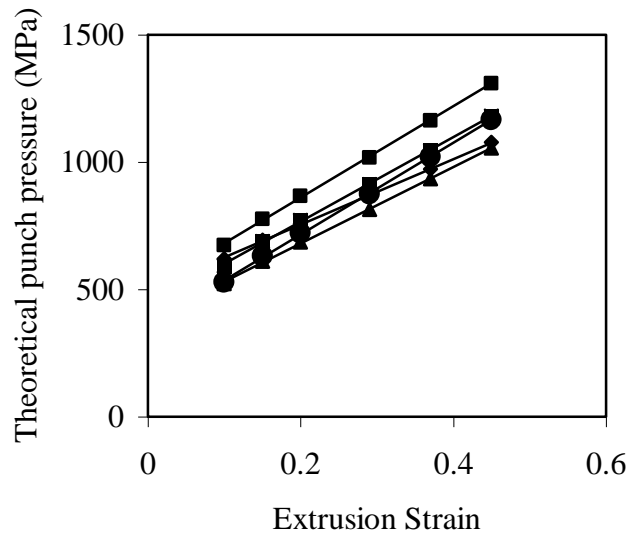
(a) Backward extrusion with a container



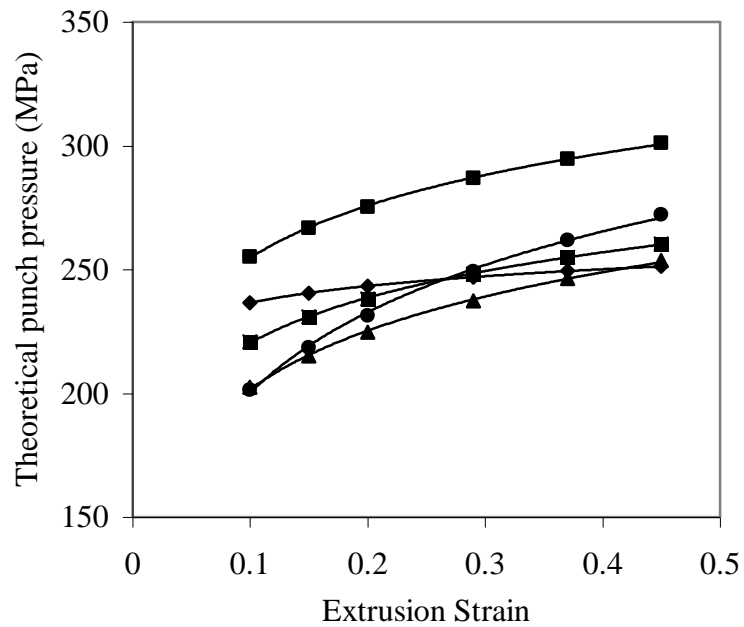
(b) Containerless backward extrusion

Fig 4.20 Variation of punch pressure against extrusion strain at various temperatures for punch depth 15 mm for (a) backward extrusion with a container and (b) containerless backward extrusion of Al-5Zn-1Mg.

■ 303 K ◆ 373 K ▲ 473 K ■ 573 K ● 673 K

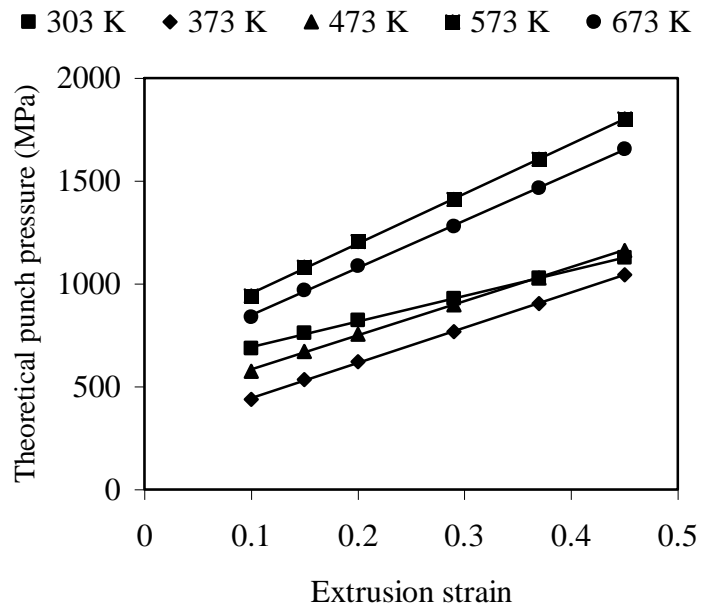


(a) Backward extrusion with a container

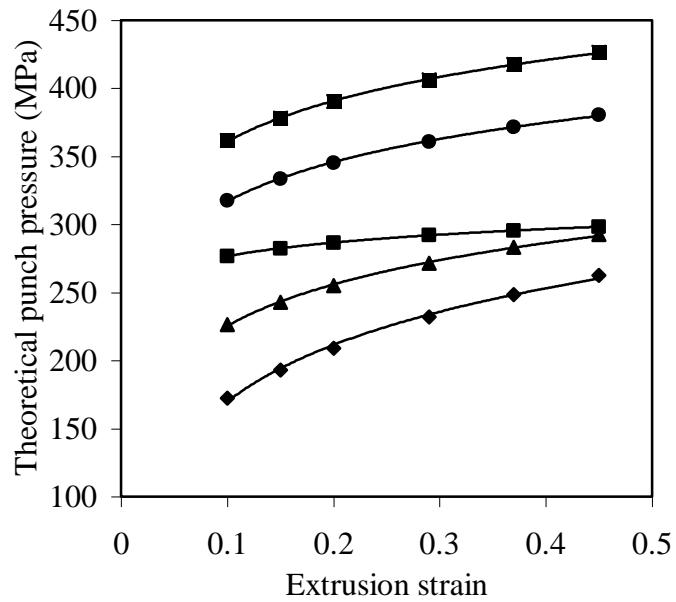


(b) Containerless backward extrusion

Fig. 4.21 Variation of punch pressure against extrusion strain at various temperatures for the punch depth of 15 mm for (a) backward extrusion with a container and (b) containerless backward extrusion of Al-10Zn-1Mg.

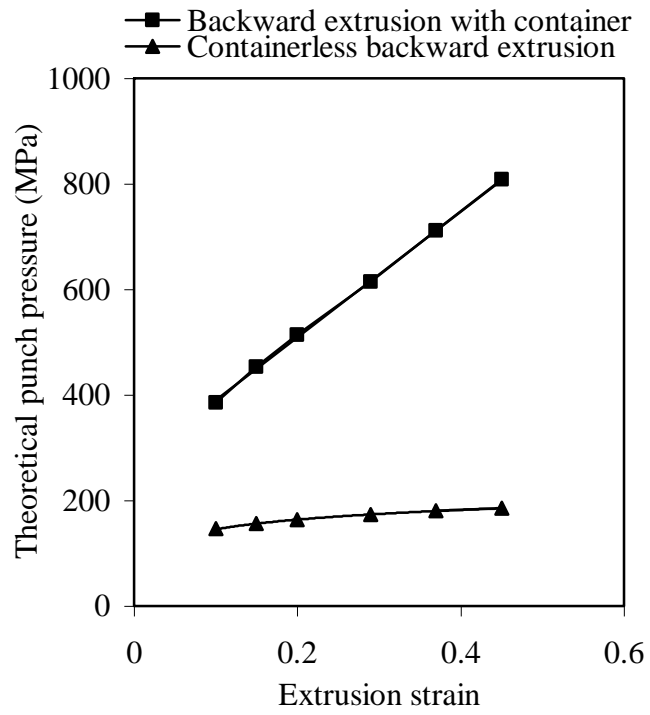


(a) Backward extrusion with a container

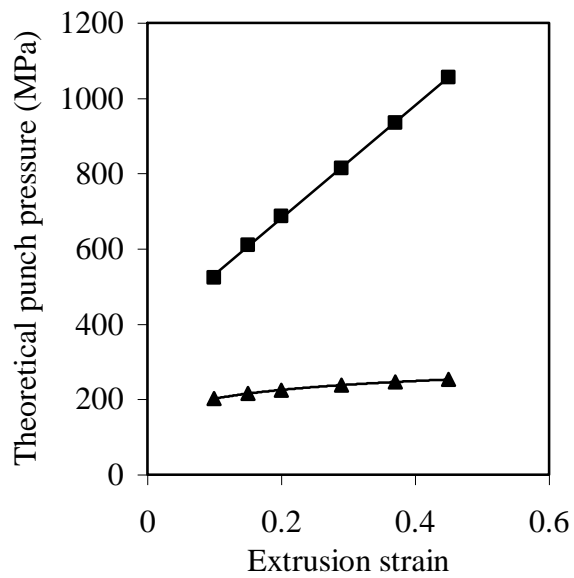


(b) Containerless backward extrusion

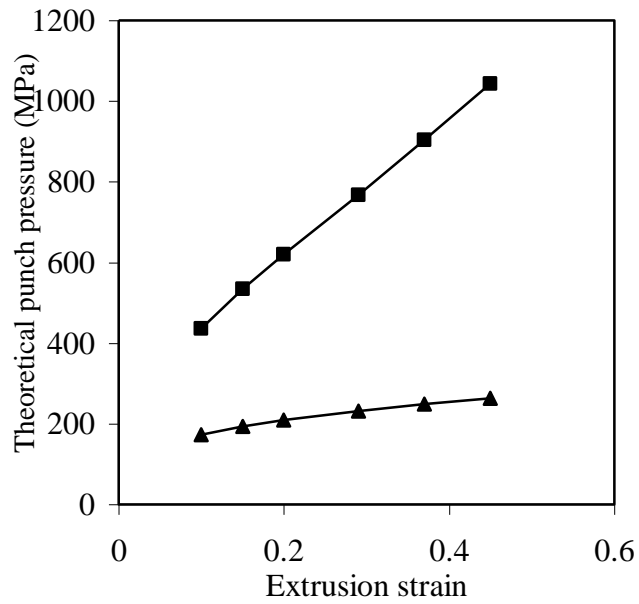
Fig. 4.22 Variation of punch pressure against extrusion strain at various temperatures for punch depth 15 mm for (a) backward extrusion with a container and (b) containerless backward extrusion of Al-15Zn-1Mg.



(a) Al-5Zn-1Mg at 373 K

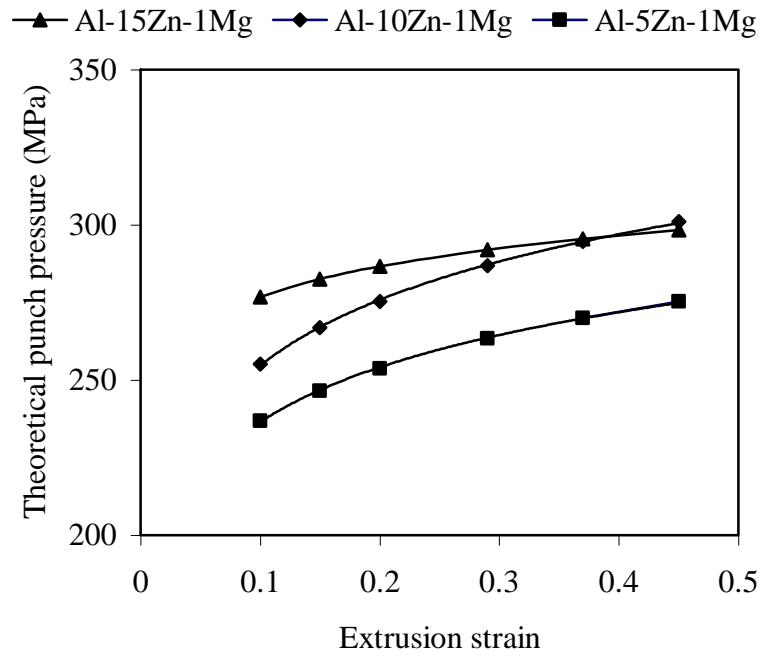


(b) Al-10Zn-1Mg at 473 K

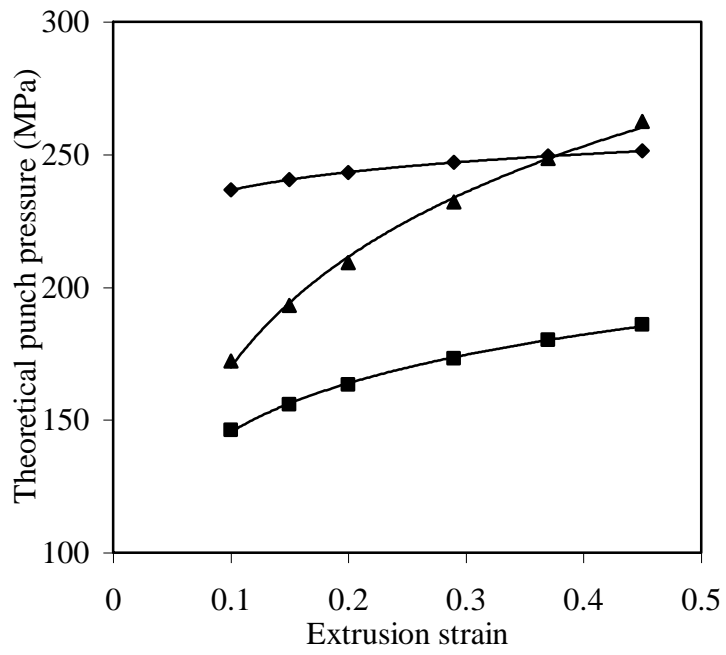


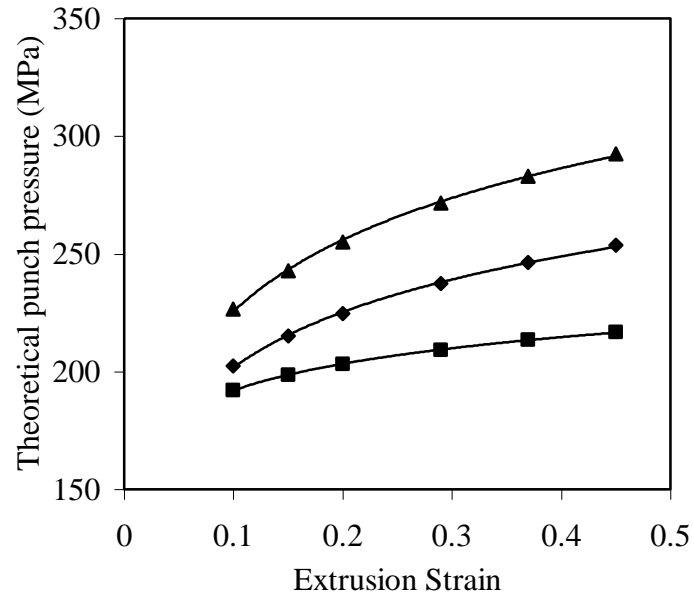
(c) Al-15Zn-1Mg at 373 K

Fig. 4.23 Variation of punch pressure with extrusion strain for the punch depth of 15 mm for backward extrusion with and without container for (a) Al-5Zn-1Mg at 373 K (b) Al-10Zn-1Mg at 473 K and (c) Al-15Zn-1Mg at 373 K



(a) 303 K





(c) 473 K

Fig. 4.24 Variation of punch pressure against extrusion strain at the punch depth of 15 mm for containerless backward extrusion of Al-Zn-Mg alloys at (a) 303 K (b) 373 K and (c) 473 K

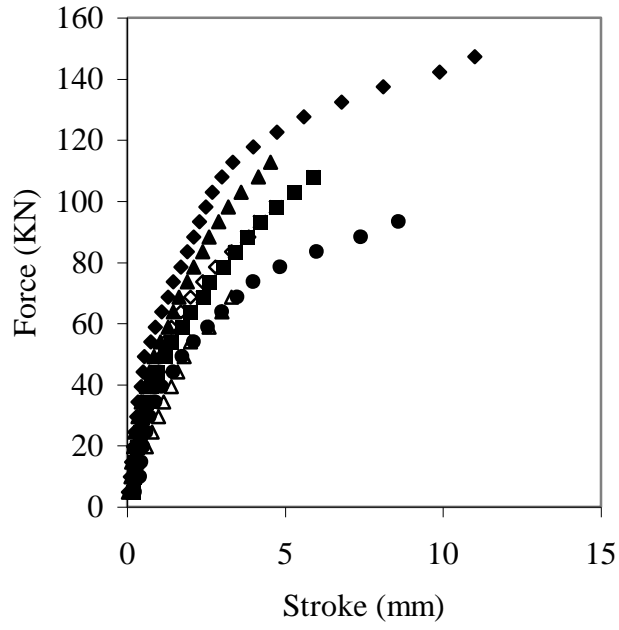
4.6.2 Punch pressure for various extrusion strain and temperatures for containerless backward extrusion

Punch pressure against extrusion strains cannot be plotted for all compositions at various temperatures since at higher strains billets failed by initiating and propagating cracks. As a result a stroke of 15 mm was impossible at all extrusion strains used in this study. However 0.1 strain could reach a punch depth of 10mm, 0.15 – 0.29 strains could reach a punch depth of 5mm each and 0.37 -0.45 could reach a punch depth of 3mm. Punch pressure was calculated by dividing punch load to the cross sectional area of the punch of 15 mm diameter. Punch pressures at various temperatures at various punch depths for various strains of Al-Zn-Mg alloys are contained in Table 4.11 to 4.16. Plot of punch pressure against temperature at selected punch depth at various strains for Al-Zn-Mg alloys are shown in Fig.4.29 to 4.31.

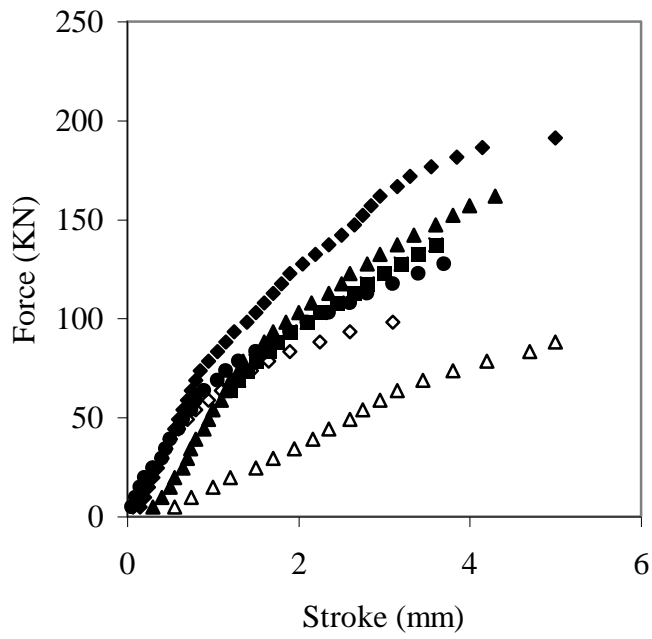
At room temperature Al-5Zn-1Mg requires lesser punch pressure, Al-10Zn-1Mg requires more punch pressure and Al-15Zn-1Mg requires maximum punch pressure for 0.1 and 0.37 strains , whereas for other strains except 0.45, Al-5Zn-1Mg requires lesser punch pressure, Al-15Zn-1Mg requires more punch pressure and Al-10Zn-1Mg requires maximum punch pressure.

At 423 K, Al-5Zn-1Mg requires lesser punch pressure, Al-10Zn-1Mg requires more punch pressure and Al-15Zn-1Mg requires maximum punch pressure for all strains except 0.1. At 523 K Al-10Zn-1Mg and Al-15Zn-1Mg showed a lesser punch pressure compared with 423 K for all the strains. At 623 K Al-5Zn-1Mg and Al-10Zn-1Mg required more punch pressure than at 523 K. Al-15Zn-1Mg showed a lower punch pressure.

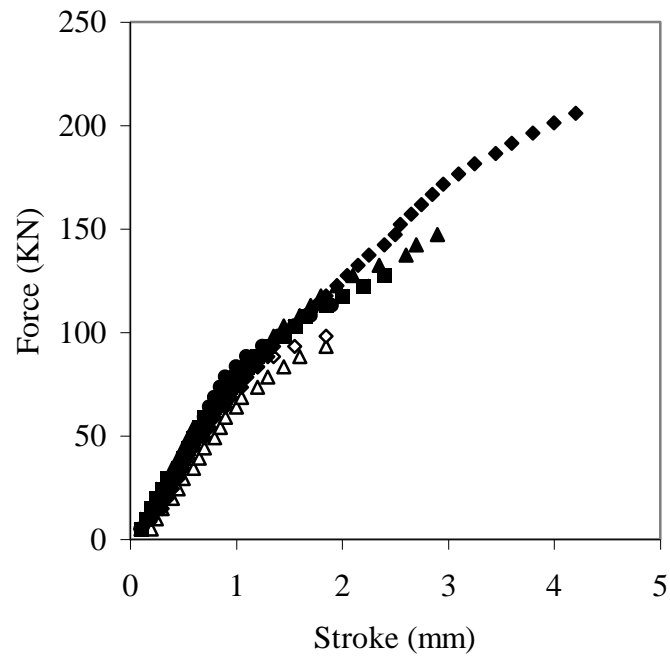
△ 0.45 Strain ◇ 0.37 Strain ● 0.29 Strain
 ■ 0.2 Strain ▲ 0.15 Strain ◆ 0.1 Strain



(a) Al-5Zn-1Mg

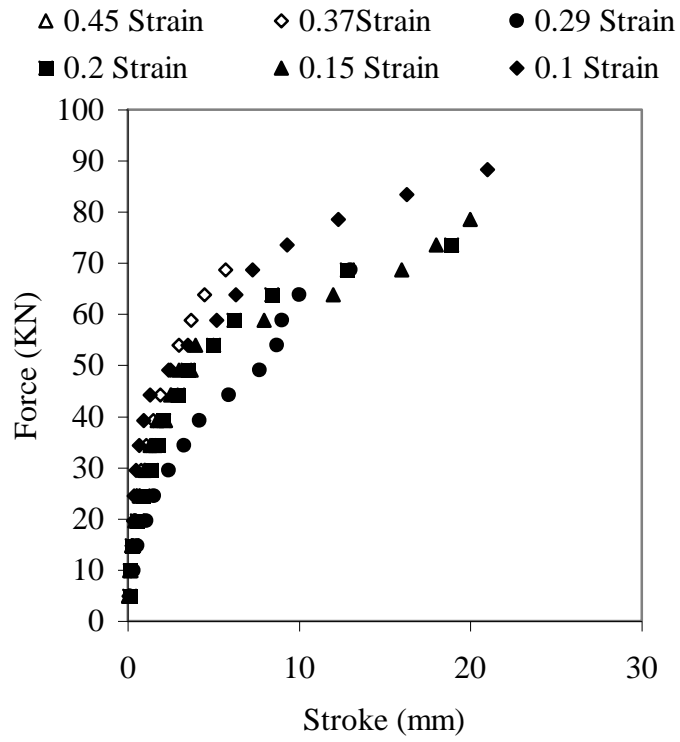


(b) Al-10Zn-1Mg

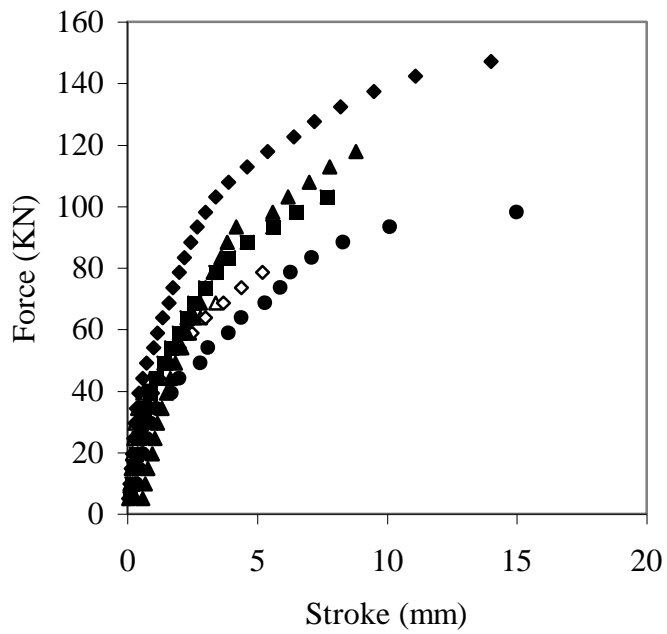


(c) Al-15Zn-1Mg

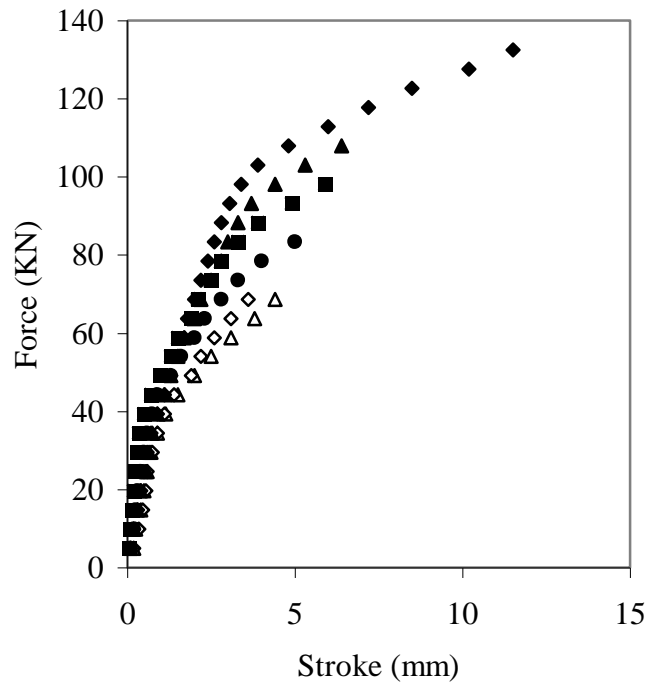
Fig. 4.25 Force-Stroke diagram of containerless backward extrusion of (a) Al-5Zn-1Mg (b) Al-10Zn-1Mg and (c) Al-15Zn-1Mg at room temperature for various extrusion strains



(a) Al-5Zn-1Mg

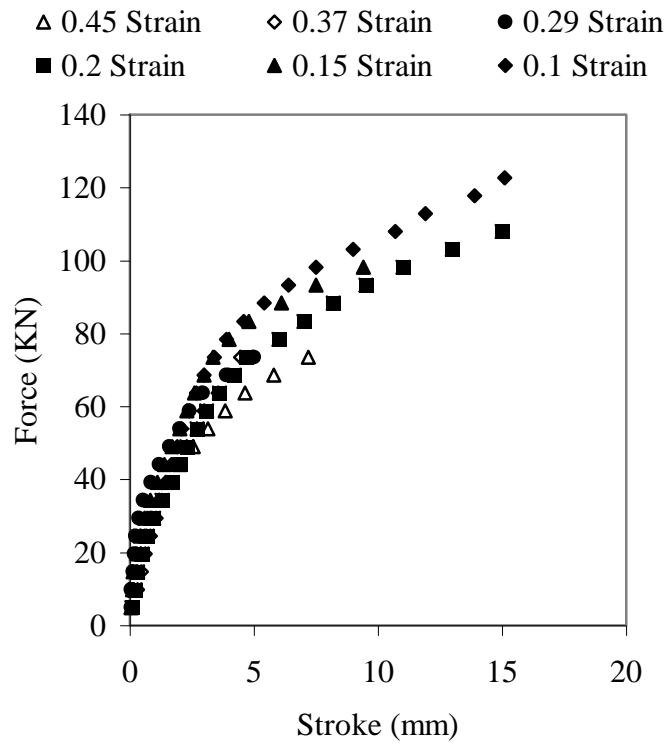


(b) Al-10Zn-1Mg

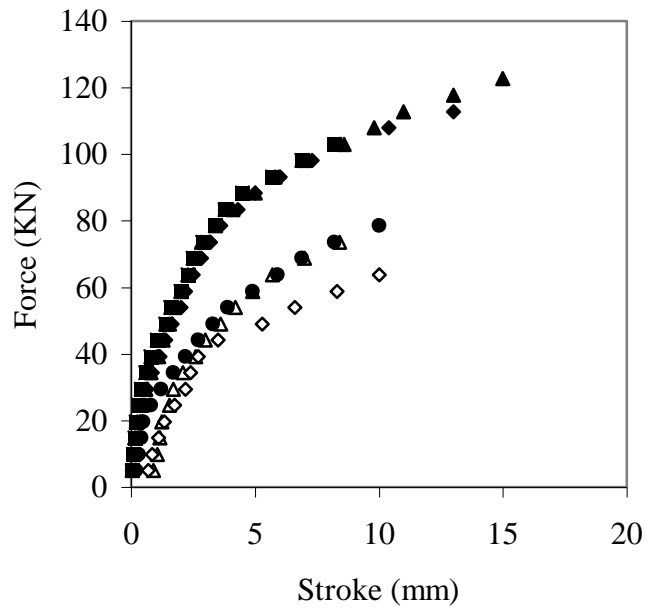


(c) Al-15Zn-1Mg

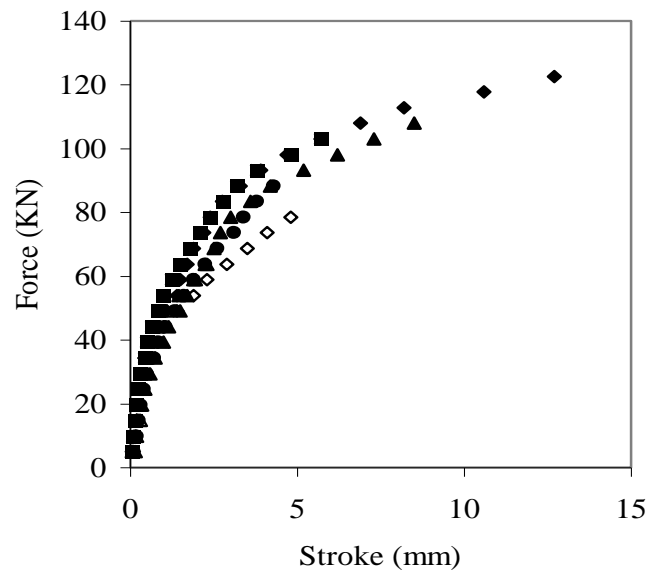
Fig. 4.26 Force-Stroke diagram of containerless backward extrusion of (a) Al-5Zn-1Mg (b) Al-10Zn-1Mg and (c) Al-15Zn-1Mg at 423 K for various extrusion strains



(a) Al-5Zn-1Mg



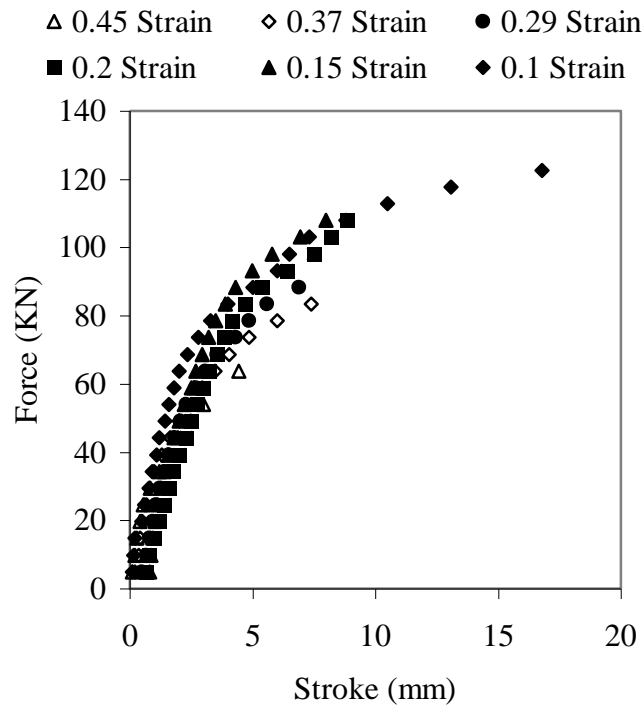
(b) Al-10Zn-1Mg



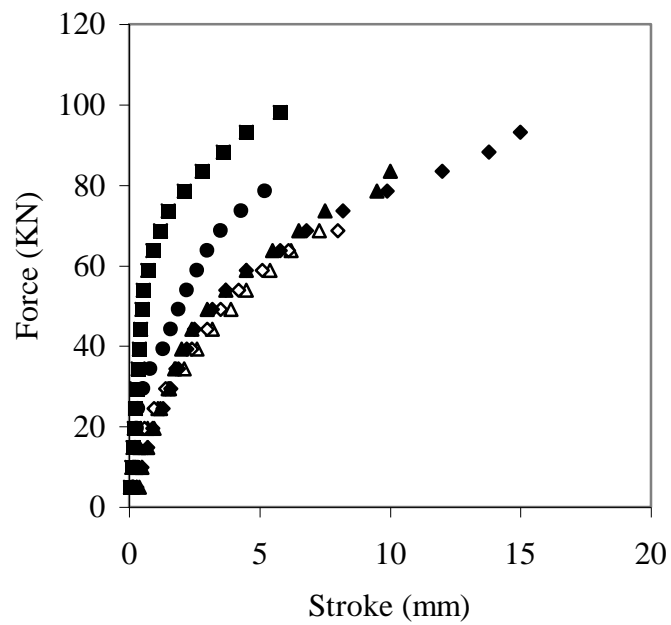
(c) Al-15Zn-1Mg

Fig. 4.27 Force-Stroke diagram of containerless backward extrusion of (a) Al-5Zn-1Mg

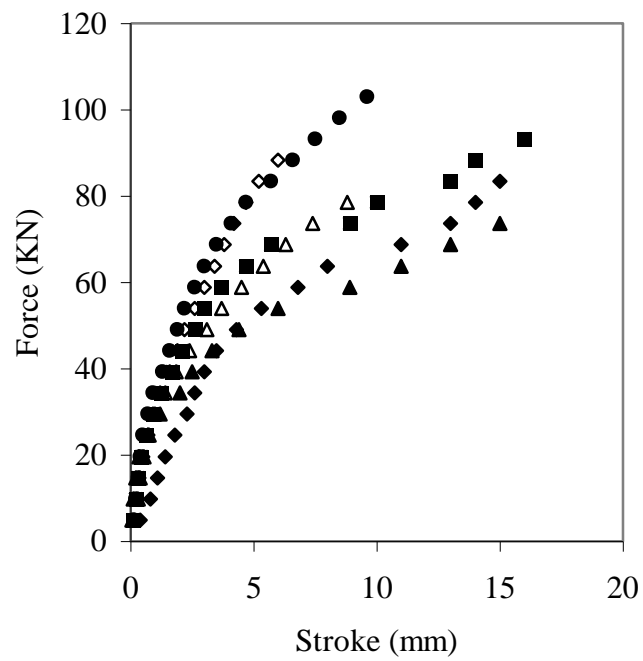
(b) Al-10Zn-1Mg and (c) Al-15Zn-1Mg at 523 K for various extrusion strains



(a) Al-5Zn-1Mg



(b) Al-10Zn-1Mg



(c) Al-15Zn-1Mg

Fig. 4.28 Force-Stroke diagram of containerless backward extrusion of (a) Al-5Zn-1Mg (b) Al-10Zn-1Mg and (c) Al-15Zn-1Mg at 623 K for various extrusion strains

Table 4.11 Punch pressure at various temperatures for a punch depth of 10mm for Al-Zn-Mg alloys at 0.1 strains

Alloy	Strain	Punch depth	Temperature (K)	Load (KN)	Punch pressure (MPa)
Al-5Zn-1Mg	0.1	10 mm	303	142	803.56
			423	73	413.10
			523	108	611.16
			623	112	633.79
Al-10Zn-1Mg	0.1	10 mm	303	195	1103.48
			423	140	792.24
			523	108	611.16
			623	78	441.39
Al-15Zn-1Mg	0.1	10 mm	303	205	1160.07
			423	126	713.02
			523	116	656.43
			623	67	379.14

Table 4.12 Punch pressure at various temperatures for a punch depth of 5mm for Al-Zn-Mg alloys at 0.15 strains

Alloy	Strain	Punch depth	Temperature (K)	Load (KN)	Punch pressure (MPa)
Al-5Zn-1Mg	0.15	5 mm	303	114	645.11
			423	56	316.9
			523	84	475.34
			623	94	531.93
Al-10Zn-1Mg	0.15	5 mm	303	162	916.74
			423	100	565.89
			523	84	475.34
			623	90	509.3
Al-15Zn-1Mg	0.15	5 mm	303	152	860.15
			423	100	565.89
			523	92	520.62
			623	52	294.26

Table 4.13 Punch pressure at various temperatures for a punch depth of 5mm for Al-Zn-Mg alloys at 0.2 strains

Alloy	Strain	Punch depth	Temperature (K)	Load (KN)	Punch pressure (MPa)
Al-5Zn-1Mg	0.2	5 mm	303	100	565.89
			423	54	305.58
			523	76	430.07
			623	86	486.66
Al-10Zn-1Mg	0.2	5 mm	303	136	769.61
			423	92	520.62
			523	90	509.3
			623	96	543.25
Al-15Zn-1Mg	0.2	5 mm	303	128	724.33
			423	94	531.93
			523	98	554.57
			623	66	373.48

Table 4.14 Punch pressure at various temperatures for a punch depth of 5mm for Al-Zn-Mg alloys at 0.29 strains

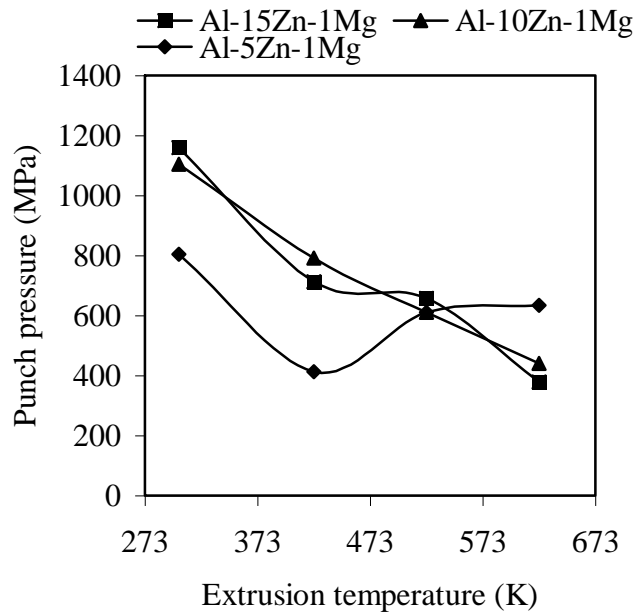
Alloy	Strain	Punch depth	Temperature (K)	Load (KN)	Punch pressure (MPa)
Al-5Zn-1Mg	0.29	5 mm	303	80	452.71
			423	42	237.67
			523	74	418.76
			623	80	452.71
Al-10Zn-1Mg	0.29	5 mm	303	128	724.33
			423	68	384.80
			523	60	339.53
			623	78	441.39
Al-15Zn-1Mg	0.29	5 mm	303	114	645.11
			423	83	469.69
			523	88	497.98
			623	80	452.71

Table 4.15 Punch pressure at various temperatures for a punch depth of 3mm for Al-Zn-Mg alloys at 0.37 strains

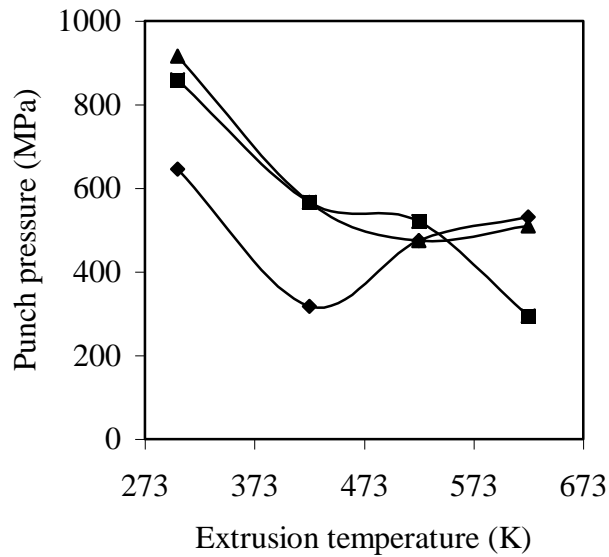
Alloy	Strain	Punch depth	Temperature (K)	Load (KN)	Punch pressure (MPa)
Al-5Zn-1Mg	0.37	3 mm	303	80	452.71
			423	54	305.58
			523	59	333.88
			623	60	339.53
Al-10Zn-1Mg	0.37	3 mm	303	98	554.57
			423	64	362.17
			523	48	271.63
			623	44	248.99
Al-15Zn-1Mg	0.37	3 mm	303	98	554.57
			423	68	384.80
			523	78	441.39
			623	80	452.71

Table 4.16 Punch pressure at various temperatures for a punch depth of 3mm for Al-Zn-Mg alloys at 0.45 strains

Alloy	Strain	Punch depth	Temperature (K)	Load (N)	Punch pressure (MPa)
Al-5Zn-1Mg	0.45	3 mm	303	64	362.17
			423	46	260.31
			523	52	294.26
			623	56	316.9
Al-10Zn-1Mg	0.45	3 mm	303	60	339.53
			423	64	362.17
			523	44	248.99
			623	42	237.67
Al-15Zn-1Mg	0.45	3 mm	303	93	526.27
			423	69	390.46
			523	64	362.17
			623	62	350.85



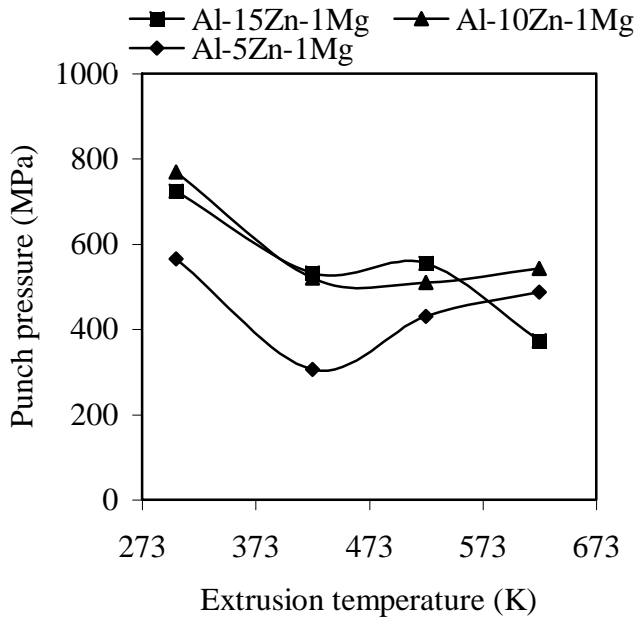
(a) Punch depth of 10mm for Al-Zn-Mg alloys at 0.1 strains



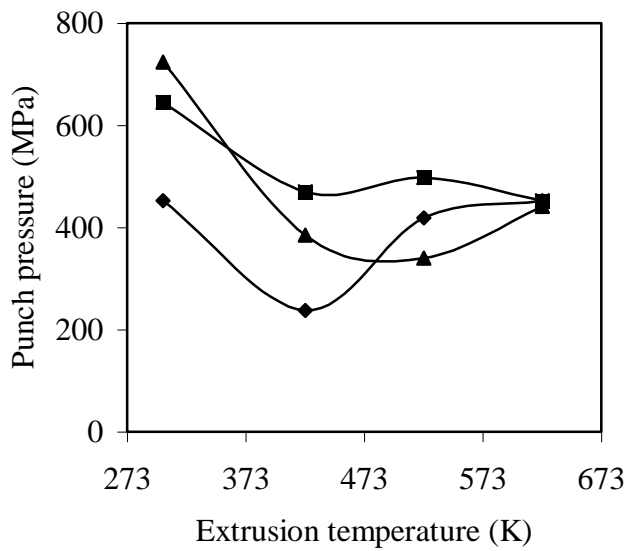
(b) Punch depth of 5mm for Al-Zn-Mg alloys at 0.15 strains

Fig. 4.29 Variation of punch pressure against temperatures for (a) punch depth of 10mm at 0.1 strains and (b) Punch depth of 5mm at 0.15 strains for

Al-Zn-Mg alloys

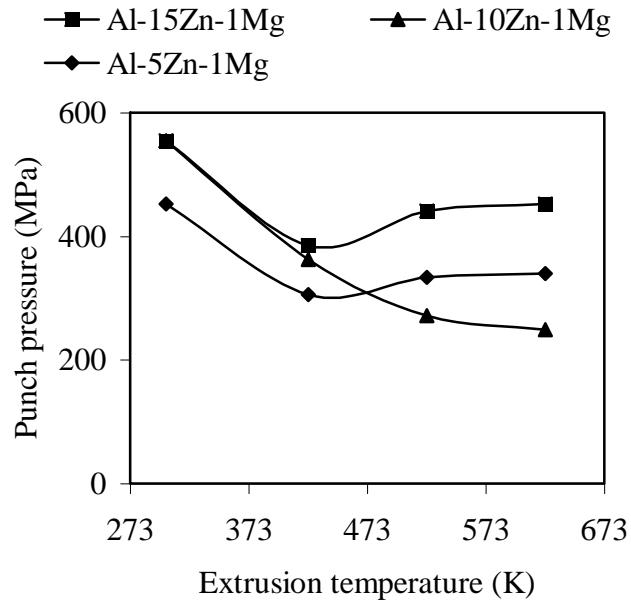


(a) 0.2 Strain

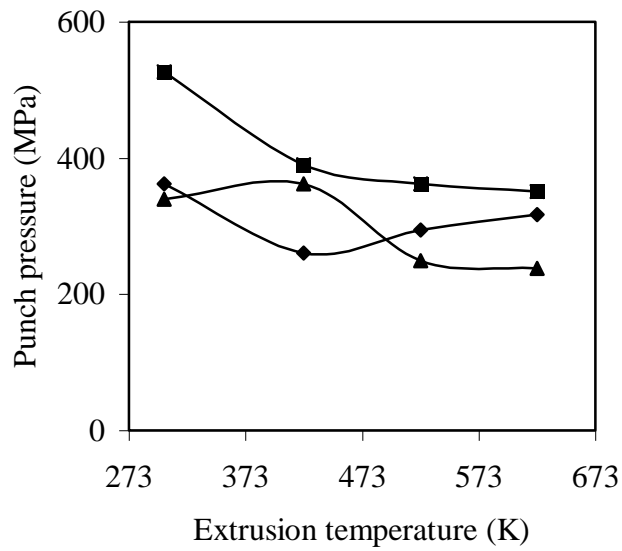


(b) 0.29 strain

Fig. 4.30 Variation of punch pressure against temperatures for a punch depth of 5mm for Al-Zn-Mg alloys at (a) 0.2 and (b) 0.29 strains



(a) 0.37 Strain



(b) 0.45 Strain

Fig 4.31 Variation of punch pressure against temperatures for a punch depth of 3mm for Al-Zn-Mg alloys at (a) 0.37 and (b) 0.45 strains

CHAPTER 5

DISCUSSIONS

5.1 MICROSTRUCTURAL ANALYSIS

In Al-Zn-Mg alloys, due to the long solidification interval (the temperature gap between the liquidus and solidus), microsegregation tends to be significant and homogenization needs lot of time, which causes the formation of second phase particles, some of which may be detrimental to the hot workability of the alloy as well as its final mechanical properties. Furthermore, the formation of a peripheral coarse grain structure is quite common in these alloys which can significantly degrade the mechanical properties. Low and higher magnification SEM images of the as-cast and homogenized microstructure of Al-Zn-Mg alloys are shown in Figs. 4.1 and 4.2 respectively. The α -Al phase with ($\alpha+\tau$) eutectic in inter dendritic regions and constitutive particles along the grain boundaries can be clearly seen. Perturbations on the surfaces of the grain boundary particles were observed in 4.2 (a to c). Similar structure was observed by Suarez et al. (2009) while working on Al-12 Zn-6 Mg alloy (Fig. 5.1). Shwe et al. (2008) also reported as cast structures of Al-5.8Zn-2.2Mg alloy Fig (5.2) which resembles the SEM images in the present investigation.

During the solidification of the Al-Zn-Mg aluminum alloys some intermetallic particles such as $MgZn_2$ phases are formed (Rokhlin et al., 2004, Lim et al., 2006, Mondal and Mukhopadhyay, 2005, Gupta et al., 2006, Ahmed et al., 2008). An X-ray diffraction (XRD, A JEOL JDX-8P-XRD) with a Cu K-alpha radiation over a range of $20^\circ - 94^\circ$ at $2^\circ/\text{min}$ on the Al-Zn-Mg alloys in the present study reveals $MgZn_2$ phases which is shown in Fig. 5.3 In addition, mutual solutions of different phases can result in the formation of new particles, for example, $Al_2Mg_3Zn_3$ compound (τ phase). Most of them have low melting points, which may result in incipient melting during hot deformation.

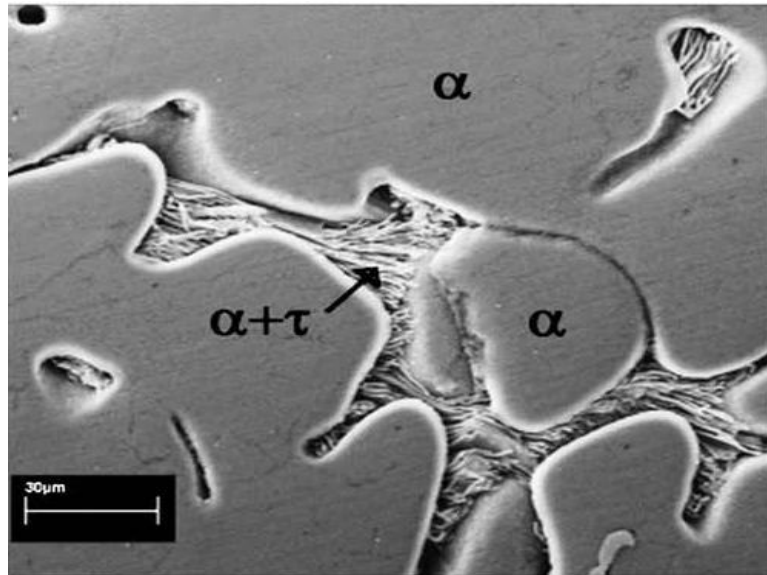
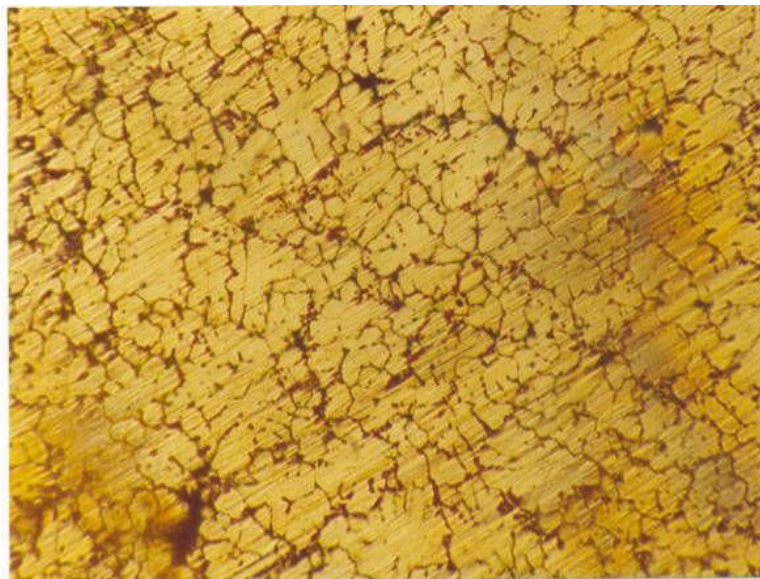
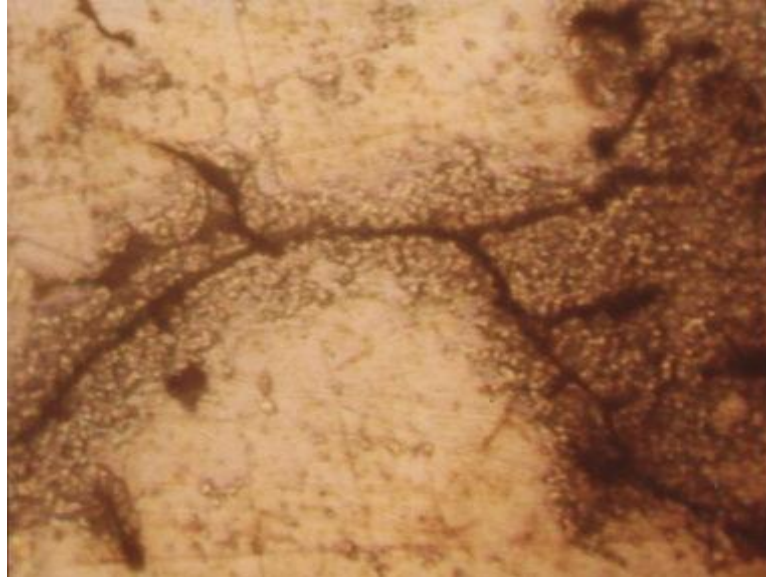


Fig. 5.1 Scanning electron micrograph of Al- 12 wt. % Zn-6 wt. % Mg alloy indicated microstructure that consists mainly by α -Al phase with ($\alpha+\tau$) eutectic in inter dendritic regions (Suarez et al., 2009).



(a) 40 X magnification



(b) Precipitate phases adjacent the grain boundaries before solution treatment, 200X

Fig. 5.2 Microstructure of as cast Al-Zn-Mg (a) 40 X (b) Precipitate phases along the grain boundaries before solution treatment, 200X (Shwe et al., 2008)

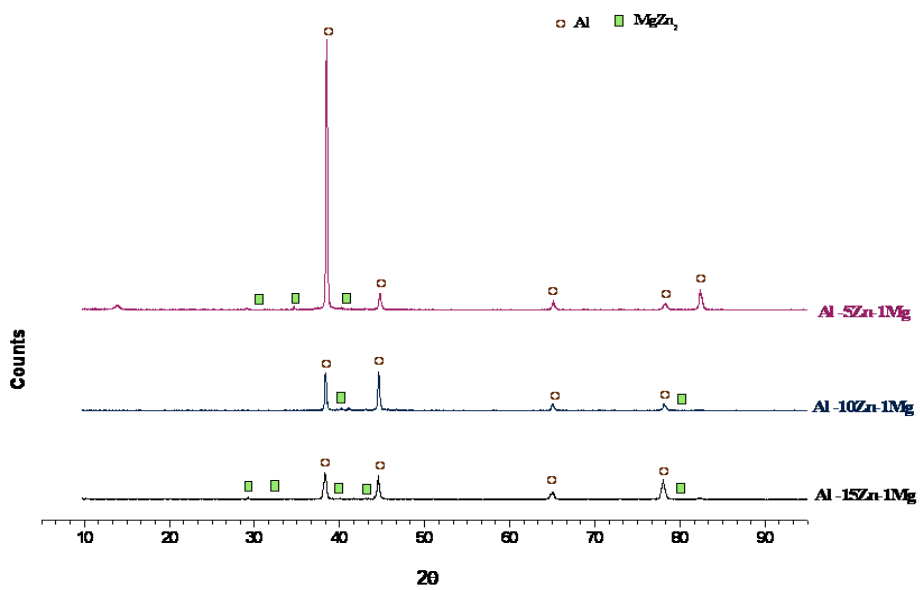


Fig. 5.3 X-Ray diffraction analysis of Al-Zn-Mg alloys

Segregation can also result in the formation of eutectic constitutive particles with low melting points in the grain boundary regions or inside the grains (Jackson and Sheppard, 1996, Robson and Prangnell, 2001). As mentioned earlier, the presence of low melting point (LMP) phases which may cause incipient melting during hot deformation can deteriorate the hot workability of aluminum alloys.

The formation of these precipitates may be attributed to the super-saturation of the structure with alloying elements occurring during solidification at high cooling rates while solidifying in a metallic mould. When the as-cast alloy is exposed to a homogenization treatment at a low temperature (< 743 K), there is a tendency for the alloying elements to precipitate out. As the temperature increases (> 743 K), the solubilities of these elements in the α -Al matrix increase (Belov et al., 2005, ASM Handbook 1992) and the formation of new particles is not expected. In the present study homogenization treatment was given at 623 K thus formation of new particles is expected.

The evolution of a typical grain boundary particle during homogenization at 663 K and 823 K was studied by Ali et al. (2011). It is clear from the above study that the dominant process at lower temperatures is the spheroidization of the grain boundary particle, while at higher temperatures the decrease in the size of the grain boundary particle is the main evolution process. Both spheroidization and decrease in the size of the grain boundary particle is observed in the present study (4.2 b).

5.2 VICKERS HARDNESS

The hardened state of the Al-Zn-Mg alloys is basically dispersion of η -precipitates that are at different stages of their development from GP-zones to the equilibrium phase. The stages entail gradual change in precipitate composition by increasing Zn/Mg ratio, which was inferred from APFIM studies conducted by (Stiller et al., 1999, Sha and Cerezo, 2004).

Prior to processing of Al-Zn-Mg alloys the precipitate volume fraction was estimated by Zhang et al. (2010) from the equilibrium phase diagram on the basis of the alloy composition. An Al alloy with 5 wt. % Zn and 1.6 wt. % Mg, each component with a

purity of better than 99.99%, was prepared by melt processing. If all Zn in solid solution had precipitated out as MgZn_2 during aging, it would form 5.93 wt. % MgZn_2 and leave 0.66 wt. % Mg in solid solution. Hence, the initial precipitate volume fraction (f_0) amounted to 3.2% in view of the densities $\rho_{\text{Al}} = 2.7 \text{ g cm}^{-3}$ and $\rho_{\text{MgZn}_2} = 5.16 \text{ g cm}^{-3}$.

It is obvious from the above estimation that as Zn content is increased in Al-Zn-Mg alloy by keeping Mg content fixed, volume fraction of MgZn_2 is supposed to increase resulting in highest hardness for Al-15Zn-1Mg and lowest for Al-5Zn-1Mg and intermediate for Al-10Zn-1Mg.

Higher strength was achieved in 7178-T6 alloy by increasing the amount of Zn over that in 7075 to obtain a higher volume fraction of the strengthening precipitates. The improved property combination in Al-Zn-Mg alloys can be achieved from careful balance of the precipitation hardening elements Zn and Mg, to maximize the strength without degrading other properties. (Krishnan and Krishna, 2007)

5.3 EFFECT OF TEMPERATURE ON YIELD STRENGTH

Difference in yield strength for different working temperatures selected for containerless backward extrusion is clear in this study. Undoubtedly, the difference in yield strength was led mainly by the differential microstructures resulted from the different temperatures. Al-Zn-Mg shows considerably good yield strength at room temperature since combination of zinc and magnesium forms second-phase particles distributed in ductile matrix, which gives rise to their very high strength. In general yield stress decreases and ductility increases as the temperature is increased. Similar behavior is shown by Al-5Zn-1Mg and Al-15Zn-1Mg till 473 K. Al-10Zn-1Mg showed similar trend till 573 K. Yield stress of Al-5Zn-1Mg and Al-15Zn-1Mg increased as temperature was increased to 573 K but further decreased at 673 K. In Al-10Zn-1Mg an increase in yield stress is found at 673 K. The increase in yield stress at 573 K and 673 K, which is against the general behavior, can be attributed to strain ageing. The diffusion coefficient increases exponentially with temperature and

thus, an increase in temperature will result in an increase in diffusivity of the solute atoms which interact with the moving dislocations and influence the yield stress. The further decrease in yield strength at 673 K for Al-5Zn-1Mg and Al-15Zn-1Mg may be due to grain growth, which eventually affects mechanical properties including the yield strength. Yield strength will generally tend to decrease with increasing grain size. The variations in yield strength at higher temperatures may be due to the microstructural difference including phases and size and distribution of MgZn₂ precipitates.

5.4 EFFECT OF ZINC CONTENT ON YIELD STRENGTH

The yield strength increased as Zn content increased from 5 to 15 wt% for all temperatures except 473 K where yield strength is not strongly dependant on Zn content. The increase in yield stress may have occurred because strength of Al-Zn-Mg alloys primarily dependent on two factors such as the amount of precipitate present in it and the morphology of the matrix. Precipitate content increases approximately in proportion to its zinc content.

If the Mg content is fixed in the phase, it is expected that the other species distribute consistently with the alloy composition in the precipitates; in other words, the alloy with the highest Zn content has the highest Zn containing precipitates.

At 473 K most of the precipitates may be dissolved thus not showing an increasing trend of yield stress in spite of the increase in Zn content.

An exception is also seen for Al-10Zn-1Mg at 573 K. This may be due to the high temperature which accelerates diffusion, leading to grain coarsening, which renders the material slightly softer. In this case, the yield strength will reduce.

5.5 EFFECT OF TEMPERATURE ON STRENGTH COEFFICIENT AND STRAIN HARDENING EXPONENT

Flow stress at room temperature for all the three chosen alloys are high since strain hardening is not relieved. So the strength coefficient at room temperature is high for all the alloys. The decrease in flow stress as the temperature is increased is as

expected for Al-5Zn-1Mg and Al-10Zn-1Mg till 573 K. The increase in flow stress upto 373 K in Al-15Zn-1Mg may be due to the dislocation pile up near the precipitates, which have been strained thus an increase in work hardening. Further increase in the temperature to 473 K decreased the flow stress. Towards 673 K flow stress increased for all the alloys. The strength coefficient is also high at 673 K. The peak or plateau in strength coefficient towards 673 K is due to the ageing processes occurring in the alloys containing atoms, which can rapidly and strongly segregate to dislocations and lock them during straining, the phenomenon is commonly referred to as dynamic strain ageing (DSA).

Dynamic strain ageing is a well-known phenomenon in a number of alloying systems, including the 7XXX series aluminium alloys. The physical origin is the repeated pinning and un-pinning of moving dislocations by diffusing solute atoms and the phenomenon is thus highly temperature and strain rate dependent (Magnus and Birger, 2010). Due to the physical nature of this interaction, the extent of it is highly dependent on temperature and strain rate through the mechanisms of diffusion and thermal activation. The process of aging occurs more rapidly at higher temperatures; because diffusion of the elements responsible for ageing is aided by raising the temperature. The maximum effect of DSA corresponds to such conditions, where the atoms can follow by diffusion the changes of the dislocation structure.

Dynamic strain ageing can cause numerous detrimental effects on the mechanical behavior such as loss of ductility, localized strain, increased stresses and inverse temperature and strain rate dependence of the flow stress as well as aesthetic problems with surface effects. The magnitude of the strain rate sensitivity (SRS) increases with temperature, indicating that the increased diffusivity promotes a more efficient DSA process (Magnus and Birger, 2010). The main signs of DSA observed in AA7030 by Magnus and Birger (2010) were serrated yielding, negative strain rate sensitivity as well as inverse temperature and strain rate dependence of the flow stress and ductility. Their findings include type D serrations, associated with moving bands

of localized deformation. They also proposed that temperature induced precipitation can play a significant role in the development of the DSA manifestations.

Studies on dynamic strain aging phenomenon of 3004 aluminum alloy by Kaiping Peng et al. (2005) in the temperature range of 253–453 K also revealed a serrated flow (DSA). They explained this behavior as; the mobile dislocations carrying by the plastic deformation are temporarily arrested at some localized obstacles, for example, the forest dislocations in the slip path.

Thus the variation of strength coefficient and strain hardening exponent with temperature are also well known physical manifestations of DSA. The increase in strain hardening exponent as temperature was increased to 373 K in Al-5Zn-1Mg and Al-15Zn-1Mg is due to the locking of pre existing dislocations either by solute atoms or precipitates and generation of new dislocations. This may be the reason for increasing the strain hardening exponent for Al-10Zn-1Mg from 373 K to 473 K too. Towards 673 K strain hardening exponent shows similar trend as strength coefficient. At these temperatures various atoms including solute atoms and a number of mechanisms can participate in the solute atom– mobile dislocation interactions thus causing dynamic strain ageing. Keh et al. (1968) were the first investigators to study DSA dislocation structures through the use of transmission microscopy. They showed that the increase in flow stress in the serrated region was attributable to significantly higher dislocation densities. This enhanced rate of dislocation multiplication with strain within the DSA region is due to the solute pinning.

It is widely accepted that a critical plastic strain, ϵ_c , is necessary for the occurrence of DSA phenomenon under certain temperature and strain rate conditions, and ϵ_c is a function of temperature under constant applied strain rate. The higher the temperature, the stronger the mobility of solute atoms, and the smaller the critical strain (Kaiping Peng et al., 2005). The local energy spectrum analysis in their study shows the existence of Mg element in that location. This strongly confirms that Mg atoms

certainly play an important role in pinning the moving dislocation and causes the serration flow.

The shift of strain ageing towards higher temperatures in this study is may be due to the presence of iron atoms in all the three chosen compositions. Bulk chemical analyses reveal the same.

5.6 EFFECT OF ZINC CONTENT ON STRENGTH COEFFICIENT AND STRAIN HARDENING EXPONENT

The strength coefficient increased as Zn content increased from 5 to 15 wt% for all temperatures selected for the study. The mechanical properties of Al-Zn-Mg alloys are largely dependent on alloying elements present in solid solution. These elements increase the strength mainly through solid solution or precipitation hardening. (Martin, 1998). An exception is seen for Al-15Zn-1Mg at room temperature. This may be due to the premature failure of the component because of lesser glide resistance of solute atoms in solid solute strengthening compared to the dislocation–dislocation interaction.

The strain hardening exponent increased as zinc content was increased to 10 wt% at 303K, 473 K and 673 K. This increase at 303 and 473 K may be due to dislocation interaction with each other and reaching configurations that restrict the movement of other dislocations. As the dislocation density increases there is an increase in the strain hardening exponent of the material. At 673 K, the increase in strain hardening exponent may be due to DSA caused by substitutional elements. This is due to the considerably lower diffusivities of the substitutional elements at room temperature and gains enough mobility, at high temperature such that the diffusivity approaches the dislocation velocity. The reduction in strain hardening at 373 and 573 K may be due to the less number of dislocations that intersect a unit area because of dissolution of pre existing precipitates. Further increase in strain hardening exponent as zinc content is increased to 15 wt% at 373 and 573 K is due to further increase in dislocation densities due to larger amount of precipitates compared to 10 wt%. The

decrease in strain hardening exponent at 303 and 673 K may be due to the premature failure of component. At 573 K the strain hardening exponent remained constant because of precipitate dissolution during deformation. Similar results were reported for Al–Zn–Mg alloy where dissolution and aging of the η phase was observed at 473 K (Gubicza et al., 2007).

5.7 EFFECT OF TEMPERATURE ON FRICTION FACTOR

The increase in friction factor from 303 to 473 K in Al-5Zn-1Mg and Al-15Zn-1Mg is due to the sticking tendency of the alloy to the die as temperature increases. Both these alloys showed a lower friction factor at 573 K since this temperature range is just enough for the diffusivity of solute atoms to segregate to the dislocations and lock them during deformation. Further increasing in friction factor at 673 K is due to the crack formation at the circumference of the ring. Friction factor decreased from 303 to 473 K in Al-10Zn-1Mg due to the increase in strain hardening exponent because of locking of pre-existing dislocations with the precipitates. The increase in friction factor at 573 K may be due to the heat losses to die thus the diffusivity is low for the solute atoms to segregate to the dislocations and lock them during deformation. The decrease in friction factor at 673 K supports this justification.

5.8 EFFECT OF ZINC CONTENT ON FRICTION FACTOR

The friction factor decreased as zinc content was increased to 10 wt% for all temperatures except 303 and 573 K. Further increase in Zn content to 15 wt% reduced the friction factor except for 473 and 673 K. The decrease in friction factor as zinc content increases is on expected line since Al-Zn-Mg alloys becomes harder with less tendency to stick towards the die as Zn content is increased. The increase in friction factor seen at 303, 573, 473 and 673 K may be due to early occurrences of plastic instabilities like shear bands. Consequently, no inferences can be drawn from these results without a more extensive investigation about the lubricating system.

5.9 EFFECT OF LUBRICATION ON FRICTION FACTOR

In the present study graphite was used as a lubricant. Graphite exhibits low friction because of their layered structures. Each layer contains strong bonds that make it resistant to breakup and thereby enable it to carry substantial load. Weak bonds between the layers enable them to slide readily over one another. Direct microscopic observations of the dynamics of solid lubrication show that sliding is accompanied by severe ductile shear of the solid lubricant film (Sloney, 1978). This implies that to provide a low friction factor, the solid lubricant must have low shear strength. The friction factor, m was low (0.31 – 0.39) while using graphite lubricant. Low shear strength alone does not ensure lubrication if the material does not adhere to the lubricated surface. It must be thermodynamically stable in the environment of application too. The change in friction factor with respect to temperature is negligible in the case of graphite lubricant. Layer lattice is a term used to describe crystal structures that consist of basal planes that are parallel to each other and consist of hexagonally oriented atoms (Fig. 5.4). The spacing between the planes is the c-spacing. The spacing between the atoms within the basal planes is the a-spacing.

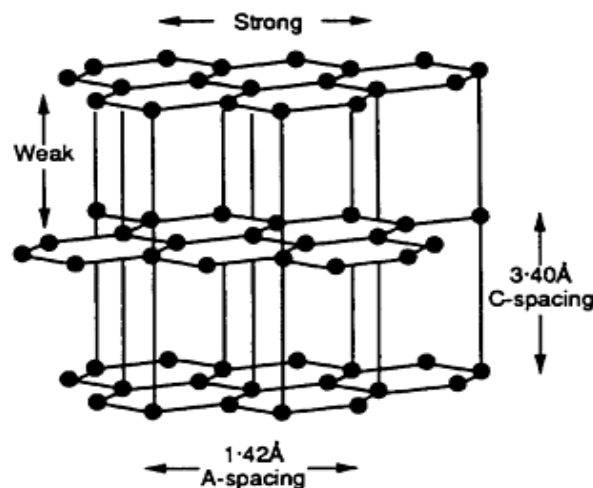


Fig.5.4 Structure of graphite (The individual sheets consist of closely packed atoms, separated by a relatively large distance from neighboring sheets).

In spite of its desirable crystal structure, graphite is not an intrinsic solid lubricant. It lubricates in a normal air atmosphere, but fails to lubricate at high altitudes or in vacuum. Savage (1948) reported convincing experimental evidence that graphite must adsorb moisture or some other condensable vapor such as hydrocarbons in order to be lubricative. This model appeared to be substantiated by the observation that, even in the presence of condensable vapors, graphite failed to lubricate above the desorption temperature. However, Peterson and Johnson (1954) observed that graphite again becomes lubricative at high temperatures when the lubricated metal becomes visibly oxidized. Restoration of lubrication at about 698 K was due to interaction of graphite with oxides of the metal. The surface oxides were thought to promote adhesion of the graphite to the lubricated surfaces. The maximum temperature for lubrication with graphite films is limited by oxidation to about 823 K. Al-Zn-Mg alloys readily oxidizes at higher temperature chosen for study and thus must have promoted adhesion of the graphite to them. Therefore the result shown by graphite lubricant is also in accordance with the above study.

5.10 STRESS ANALYSIS OF BACKWARD EXTRUSION IN Al-Zn-Mg ALLOYS WITH AND WITHOUT CONTAINER BASED ON“DIPPER MODEL”

5.10.1 The Force-Stroke Diagram

Force decreases with stroke for container backward extrusion because the force for axial upsetting zone decreases as material under punch decreases while that for vertical upsetting zone increases. The decrease is more and the increase is less as undeformed depth, b decreases continuously. At higher extrusion strains the decrease in force with stroke is rapid.

In containerless extrusion as material below the punch decreases, force increases. Force is increasing with stroke. At all strains force-stroke diagram is parallel to each other for deformation at room temperature. Higher the strain higher is the punch pressure. At room temperature Al-5Zn-1Mg requires lesser force, Al-10Zn-1Mg requires more force and Al-15Zn-1Mg requires maximum force for each strain.

5.10.2 Theoretical Punch Pressure Analysis

Theoretical punch pressures are obtained by dividing force by area of punch, which is constant. Containerless extrusion requires lower punch pressure than container extrusion due to absence of container wall billet friction. Punch pressure for containerless extrusion follows power law while that for container extrusion is linear. Rate of increase ($dP_p/d\epsilon$) is very high for container extrusion than in containerless extrusion at the optimum temperature of warm extrusion for each composition. At different temperatures the flow stress is different for each composition as K and n varies with temperature.

Optimum temperature is 373 K for Al-5Zn-1Mg and Al-15Zn-1Mg and 473 K for Al-10Zn-1Mg for warm extrusion as the forces are the least. This effect is explained due to dynamic strain ageing. The diffusion coefficient increases exponentially with temperature and thus, an increase in temperature will result in an increase in diffusivity of the solute atoms which helps to catch up with the faster moving dislocations and sustain DSA at hot working temperatures.

All the three compositions are used in equilibrium conditions. There will be more amount of $MgZn_2$ in Al-15Zn-1Mg, less in Al-10Zn-1Mg and least in Al-5Zn-1Mg at room temperature. Workability depends not only on material characteristics but also on process variables, such as strain, temperature, and stress state. In other words, extrudability can be deteriorated by two factors: (i) unfavorable processing conditions and (ii) the presence of large second-phase particles. The effect of composition for containerless extrusion at room temperature, 373 K and 473 K reveals the same

5.11 STRESS ANALYSIS OF BACKWARD EXTRUSION IN Al-Zn-Mg ALLOYS WITH AND WITHOUT CONTAINER BASED ON EXPERIMENTATION

5.11.1 The Force-Stroke Diagram

Force-stroke diagrams of Al-Zn-Mg alloys at various temperatures did not show a trend of increasing forces with respect to extrusion strains. It can also be noted that

punch travel is maximum in the case of 0.1 strain and minimum in the case of 0.45 strains for all temperatures. It is because there is an excessive material to material shearing taking place in the vicinity of punch corner face and thus, tresca shear friction coefficient of 0.5 plus the slip coefficient of friction are encountered. This high friction may result in various limits to the attainable deformation. It is obvious that tearing and cracking are accentuated by high friction. The cracks developed on a billet of 25 mm diameter may propagate at a faster rate compared to a billet of 50 mm diameter. Zhang et al. (2010) found that the average size of η (MgZn_2) precipitates decreased slightly during deformation. This may be due to (1) disintegration of precipitates during deformation, (2) formation of new small precipitates, and (3) dissolution of pre-existing large precipitates. To analyze the effect of processing and constitution on the strength of the material, the simplifying assumption is made that the various contributions to the strength of the material from solutes (σ_{SS}), precipitates (σ_P), dislocations (σ_{Disl}) and grain boundaries (σ_{GB}) can be simply linearly superimposed:

$$\sigma = \sigma_{SS} + \sigma_P + \sigma_{GB} + \sigma_{Disl}$$

The strengthening effects of solutes in Al–Zn–Mg alloys can be represented according to Dixit et al. (2008) as

$$\sigma_{SS} = MA_{Zn}c_{Zn}^{2/3} + MA_{Mg}c_{Mg}^{2/3}$$

Where M (≈ 3) is the Taylor factor for tensile deformation and $A_{Zn} = 3.1$, $A_{Mg} = 20.5$ are the strengthening coefficients of Zn and Mg in Al, respectively. The concentrations c_{Zn} and c_{Mg} are given in weight per cent. They found that in contrast to σ_{SS} and σ_P , the strengthening from cells/subgrains (σ_{GB}) or forest dislocations (σ_{Disl}) increased monotonically with imposed strain, owing to increased dislocation density, with progressing deformation. The trend shown by force stroke diagrams during containerless backward extrusion and cracking of billets may be because of these high dislocation densities.

5.11.2 Experimental Analysis Of Punch Pressure

Punch pressure against temperature at selected punch depth at various strains for Al-Zn-Mg alloys were plotted in Fig.4.29 to 4.31. At room temperature Al-5Zn-1Mg requires lesser punch pressure, Al-10Zn-1Mg requires more punch pressure and Al-15Zn-1Mg requires maximum punch pressure for 0.1 and 0.37 strains, whereas for other strains except 0.45, Al-5Zn-1Mg requires lesser punch pressure, Al-15Zn-1Mg requires more punch pressure and Al-10Zn-1Mg requires maximum punch pressure. This behavior is because of large amount of $MgZn_2$ precipitates in Al-15Zn-1Mg compared to Al-10Zn-1Mg which increases the strength but reduces the ductility. The properties of these alloys, determined by microstructural features, are affected by the nature of the aluminium matrix phase, the various second phases as well as the interaction between them. Workability is in fact affected by all parameters affecting the fracture of the material under processing. It is strongly dependent on the size and density of second-phase particles which are in turn dependent on the chemical composition and homogenization treatment. On the other hand, compressive stresses superimposed on shear stresses during the deformation process can have a significant influence on closing small cavities or limiting their growth and thus enhancing workability. Because of the important role of the stress state, it is not possible to express workability in absolute terms.

It's to be noted that at 423 K, where most of the precipitates are dissolved, Al-5Zn-1Mg requires lesser punch pressure, Al-10Zn-1Mg requires more punch pressure and Al-15Zn-1Mg requires maximum punch pressure for all strains except 0.1, where billet is fractured as a result of the presence of large intermetallic particles or even the multiplication of local melting and large particles. As the liquation occurs of the compound at the grain boundary regions, which render the alloy brittle and thus adversely affects the ductility and other mechanical properties. Failure at low levels of plastic strain can also be due to the early occurrence of plastic instabilities, such as shear bands and can be attributed to insufficient strain hardening and strain rate hardening capability of these materials (Wang, 2004). Therefore, in warm extrusion,

extrusion strain depends on the alloy composition and the microstructure formed during casting and developed during homogenization.

At 523 K, Al-10Zn-1Mg and Al-15Zn-1Mg showed a lesser punch pressure compared with 423 K for all the strains. This may be due to the change in morphology of the precipitates in Al-5Zn-1Mg at 523 K. In practice, the morphology of precipitates is seldom a suitable variable for manipulation using conventional forming, although the same precipitation phases, such as the η phase in Al-Zn-Mg alloys (Gjonnes and Simesen, 1970, Degischer et al., 1980) have multiple morphologies. During thermo-mechanical treatments, the precipitation process follows a fixed transformation sequence dominated by the precipitation kinetics and thermodynamics so that the precipitates generally have a simple orientation relationship with the matrix and this determines their unique morphology, such as rods or platelets (Degischer et al., 1980). The results to date have established that the high local strains imposed by containerless backward extrusion are effective in altering the precipitate orientations within the matrix. This potentially may provide an effective method for manipulating the precipitate morphology and obtaining unique microstructures that are significantly different from those formed by conventional forming. Presence of comparatively coarse dendrite also has a role in enhancement of properties. Role of matrix morphology on the punch pressure becomes more pronounced in Al-Zn-Mg. These microstructural changes are, however, not the subject of this study

At 623 K, Al-5Zn-1Mg and Al-10Zn-1Mg requires more punch pressure than that at 523 K. This effect is explained due to dynamic strain ageing. It occurred in the range of 523-623 K, for Al-5Zn-1Mg and at 623K, for Al-10Zn-1Mg and Al-15Zn-1Mg alloys. Dynamic strain ageing is totally undesirable during mechanical processing. Therefore this temperature range should be avoided while working Al-Zn-Mg alloys. Below the recrystallization temperature and above room temperature warm working is to be done to maximize the advantages and minimize the disadvantages of both hot and cold working.

Al-15Zn-1Mg showed a lower punch pressure because of fracture of billet along vertical direction. Al-Zn-Mg alloys are known for having rather poor hot workability

due to the presence of dissolved and later precipitated elements in the form of large particles that raise flow stress and cause the actual temperature of the extrudate to increase above the solidus temperature, leading to hot tearing. Hot tearing represents the separation or failure of the product as a result of a sequence of phenomena consisting of local melting, crack formation and final fracture of the product. In the case of the Al-Zn-Mg alloys, the phases that deteriorate the extrudability are Al-Mg-Zn eutectic phases which are mostly located at the dendrite boundaries. GB particles deteriorate the hot workability of the alloy in addition to mechanical properties since they are hard and brittle especially when located at the grain boundary regions. In order to avoid the detrimental effects of these particles, they should be dissolved during the homogenization treatment. If the particles are not dissolvable, they should be spheroidized.

A very noticeable feature of Al-Zn-Mg-based alloys aged at high temperatures is the existence of “precipitate free zones” (PFZs) along grain boundaries (Cornish and Day, 1969, Unwin et al., 1969). So the possibility of the same in the fracture of billets at high temperatures cannot be ruled out. These features are believed to affect the mechanical properties of Al-Zn-Mg alloys (Thomas and Nutting, 1960, Ryum 1969, Unwin and Smith, 1969, Muraki et al., 1969, Domont et al., 2004, Morgeneyer et al., 2008). Researches correlating mechanical properties (proof stress and elongation) to microstructural parameters (width of PFZ and the size of grain boundary precipitates) have revealed that the presence of PFZ adversely affects the fracture properties of the alloys (Ogura et al., 2006). The presence of PFZs also implies that the nucleation of precipitates is affected in the vicinity of grain boundaries. Formation of PFZs is generally explained by one of two mechanisms, either vacancy depletion or solute depletion. The vacancy depletion mechanism (Taylor, 1963, Embury and Nicholson, 1965, Lorimer and Nicholson, 1966) takes into account the effects of vacancy sinks during quenching, which result in retarded precipitation around grain boundaries compared with that in grain interiors. Embury and Nicholson (1965) attributed the formation of PFZs to the vacancy concentration being depleted to a level below the critical concentration required for precipitation. On the other hand, solute depletion theory takes into account depleted solute concentrations near grain boundaries

(Cornish and Day, 1969, Varley et al., 1957). However, it is not studied which of these mechanisms is the most important in Al–Zn–Mg alloy subjected containerless backward extrusion at various temperatures.

The present study shows that the composition of precipitates and correspondingly that of the residual solid solution can be tuned by adjusting the alloy composition and the processing temperature.

The optimum temperature for containerless backward extrusion would be 423 K for Al-5Zn-1Mg and 573 K for Al-10Zn-1Mg and Al-15Zn-1Mg alloys since the punch pressures are least at those temperatures.

CHAPTER 6

FINITE ELEMENT ANALYSIS OF CONTAINERLESS BACKWARD EXTRUSION OF Al-Zn-Mg ALLOYS

6.1 PROBLEM STATEMENT

Finite element method is applied to containerless backward extrusion of Al-Zn-Mg alloy billets using a high speed steel punch and a base plate, with an objective to generate the finite element grid deformation of the billet which can be used to judge the material deformation pattern during the process and to determine the Von-Mises stress from each analysis.

6.2 PROBLEM DESCRIPTION

- (i) Finite element model of the containerless backward extrusion is formulated using ANSA by taking values of friction factor and other material properties from the present experimental work on “Flow and frictional properties of Al-Zn-Mg alloys”.
- (ii) The height and diameter of billets are kept constant except for one case where diameter is chosen as 40 mm for the same height.

6.3 DETAILED STEPS OF THE FINITE ELEMENT ANALYSIS

Flow properties of Al-Zn-Mg alloys estimated from compression and ring compression tests are taken as basis to formulate the present problem.

6.3.1 Pre-processing

The geometrical dimensions and other properties are listed as follows.

Die: - Base plate diameter = 100 mm
Punch diameter = 15 mm

Billet: - Cylindrical billet of 100 mm diameter and 50 mm height

Die properties: The material selected for the die is high speed steel with following mechanical properties

- (i) Young's modulus = 210GPa
- (ii) Poisson's ratio = 0.29
- (iii) Yield strength = 2000 MPa

6.3.2 Model Generation

The ultimate purpose of a finite element analysis is to recreate mathematically the behavior of an actual engineering system. In other words, the analysis must be an accurate mathematical model of a physical prototype. In the broadest sense, this model comprises all the nodes, elements, material properties, real constants, boundary conditions, and other features that are used to represent the physical system.

The steps involved in model generation are

- (i) CAD will be generated using PRO E. Convert the PRO E file into IGES.
- (ii) Import the IGES file in the ANSA. Change the LENGTH into the required element size.
- (iii) Clean up the CAD. Fix the blue & red lines if any.
- (iv) Start the 2D surface meshing.
- (v) Create volumes as per the requirements and create solid elements like tetrahedral brick using those volumes.
- (vi) Give the section properties to the solid elements as per the DYNA section card and apply the element formulation No 13 (Tetrahedron with bulk forming formulation).

- (vii) Apply the Material properties to the solid elements as per the DYNA MAT card. There are many material models available in the LS Dyna. “Strain rate sensitive Power law Plasticity” is the material model chosen for the present study.
- (viii) Apply the boundary conditions like CONTACT, SPC and NODAL RIGID BODIES. As per the requirement, “CONTACT_SURFACE_TO_SURFACE” is used in the present study.
- (ix) Apply the load in the form of Load Vs Time graph.
- (x) Give the output requests like D3PLOT, GLSTAT, MATSUM etc. where D3PLOT is the animation file which contains stress, strain, deformation plot. GLSTAT will give the total energy consumed in the process and MATSUM will give the energy stored in each material.
- (xi) Give the control cards which are useful while running the solution (CONROL_CONTACT, CONTROL_PARALLEL_CONTROL_REMESHING, CONTROL_TERMINATION etc)

6.3.3 Solving

LS DYNA is the solver used for the solving the present problem. This will solve the problem using the below said equation.

$$F = Mx'' + Cx' + Kx \quad (6.1)$$

where M=Mass

C= Damping coefficient

K=Stiffness

x= Displacement.

x'' = Acceleration

x' =Velocity

F= Load or Force.

This equation is purely time dependent. The region solver will calculate the parameter called “Time step”. i.e. time at which each calculation cycle will complete and give the result.

$$DT=L/C \tag{6.2}$$

where L= Characteristic length of the element. i.e. minimum length of the element whether it may be side length or the diagonal length whichever is minimum. It will calculate for each element and finally consider whichever is least of all for further calculation purposes.

C=Velocity of the sound wave passing through that element. Velocity of the sound wave in turn depends on the below-said relation.

$$C = (\sqrt{E}) / \rho \tag{6.3}$$

where E =Young’s modulus.

ρ = Density of the material.

From the above relation it can be concluded that time step can be improved by varying E and ρ . Actually in physical meaning varying length is better than varying of E and ρ because the latter will affect the stress and strain values due to variation in material properties which is not so in real condition.

6.3.4 Material Model 64: Strain Rate Sensitive Power-Law Plasticity

This material model follows a constitutive relationship of the form:

$$\sigma = k\varepsilon^m \dot{\varepsilon}^n \tag{6.4}$$

where σ is the yield stress, ε is the effective plastic strain, $\dot{\varepsilon}$ is the effective plastic strain rate, and the constants k , m , and n can be expressed as functions of effective plastic strain or can be constant with respect to the plastic strain. The condition of no strain hardening can be obtained by setting the exponent of the plastic strain equal to a very small positive value, i.e. 0.0001. This model can be combined with the superplastic

forming input to control the magnitude of the pressure in the pressure boundary conditions in order to limit the effective plastic strain rate so that it does not exceed a maximum value at any integration point within the model. A fully viscoplastic formulation is optional. An additional cost is incurred but the improvement in results can be dramatic.

6.4 CONTACT ALGORITHM

Contact algorithms in LS-DYNA currently can treat any arbitrarily shaped surface by representing the surface with a faceted mesh. Occupant modeling can be treated this way by using fine meshes to represent the head or knees. The generality of the faceted mesh contact suffers drawbacks when modeling occupants, however, due to storage requirements, computing costs, and mesh generation times. The geometric contact entities were added as an alternate method to model cases of curved rigid bodies impacting deformable surfaces. Much less storage is required and the computational cost decreases dramatically when compared to the more general contact.

Geometric contact entities are developed using a standard solid modeling approach. The geometric entity is defined by a scalar function $G(x, y, \text{ and } z)$. The solid is determined from the scalar function as follows:

When $G(x, y, z) > 0$, the point (x, y, z) is outside the solid.

$G(x, y, z) = 0$, the point (x, y, z) is on the surface of the solid.

$G(x, y, z) < 0$, the point (x, y, z) is inside the solid.

Thus, by a simple function evaluation, a node can be immediately determined to be outside the solid or in contact. If the node is in contact with the solid, a restoring force must be applied to eliminate further penetration. A number of methods are available to do this such as Lagrange multipliers or momentum based methods. The penalty methods were selected because it is the simplest and most efficient method. Also, in the present application the impact velocities are at a level where the penalty methods provide

almost the identical answer as the exact solution.

Using the penalty method, the restoring force is proportional to the penetration distance into the solid and acts in the direction normal to the surface of the solid. Thus, the penetration distance and the normal vector must be determined. The surface normal vector is conveniently determined from the gradient of the scalar function.

6.4.1 Tetrahedron Element With 12 Degrees-of-Freedom

Automatic mesh generators often use tetrahedron element extensively and add the simple element rule which is used to place node 4. The parametric coordinates, (r, s, t), take on values between 0 and 1. The shape functions are given by:

$$N1(r, s, t) = r$$

$$N2(r, s, t) = s$$

$$N3(r, s, t) = 1 - r - s - t$$

$$N4(r, s, t) = t$$

6.4.2 Fully Integrated Tetrahedron Element With 24 Degrees-of-Freedom

The twenty-four degrees of freedom tetrahedron element is derived from the ten node tetrahedron element by following the same procedure used for the forty-eight degree of freedom brick element (Yunus et al., 1989, 1991). This element has the advantage that shell nodes can be shared with its nodes and it is compatible with the brick element discussed above. The accuracy of this element is relatively good, at least when compared to the constant strain tetrahedron element.

During implementation the references (Yunus et al., 1989, 1991) is not strictly followed. In order to prevent locking in applications that involve incompressible behavior, selective reduced integration is used with a total of 5 integration points. Although this is rather expensive, no zero energy modes exist. The same approach is used in determining the rotary mass that is used in the implementation of the shell elements.

When two sides of the adjacent bricks made from five tetrahedron are together, it is likely that four unique triangular segments exist. This creates a difficulty in TAURUS which uses the numbering as a basis for eliminating interior polygons prior to display. Consequently, the graphics in the post-processing phase can be considerably slower with the degeneration. However, marginally better results may be obtained with five tetrahedrons per hexahedron due to a better constraint count.

6.4.3 Post Processing

Post processing was done in hyperview tool which has been developed by Altair Inc. In the post processing it was found that the results from the solver after solution are completed. This tool will support many solvers like Abacus, Nastran, LS Dyna, Pamcrash, Radioss etc. The output results in the present study were concerned with LS Dyna.

6.5 FINITE ELEMENT FORMULATION OF THE PROBLEM

6.5.1 Assumptions Made in Finite Element Formulation of the Problem

The following assumptions are made when creating this model:

- i) Material is homogeneous and isotropic.
- ii) Material obeys power law equation of plasticity.
- iii) The bottom surface of the billet material is fixed.
- iv) The load applied on the billet by the punch is time dependent
- v) The punch is a non deformable part.
- vi) The punch and the billet are in surface to surface contact.

Conventional steps followed in finite element analysis of the problem are as follows.

6.5.2 Pre-processing

This step involves geometrical modelling of the physical problem, assigning the material properties, choosing the proper material behaviour model, meshing the model with suitable elements, generating required contact pairs, and assigning boundary conditions.

6.5.3 Solving

This step involves solving the problem with suitable solver settings. In this step, the solver performs the finite element computations using the inputs given at the pre-processing stage and solver settings.

6.5.4 Post-processing

At this stage, the solution of the problem could be read and graphically visualised as per the analysis requirement. To open the model



6.5.5 Steps involved for running the program

The steps are enumerated below:

- (i) Click on file
- (ii) Click input, then LS-DYNA option
- (iii) Select the folder required
- (iv) Click on the file, then click ok
- (v) Give all the inputs like load, time, material property, etc
- (vi) Then go for file option again, click output ls-dyna option
- (vii) Select the previous folder, file
- (viii) Select the model option in output window displayed, click ok
- (ix) Copy the solver file (ls_970_win32.exe) in to the above selected folder
- (x) Double click on the solver file, a window will be displayed
- (xi) Type as i=key file name, then enter
- (xii) Programs starts running

```
LS-DYNA, A Program for Nonlinear Dynamic
Analysis of Structures in Three Dimensions
Version: 1570a      Date: 11/28/2005
Revision: 6763.169  Time: 19:00:26

Features enabled in this version:
Shared Memory Parallel
ANSYS Database Format
ANSYS License

Licensed to:
Platform : PC WIN32(IUP8.1 SSE)
OS Level : Windows 2000/NT/XP
Hostname  : lenovo
Precision : Single precision (14M)
Unauthorized use infringes LSTC copyrights

please define input file names or change defaults :
>l=part.key ncpu=2 Input file: part.key

The native file format      : 32-bit small endian
Memory size from default   : 20000000

on UNIX computers note the following change:
ctrl-c interrupts ls-dyna and prompts for a sense switch.
type the desired sense switch: sw1., sw2., etc. to continue
the execution. ls-dyna will respond as explained in the users manual

type      response
-----
sw1.      a restart file is written and ls-dyna terminates.
sw2.      ls-dyna responds with time and cycle numbers.
sw3.      a restart file is written and ls-dyna continues calculations.
sw4.      a plot state is written and ls-dyna continues calculations.

***** notice ***** notice ***** notice *****
* This is the LS-DYNA Explicit Finite Element code. *
* Neither LSTC nor the authors assume any responsibility for *
* the validity, accuracy, or applicability of any results *
* obtained from this system. The user must verify his own *
* results. *

```

```
memory needed after input phase
memory required for explicit solution : 4856723
additional dynamically allocated memory: 134760

input of data is completed

initial kinetic energy = 0.0000000E+00
initialization completed

dt of cycle      1 is controlled by solid      element 42270

time..... 0.00000E+00
time step..... 4.35248E-09
kinetic energy..... 0.00000E+00
internal energy..... 1.00000E-20
spring and damper energy..... 1.00000E-20
system damping energy..... 0.00000E+00
sliding interface energy..... 0.00000E+00
external work..... 0.00000E+00
eroded kinetic energy..... 0.00000E+00
eroded internal energy..... 0.00000E+00
total energy..... 1.00000E-20
total energy / initial energy... 1.00000E+00
energy ratio w/o eroded energy... 1.00000E+00
global x velocity..... 0.00000E+00
global y velocity..... 0.00000E+00
global z velocity..... 0.00000E+00
cpu time per zone cycle..... 0 nanoseconds
average cpu time per zone cycle... 0 nanoseconds
average clock time per zone cycle... 5287 nanoseconds

estimated total cpu time = 9 sec ( 0 hrs 0 mins)
estimated cpu time to complete = 0 sec ( 0 hrs 0 mins)
estimated total clock time = 60892 sec ( 16 hrs 54 mins)
estimated clock time to complete = 60884 sec ( 16 hrs 54 mins)

1 t 0.00000E+00 dt 4.35E-09 flush i/o buffers
1 t 0.00000E+00 dt 4.35E-09 write d3plot file
2298 t 9.9776E-06 dt 4.35E-09 write d3plot file
4536 t 2.0000E-05 dt 4.35E-09 write d3plot file
5000 t 2.1768E-05 dt 4.35E-09 flush i/o buffers
6893 t 2.9997E-05 dt 4.35E-09 write d3plot file
9191 t 3.9999E-05 dt 4.35E-09 write d3plot file
10000 t 4.3520E-05 dt 4.35E-09 flush i/o buffers
11488 t 4.9997E-05 dt 4.35E-09 write d3plot file
13785 t 5.9999E-05 dt 4.35E-09 write d3plot file
15000 t 6.5283E-05 dt 4.35E-09 flush i/o buffers
16083 t 6.9997E-05 dt 4.35E-09 write d3plot file
18381 t 7.9999E-05 dt 4.35E-09 write d3plot file
20000 t 8.7045E-05 dt 4.35E-09 flush i/o buffers
20678 t 8.9996E-05 dt 4.35E-09 write d3plot file
22976 t 9.9998E-05 dt 4.35E-09 write d3plot file
25000 t 1.0881E-04 dt 4.35E-09 flush i/o buffers

```

6.5.6 Steps involved for applying load

The steps are enumerated below:

- (i) Click on file option on ANSA screen
- (ii) Input the file
- (iii) Click DECK option, then click LS - DYNA
- (iv) For applying load click node option, sub folders will be displayed
- (v) Select LIST option from the sub folders
- (vi) A load node window will be displayed, click on 1 in the window displayed then click edit
- (vii) Remove 1 in LCID box, press shift question mark on the keyboard
- (viii) Select on anonymous define curve, then click edit
- (ix) Apply load as per your requirements, then click ok
- (x) Click escape
- (xi) Go for database option and request for output files like d3plot, glstat, matsum etc

6.5.7 Steps involved for assigning material properties

The steps are enumerated below:

- (i) Click on the MATLIST option on ANSA screen
- (ii) Materials window will be displayed
- (iii) Click on any default MAT file (ex: MAT 24, MAT60, etc)
- (iv) Click on edit, a window of selected MAT file will be displayed.
- (v) Assign the material properties required like density, Young's modulus, Poisson's ratio etc
- (vi) Then press escape, all windows displayed will be closed

6.5.8 Steps involved in setting the time

The steps are enumerated below:

- (i) Click on CONTROL option and hold it
- (ii) 3 sub-buttons like control, keyword and title will be seen
- (iii) Go for control option
- (iv) sub-buttons like (A-B, I-L, S-S, T-Z etc) will be seen
- (v) Select the appropriate button as per your requirement. For example, when you click on T-Z button, a control card window will be displayed
- (vi) Give the time (termination time) required in the ENDTIM box (ex: 10 millisecond, 5 millisecond, etc.)
- (vii) After setting time click ok

6.6 SIMULATION PROCEDURE

The following procedure was adopted:

- 1) The FE model was built in ANSA, and discretising the plate with hexahedron elements were done
- 2) Boundary conditions were applied like SPC (single point constraint), load, control cards, output request, etc.
- 3) By doing so the model was ready for solving.
- 4) The file was Run in the solver (LS-DYNA)
- 5) Once running was completed, results were viewed

6.7 RESULTS AND DISCUSSION

The stress and strain distribution for Al-Zn-Mg alloys with diameter d_0 of 100 mm and height h_0 of 50 mm during containerless backward extrusion at room temperature was studied. It is seen that internal stresses developed by Al-15Zn-1Mg was maximum while Al-5Zn-1Mg was the least. The high internal stresses of the Al-15Zn-1Mg alloys compared with Al-10Zn-1Mg and Al-5Zn-1Mg is because of the

dispersion of η -precipitates that are at different stages of their development from GP-zones to the equilibrium phase.

It is noted that billet of h_0/d_0 ratio of 0.5 didn't show lateral displacement of material in Al-Zn-Mg alloys, which is a characteristics of containerless backward extrusion (Fig. 6.1 to 6.3) where as a billet with h_0/d_0 ratio of 1.25 shows bulging which is due to upsetting(Fig 6.4).

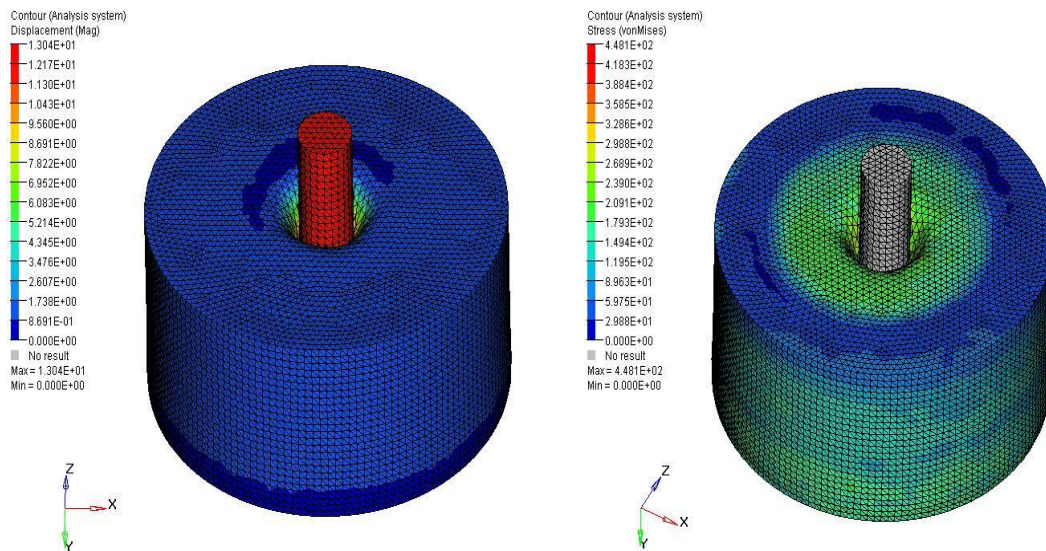


Fig.6.1 Stress and displacement distribution for Al-5Zn-1Mg billets of 100 mm diameter and 50 mm height during containerless backward extrusion at room temperature.

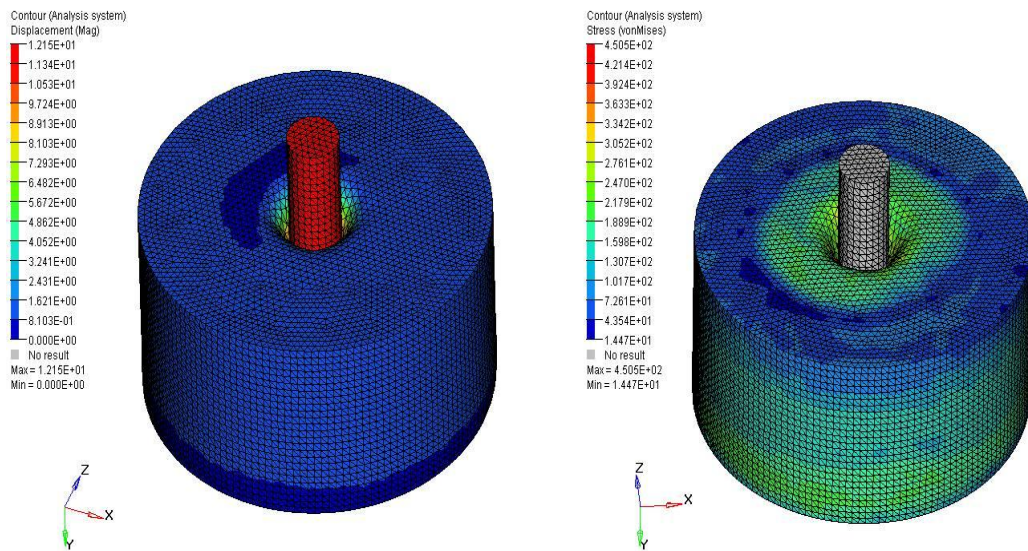


Fig.6.2 Stress and displacement distribution for Al-10Zn-1Mg billets of 100 mm diameter and 50 mm height during containerless backward extrusion at room temperature.

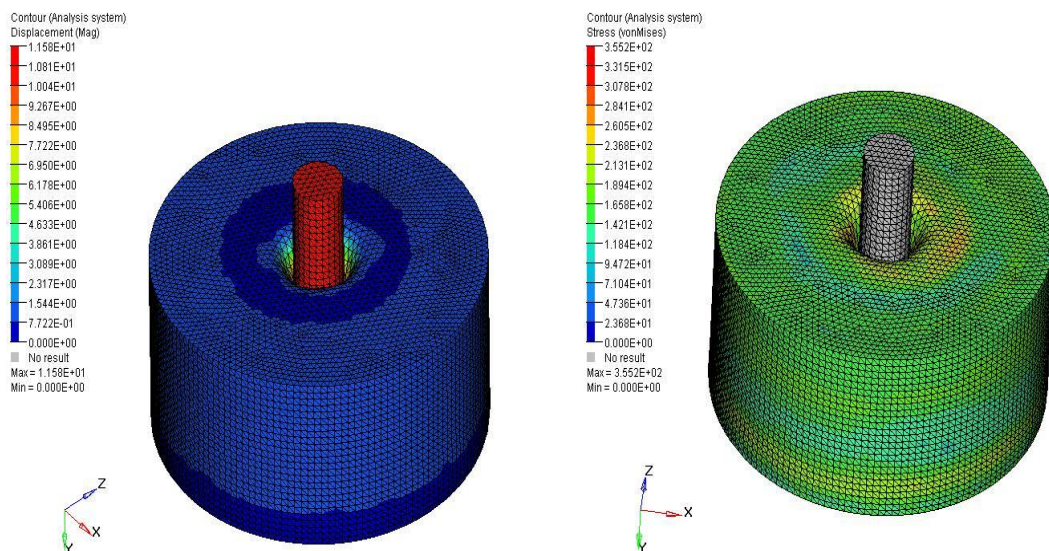


Fig.6.3 Stress and displacement distribution for Al-15Zn-1Mg billets of 100 mm diameter and 50 mm height during containerless backward extrusion at room temperature.

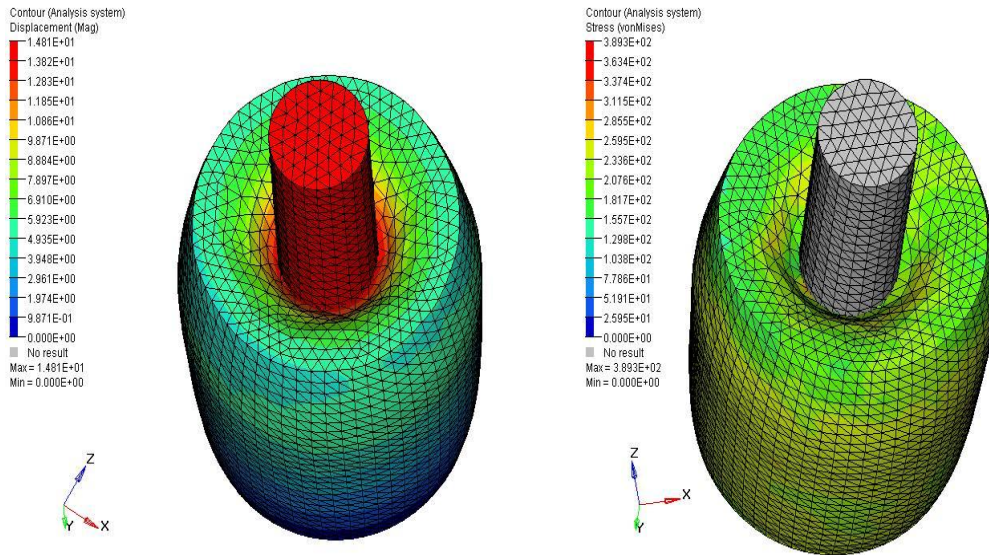


Fig.6.4 Stress and displacement distribution for Al-10Zn-1Mg billets of 40 mm diameter and 50 mm height during containerless backward extrusion at room temperature.

CHAPTER 7

CONCLUSIONS

1. From the flow stress and frictional analysis of Al-Zn-Mg alloys it can be concluded that all the three chosen Al-Zn-Mg alloys can be mechanically processed economically and with ease between 373 K and 573 K when coated with graphite as an effective lubricant. This would demand lesser forces; ensure adequate plasticity, minimization of embrittlement and reduced wear and tear of dies.
2. From the theoretical investigation on containerless backward extrusion of Al-Zn-Mg alloys it can be concluded as follows:
 - (i) Optimum warm extrusion temperature for Al-5Zn-1Mg and Al-15Zn-1Mg is 373 K and for Al-10Zn-1Mg is 473 K when coated with graphite as an effective lubricant. Lesser forces imply the possibility of the use of lower capacity presses and simplified design of tooling.
 - (ii) Containerless backward extrusion requires less than half of the force compared to conventional container extrusion.
 - (iii) Theoretical punch pressure is minimum for Al-5Zn-1Mg and maximum for Al-15Zn-1Mg and intermediate for Al-10Zn-1Mg at room temperature and at warm working temperatures.
3. From the experimental investigation on containerless backward extrusion of Al-Zn-Mg alloys it can be concluded as follows
 - (i) Initial height h_0 of billet, should be as small as possible to make upsetting difficult and diameter (d_0) of the billet should be large in comparison to punch diameter (d_p) to make extrusion strain smaller and extrusion process easier. In the present case the value of undeformed depth (b) is high and h_0/d_0 are varying from 1 to 2.5. Extrusion occurs

only at lower strains where the ratio is less than one. A study with h_o/d_o ratio much lesser than 1 and for smaller undeformed depth (b) is found feasible.

- (ii) Optimum warm extrusion temperature for Al-5Zn-1Mg is 423 K and for Al-10Zn-1Mg and Al-15Zn-1Mg is 523 K when it was carried out with graphite coating on the alloy to act as an effective lubricant. Lesser forces imply the possibility of the use of lower capacity presses and less simplified design of tooling. Hence, it could be concluded that theoretical predicted values using Dipper model agrees with experimentally determined values.
 - (iii) The punch pressure is minimum for Al-5Zn-1Mg, maximum for Al-15Zn-1Mg and intermediate for Al-10Zn-1Mg for billets which are not fractured at warm working temperatures. This fact too is agreeing with theoretical predicted values.
4. From the finite element analysis of containerless backward extrusion of Al-Zn-Mg alloys it can be concluded that for a billet of h_o/d_o ratio of 0.5 shows an absence of lateral displacement of material, which is a characteristic of containerless backward extrusion. Selection of optimum warm working temperature will reduce the forces for extrusion.
5. The domain where dynamic strain ageing exists must be considered when selecting operating conditions like working temperature and extrusion strain. Parameters such as composition and microstructure should also be considered because the existence of dynamic strain ageing is strongly dependent on if and how the solute species are present in the material. Dynamic strain ageing can also be a positive phenomenon if its domain is well-known. For example, it can be used as a thermo-mechanical treatment to increase the room temperature strength. It can also serve as a strengthener at elevated temperatures because of the associated increased strength and higher work hardening rate.

REFERENCES

- Ahmed, H., Eivani, A.R., Zhou, J., Duszczuk, J. (2008), Proc. Symp. Aluminum Alloys: Fabrication, Characterization and Application, TMS Annual Meeting, New Orleans
- Ali, Reza, Eivani, Jie, Zhou, Jurek, Duszczuk. (2011), "Microstructural Evolution During the Homogenization of Al-Zn-Mg Aluminum Alloys, Recent Trends in Processing and Degradation of Aluminium Alloys, 477-516.
- Altan, T., Oh, S. and Gegel, H.L. (1983)."Metal forming:Fundamentals and application." American society of Metals, USA., 48-53
- Altan, T., Oh, S. and Gegel, H.L. (1983)."Metal forming:Fundamentals and application." American society of Metals, USA. 83-88
- Altan, T., Ngaile, G. and Shen, G. (2004). "Cold and Hot Forging." ASM International, Materials Park., Ohio.
- Altinbalik, T., and Ayer, Ö.(2008). "A Theoretical and Experimental Study for Forward Extrusion of Clover Sections." Material and Design., Vol., 29-6, 1182-1189
- Aluko, O. and Adeyemi, M.B. (1998). "Warm Compression Test of Aluminium Alloy." J. Mat. Eng. Performan, ASM International, 7., 474-478
- Alvarez, O., Gonzalez, C., Aramburu, G., Herrera, R., Juarez-Islas, J., A. (2005), Materials Science and Engineering, A402, 320 -324.
- ANSYS, (1994), "ANSYS User's Manual: Theory", Vol.,IV, Swanson Analysis Systems, Inc, William, F H., Robert, M, C. (1993), "Metal Forming -Mechanics and metallurgy", prentice Hall, New Jercey, 62-65.
- ASM Handbook.(1992).10th ed., vol. 3, Alloy Phase Diagrams, ASM International, Metals Park, OH

ASM Handbook (1992), 10th ed., vol. 14, Metal Forming, ASM International, Metals Park, OH.

Avitzur, B. (1968) "Metal Forming, Processes and Analysis", McGraw-Hill, New York, 188.

Avitzur B. (1983), "Handbook of Metal Forming Processes", Wiley, New York, 150-151

Avitzur, B (1987), "Metal forming", Encyclopedia of Physical Science & Technology, 8, San Diego: Academic Press, Inc., 80–109

Ban, B, A. (2013), "The Study of Stress State in Indentation of a Flat Punch with Rounded Edge in Axisymmetric Backward Extrusion", International Journal of Mining, Metallurgy & Mechanical Engineering , Vol. 1, Issue 2, 122 - 127

Barisic, B., Jurkovic, M, and Kuzman, K(2002), "Numerical – experimental analysis of backward extrusion force", in: R. Cebalo, H. Schulz (Eds), Proceedings of the Eighth International Scientific Conference CIM 2002, Brijuni, Croatia, IV001-IV009

Barisic, B., Cukor, G and Math, M. (2004) "Estimate of consumed energy at backward extrusion process by means of modeling approach", Journal of Materials Processing Technology 153-154, 907-912.

Bashir, R., Mustafa Al-Maghrabi.(2012), "An Investigation of Metal Flow Behavior between Flat and Overlapping Dies during Copper Forging", 2nd International Conference on Materials, Mechatronics and Automation, Libya, 104 – 108

Belov, N., A., Eskin, D., G., Aksenov, A., A. (2005), "Multicomponent Phase Diagrams: Applications for Commercial Aluminum Alloys", Elsevier Science, New York

Berg, L, K, Gjønnnes, J, Hansen, V, Li, X, Z, Knutson-Wedel, M, Waterloo,G.(2001), "GP-zones in Al–Zn–Mg alloys and their role in artificial aging"Acta Mater., 49, 3443-3451.

- Betzalel Avitzur. (1992), "Friction during metal forming", ASM Handbook, – Friction, lubrication and wear technology, Vol. 18, 85
- Binder, H, and Lange, K. (1980), "Investigation on Open Die Extrusion of Solid Cylindrical Workpieces" (in German), Springer, Berlin, 124.
- Branimir, B, Nicolae, U, Zlatan, C.(2008), "Investigation of forming force at backward extrusion process on different aluminum materials", The International Conference of the Carpathian Euro-Region Specialists in industrial systems, 7th edition, Baia Mare, Romania
- Campbell, F.C. (2008). "Elements of Metallurgy and Engineering Alloys." ASM International, USA., 282-283
- Can, Y., Altinbalik, M.T., and Misirli, C, (2002), "An Investigation of the Early Stages of Open Die Forging-extrusion Process for Different Die Geometries." The Tenth International Conference on Machine Design and Production, ISBN 975-429-187-X, September 4-6, 2002, Umtik, Cappadocia, Turkey, 375-384
- Cannizzaro. (1992). "Limits of Open Die Forward Extrusion: Numerical Analysis and Experimental Tests." Twenty-ninth International Matador conference., Manchester., 441-444
- Chakraborty, J. (1988). "Theory of Plasticity." Butterwoth-Heinmann, UK., 7-10
- Charles,W., John, T. B, Raymond, F, V (1984), Tool and Manufacturing Engineering Handbook, Society of Manufacturing, Fourth Edition, Volume 2 Formic, 13.11-13.37.
- Cockcroft, M.G, and Latham, D.J (1968), "Journal of the Institute of Metals", Vol., 96, 33.
- Cooke, M. and Larke, E.C. (1945). J. Inst. Met., Vol. 71., 371-390
- Cornish, A, J, Day, M, K, B.(1969), J Inst Metals, 97, 44-52

Davis, J. R., Davis & Associates.(2007), ASM specialty Handbook, Aluminum and Aluminum Alloys, The Materials Information Society, ISBN-13: 978-087170-496-2, United States of America

Degischer, H. P., Lacom, W., Zahra, A., Zahra, C, Y. (1980), “Decomposition process in an Al-5% Zn-1% Mg alloy”, *Metallk Z*, 71(1), 231–238.

Dennis, W. H. (1961), *Metallurgy of the Non-Ferrous Metals*

Dieter, G. E. (2003) “Handbook of Workability and Process Design”, ASM International, USA.

Dixit, M., Mishra, R. S., Sankaran, K. K. (2008), “Structure-property correlations in Al 7050 and Al 7055 high-strength aluminum alloys” , *Materials Science and Engineering, A*, 478, 163–172.

Drozda, T., Wick, C, Bakerjian, R, Veilleux, R, F, Petro, L. (1984), *Tool and manufacturing engineer’s handbook: Forming*, 2, SME, 13-14

Dumont, D., Deschamps, A., Brechet, Y.(2004), “A model for predicting fracture mode and toughness in 7000 series aluminium alloys” *Acta Materialia*, 52, 2529-2540

Emad, M, A. (2014), “Microstructure Properties of Rapidly Solidified Al-Zn-Mg-Cu Alloys”, *Indian Journal of Materials Science*, Vol. 2014, <http://dx.doi.org/10.1155/2014/353698>

Embury, J, D., Nicholson, R, B. (1965), “The nucleation of precipitates: The system Al–Zn–Mg”, *Acta Materialia*, 13, 403-417

Frank, F, K., and Jay, S, G. (2005), “Metalworking: Bulk Forming”, *ASM Handbook Volume 14A*, ASM International, 421-439

Friauf, J, B. (1927), “The crystal structure of magnesium di- zincide”, *Phys, Rev*, 29, 34–40.

- Fukui, S., and Seino J. (1960), "Studies on the Cold Open-die Extrusion of Metals." J.Jap.Aero.Expl.Agency., 6., 82-92 (In Japanese)
- George, E, Dieter. (1988) "Mechanical Metallurgy", Mc-Graw Hill, 503-515, 616-634.
- Gjonnes, J., Simensen, C, J. (1970), "An electron microscope investigation of the microstructure in an aluminium–zinc–magnesium alloy", Acta Materialia, 18, 881-890
- Gubicza, J., Schiller, I., Chinh, N, Q., Illy, J., Horita, Z., Langdon T, G. (2007), "The Effect of Severe Plastic Deformation on Precipitation in Supersaturated Al-Zn-Mg Alloys", Materials Science and Engineering, A, 460-461, 77-85
- Gupta, R., K., Nayan, N., Ghosh, B., R. (2006), "Design of Homogenization Cycle for Various Grain Sizes of Aluminum Alloy AA2219 Using Diffusion Principles", Canadian Metallurgical Quarterly, 45(3), 347-352
- Haarschiedt K. and Lange, K. (1983), "Investigations on Open Die Extrusion of Thickwalled Hollow Cylindrical Workpiece", Springer-Verlag, Berlin, (in German)
- Hassan Sofuoglu, Hasan Gedikli, and Jahan Rasty. (2001) "Determination of friction coefficient by employing the ring compression tests", Journal of engineering materials and technology, Vol., 123, 338-348
- Hatch, J, E. (1985), "Aluminium – Properties and Physical Metallurgy", American Society for Metals, Ohio, USA, 50-52
- Hsu, T.C. and Young, A.J. (1967) "Plastic Deformation in the Compression Test of Pure Copper." J. Str. Analy. For Eng. Design, 2-2., 159-170
- Hsu, T.C. (1969). Standard Methods of Compression testing of Metallic materials at Room Temperature, ASTM Standards, pt. 31, Designation E9-70; elevated temperature compression tests, ASTM E209; Mater. Res. Stand, Vol. 9., 20-25, 47-53

Huang, Z., and Fu P. (2001). "Solution to Bulging Problem in the Open Die Cold Extrusion of a Spline shaft and Relevant Photoplastic Theoretical Study." J. Mater. Process. Technol., 114., 185-188

Ishikawa, T., Sano, H. Yoshida, Y. Yukawa, N. Sakamoto, J. and Tozawa, Y. (2006). "Effect of Extrusion Conditions on Metal Flow and Microstructures of Aluminum Alloys." Annals of the CIRP. Vol., 55/1

Jabbar, K, J (2010), "Calculation of relative extrusion pressure for circular section by local coordinates system by using finite element method F.E.M", Diyala Journal of Engineering Sciences, Vol., 03, No. 02, 80-96

Jackson, A., and Sheppard, T.(1996), Proc. 6th Int. Aluminum Extrusion Technology Conf., Chicago, Aluminum association, Washington DC, vol., 1 [15]

Jain, S.C. and Bramley, A.N. (1968) "Speed and Frictional Effects in Hot Forging." Proc. Inst. Mech. Eng, 182., 783-798

Javanmard, S, A, S., Daneshmand, F, Moshksar, M, M, and Ebrahimi, R (2011), "Meshless analysis of backward extrusion by natural element method", IJST, Transactions of Mechanical Engineering, Vol. 35, No. M2, 167-180

John Rumierz (1992), "Lubricants for rolling – element bearings", ASM Hand book, Friction, Lubrication and Wear Technology, Vol., 18 , pp. 254

Kaiping Peng, Wenzhe Chen and Kuangwu Qian. (2005). "Study on dynamic strain aging phenomenon of 3004 aluminum alloy", Materials Science and Engineering, A 415, 53–58

Kalpakjian (1992), "Manufacturing Engineering and Technology", 3rd Edition, Addison-Wesley Publishing Company, 300-312

Kammer, I, C. (1999), "Aluminium Handbook, Vol., 1" Aluminium – Verlag, Germany, 127-128

Keh, A. S., Nakada, Y., and Leslie, W. C. (1968) "Dynamic Strain Aging in Iron and Steel in Dislocation Dynamics", McGraw-Hill, 381

Komura, Y., Tokunaga, K (1980), "Structural studies of stacking variants in Mg-base Friauf-Laves phases", Acta Cryst. B36, 1548–1554.

Krishnan, K, S and Krishna, R (2007), "Development of Aerospace Aluminum Alloys and Processes by Design: Potential and Challenges", Frontiers in the Design of Materials, 185-194

Krishnamoorthy, C.S (1994), "Finite Element Analysis, Theory and Programming", McGraw-Hill

Kumar, S., and Vijay, P. (2007). "Die design and experiments for shaped extrusion under cold and hot condition." J. Mat. Pro. Tech., 190., 375-381.

Kuntz, C., M. Keddani, D. Schuster and H. Takenouti. (1997) "Study of Exfoliation Corrosion of the Aluminium Alloys by various electrochemical techniques." ABT Metallurgie, 37(2-3-4): 285-288.

Kunogi, M. (1954). "A New Method of Cold Extrusion." J.Sci.Research Inst, Tokyo, Japan, 50., 215-246

Kurtz, Laue, and Helmut Stenger. (1981), "Extrusion Processes, Machinery, Tooling" "ASM, Ohio, 76- 77

Kurtz, M. (2006), "Mechanical Engineer's hand book: Materials and Mechanical Design", John Wiley and Sons, Inc., USA, 92-113

Lange, K. (1985) "Hand book of Metal Forming", McGraw-Hill, New Delhi, 15.36 - 15.73

Laue, K., and Stenger, H. (1976), ASM, Ohio, 2-5

Laves, F, Löhberg, K, Witte, H. (1935), "Isomorphism of the ternary compounds $Mg_3Zn_3Al_2$ and Mg_4CuAl_6 " Metallwirtschaft, Metallwissenschaft, Metalltechnik 14 793–794.

Lee, G.A., Kwak, D.Y. Kim, S.Y. Im, Y.T. (2002). "Analysis and design of flat-die hot extrusion process, Three-dimensional finite element analysis." *Int. J. Mec. Sci.*, 44., 915-34.

Lendvai, J. (1996), "Precipitation and strengthening in aluminium alloys" *Mater. Sci. Forum*, 43-56, 217–222

Li Jun. (1997) "Research on Open-die Cold Extrusion Forming's modeling and Its Technological Parameters Application," Tianjin University, (In Chinese)

Li, Z, H, Xiong, B,Q, Zhang, Y,G, Zhu, B,H, Wang, F, Liu, H,W.(2008), "Effect of one-step aging on microstructure and properties of a novel Al-Zn-Mg-Cu-Zr alloy", *Sci China Ser E-Tech Sci.*, vol. 52, no.1, 67-71.

Lim, S., T., Lee, Y., Y., Eun, I., S. (2006), *Mater. Sci. Forum* 519-521, 549.

Lorimer, G, W., Nicholson, R, B. (1966), "Further results on the nucleation of precipitates in the Al-Zn-Mg system", *Acta Materialia*, 14, 1009-1013

Maccarini, G., Giardini, C., Pellegrini, G. and Bugini, A. (1991). "The influence of Die Geometry on Cold Extrusion Forging Operations: FEM and Experimental Results". *Mater Process Technol.*, Vol., 27, 227-238

Magnus Hörnqvist and Birger Karlsson. (2010). "Dynamic strain ageing and dynamic precipitation in AA7030 during cyclic deformation", *Procedia Engineering*, Vol. 2, 265–273

Male, A.T. and Cockroft, M.G. (1964). "A Method for the Determination of the Coefficient of Friction of Metals under condition of Bulk Plastic Deformation." *J. Inst. Metals*, 93., 38-46

Male, A.T. (1966). "Variations in Friction Coefficients of Metals during Compressive Deformation." *J. Inst. Metals*, 94., 121-125

- Male, A.T., Depierre, V. and Saul, G. (1973). "The relative Validity of Concept of Coefficient of Friction and Interface Friction shear Factor for Use in Metal Deformation Studies." ASLE Trans., 16, 177-184
- Marlaud, T., Deschamps, A, Bley, F, Lefebvre, W, Baroux, B (2010), "Influence of alloy composition and heat treatment on precipitate composition in Al-Zn-Mg-Cu alloys", Acta Materialia, 58, 248-260
- Martin, J., W. (1998), Precipitation Hardening, 2nd ed., Butterworth-Heinemann, Oxford
- McQueen, H.J. and Jonas, J.J. (1971). Hot Workability Testing Techniques, in Hoffmann, A.L. (ed.), "Metal Forming: Interrelation Between Theory and Practice," Plenum Publishing Corporation., New York.
- Miroslav Plančak, Dejan Movrin, Dragiša Vilotić, Zlatan Car, Aljoša Ivanišević and Igor Kačmarčik (2012), "An analysis of non-axisymmetric backward extrusion", Technical Gazette 19, 4(2012), 953-957
- Mondal, C., Mukhopadhyay, A. K. (2005), "On the nature of T(Al₂Mg₃Zn₃) and S(Al₂CuMg) phases present in as-cast and annealed 7055 aluminum alloy." Materials Science and Engineering, A., 391, 367.
- Mondolfo, L, F. (1976), "Aluminium alloys: Structure and Properties", Butterwoths, London, UK, 576-587
- Morgeneyer T.F., Starink M.J., Wang S.C., Sinclair I. (2008) "Quench sensitivity of toughness in an Al alloy: direct observation and analysis of failure initiation at the precipitate free zone" Acta Materialia, 56, 2872-2884
- Muraki, H., Yoshinaga, H., Koda, S. (1969), "Mechanical properties of age-hardened Al-Zn-Mg alloys", Journal of Japan Institute of Light Metals, 19, 344-351
- Murray, J, L., (1983), "Al (Aluminum) Binary Alloy Phase Diagrams", Alloy Phase Diagrams", ASM International, Vol., 3

Narayanasamy, R. (2000), Metal Forming Technology, Ahuja Book Company Pvt. Ltd, , 1-80, 105-118.

Nishimura, T., Sato, T. and Tada Y. (1995). "Evaluation of Frictional Conditions for Various Tool Materials and Lubricants Using the Injection-upsetting Method." J. Of Materials Proc. Tech., Vol., 53, 726-735

Oberg, Jones, E, Franklin, D, Horton, Holbrook, L, Ryffel and Henry, H, (2000), Machinery's Handbook, 26th ed, Industrial Press, New York, 1348–1349

Ogura, T., Hirosawa, S., Cerezo, A., Sato, T., (2006), "Quantitative Correlation between Strength, Ductility and Precipitate Microstructures with PFZ in Al-Zn-Mg (-Ag, Cu) Alloys", Materials Science Forum, 519–521, 431-436.

Ogura, T., Hirosawa, S., Sato, T., (2006), "Effects of precipitate microstructures near grain boundaries on strength and ductility in Al-Zn-Mg (-Ag) alloys", Journal of Japan Institute of Light Metals, 56, 644-650

Pearsall, G.W. and Backofen, W.A. (1963). Trans. ASME, Ser. D: J. Basic Eng, Vol.85., 68

Peterson, M, B., and Johnson, R, L., (1954)"Friction of Possible Solid Lubricants with Various Crystal Structures", NACA TN-3334

Pohlandt, K., Banabic, D. and Lange, K. (2004). "On the Determination of Friction Coefficient by Ring Compression." www.UTFscience.deIII, 1-3

Polmear, I, J. (1995), "Light Alloys – Metallurgy of Light Metals", Arnold Publication, London, 115-118

Rao, B.K., Khadar, M.S.A. and Srinivasan K. (1999) "High temperature Compression Testing and Determination of Warm Working Temperature for Commercial Purity Aluminium." Bull. Mat. Sci, Springer, 22-1., 17-20

Robson, J.,D., and Prangnell, P.,B. (2001), Acta Materialia, 49, 599

- Rokhlin, L. L., Dobatkina, T. V., Bochvar, N. R., Lysova, E. V. (2004), "Investigation of phase equilibria in alloys of the Al–Zn–Mg–Cu–Zr–Sc system." *J Alloys Compd*; 367, 10
- Rowe, G. W. (1977), "Principles of Industrial Metalworking Processes", Edward Arnold, London.
- Ryum, N. (1969), "The influence of dislocation arrangement on recrystallization in an Al-Mg-Zn alloy", *Acta Materialia*, 17, 831-837
- Saha, P., K. (2008) "Aluminium Extrusion Technology", The Materials Information Society, ASM International, 1-29.
- Samuel H. Talbert, and Betzalel Avitzur.(1996), "Elementary mechanics of Plastic Flow in Metal Forming", John Wiley & Sons, Chichester, 232-282
- Savage, R. H. (1948), Graphite lubrication, *J. Appl. Phys.*, Vol. 19(1), 1-10
- Schey, J.A. (1983), "Tribology in metal working" ASM, Ohio 450 – 452
- Shuang-jie Zhan., Ying Gao, FumingZeng. and lun Li (2010). "Research on Open-die Cold Extrusion Technology of the Electromotor Shaft Shoulder Fillet." 2nd International Conference on Computer Engineering and Technology, Vol 1., China., VI-702 - VI-704
- Schmitt, G., Schmoeckel, D. and Kurt Lange. (1965) "Investigation of Cup Piercing without Restriction", (in German), Institute for Metal forming, University of Stuttgart, 2/3, 1-42
- Schmitt, G. (1968) "Investigations on Backward Can Extrusion of Steel at Room Temperature" (in German), *Berichte aus dem Institut für Umformtechnik*, Universität Stuttgart, no7, Essen, Girardet, 1968.
- Sha, G., Cerezo, A. (2004), "Early-stage precipitation in Al-Zn-Mg-Cu alloy (7050)", *Acta Materialia*, 52(15), 4503-4516

Shahriari, D., Amiri, A. and Sadeghi, M.H. (2010). "Study on Hot Ring Compression Test of Nimonic 115 Superalloy using Experimental Observations and 3D FEM Simulation." J. Mat.Eng.Performan, ASM International, 19., 633 – 642

Shuang-jie Zhan., Ying Gao, Fuming Zeng. and Lun Li (2010). "Research on Open-die Cold Extrusion Technology of the Electromotor Shaft Shoulder Fillet." 2nd International Conference on Computer Engineering and Technology, Vol. 1, China., VI-702 - VI-704

Shwe, W, H, A, Kay T, L, and Waing, W, K, K, O. (2008), "The Effect of Ageing Treatment of Aluminum Alloys for Fuselage Structure-Light Aircraft", World Academy of Science, Engineering and Technology 46, 696-699

Sliney, H, E. (1978), "Dynamics of Solid Lubrication as Observed by Optical Microscopy", ASLE Trans., 21(2), 109-117

Sofuoglu, H., and Gedikli, H, (2002) "Determination of friction coefficient encountered in large deformation processes", Tribology International 35, 27-34

Srinivasan, K., (2005), "Friction in metal forming processes", 2nd international conference on recent advances in material processing technology, 39-44

Srinivasan, K., and Venugopal P. (1990). "Some Experience with Open Die Extrusion." Proc. 14th All India Machine Tool Design and Research Conference, IIT, Bombay, India, 193-198

Srinivasan, K., and Venugopal P. (1993), "Warm Open Die Extrusion of Ti-6Al-4V." J.Mater.Process.Technol., 38,265-278

Srinivasan, K., and Venugopal P. (1997), "Adiabatic and Friction Heating on the Open Die Extrusion of Solid and Hollow Bodies." J.Mater.Process.Technol., 70.,177-179

Srinivasan, K., and Venugopal P (1999), "Hardness Stress-Strain Correlation in Titanium Open Die Extrusion: An Alternative to Viscoplasticity." J.Mater.Process.Technol., 95., 185-190

Srinivasan, K., and Venugopal P. (2004). "Direct and Inverted Open Die Extrusion of Rods and Tubes." *J.Mater.Process.Technol.*, 153-154, 765-770

Srinivasan, K., and Venugopal P. (2007). "Influence of Die Angle on the Open Die Extrusion of Commercially Pure Titanium Tubes." *Material and Manufacturing Processes*, 22, 238-242

Srinivasan, K., and Venugopal P. (2008). "Formability Limit in Containerless (open die) Extrusion of Commercial Purity Titanium Rods and Tubes." *Material and Manufacturing Processes*, 23, 347-351

Stiller, K., Warren, P, J, Hansen, V, Angenete, J, Gjønnnes. (1999), *Materials Science and Engineering*, A, 270, 55–63.

Suarez, M, A., Lara, A, G., Sánchez-Arévalob, F, M., Alvarezb, O., Colin J., Juarez-Islas, J, A. (2009), "Prediction and characterization of growth temperatures in Al–Zn–Mg alloys", *Materials Characterization*, 60, 420 – 424

Surendra K. (1985) "Principles of metal working", Oxford and IBH, India, 311 – 316

Takahashi, W., and Fukuda, T. (1987), "Effect of Structure and Skinpass Reduction of Area on Process Limitation in Open Die Forward Extrusion." *Trans. Min. Metall. Assoc.*, Kyoto, 20-9., 630-636

Takahashi, W., and Fukuda, T. (1988), "Process Limitations for Open Die Forward extrusion of Rod" *Sumitomo Met.*, 40-2., 15-24

Taylor, J, L. (1963), "The effect of heat treatment on the grain boundary zones in a high purity Al–Zn–Mg alloy", *J Inst Metals*, 92, 301-302.

Thomas, G., Nutting, J. (1960), "The ageing characteristics of aluminium alloys- Electron microscope studies of alloys based on the aluminium-zinc-magnesium system", *J., Inst., Metals*, 88, 81-90.

Tiernan, P., Hillery, M, T, Draganescu, B, and Gheorghe, M. (2005), “Modelling of cold extrusion with experimental verification”, *Journal of Materials Processing Technology*, 168, 360-366.

Unwin, P, N, T, Smith, G, C. (1969), *J Inst Metals*, 97, 299-310

Unwin, P, N, T., Lorimer, G, W., Nicholson, R, B. (1969), “Origin of the grain boundary precipitate free zone”, *Acta Materialia*, 17, 1363-1377

Van Rooyen, G.T. and Backofen, W.A. (1960), *Int. J. Mech. Sci. Vol. 1.*, 1-27

Varley, P, C., Day, K, B., Sendorek, A., (1957), “The structure and mechanical properties of high purity Al–Zn–Mg alloys”, *J. Inst. Metals*, 86, 337-350.

Varley, P, C. (1970), “Aluminium and its alloys”, *Newnes-Butterworths, London*, 53-54

Varun Bhat, D. N., Vishav Bandhu Sharma and Srinivasan, K. (2007), “Friction Factor of CP Aluminium, Aluminium-Zinc and Aluminium-Zinc-Magnesium Alloys at an Elevated Temperature of 773K”, *Aluminium in India, Vol b No 4*, 21-24

Wagoner, R.H. and Chenot, J.L. (1997), “Fundamentals of metal forming”, *John Wiley and Sons*, 313-338

Wang, Y, M., Ma, E. (2004), “Three strategies to achieve uniform tensile deformation in a nanostructured metal”, *Acta Materialia*, 52(6), 1699-1709

Warner, T. (2006), “Recently-Developed Aluminium Solutions for Aerospace Applications”, *Mater Sci Forum*, 519–521, 1271

Watkins, A, K and Kondic, V. (1963), “Structure and Tensile Properties of Aluminum Alloys”, *Foundry Journal*, 53-63.

Waterloo, G., Hansen, V, Gjønnnes, J, Skjervold, S, R.(2000), “Effect of predeformation and preaging at room temperature in Al-Zn-Mg-(Cu,Zr) alloys”, *.Mater, Sci, Eng, A*, 303, 226-233

Wiley, L. A. (1973) "Metallography, Structures and Phase Diagrams", Metals Handbook, 8th ed., Vol 8, American Society for Metals, Metals Park, OH.

William F, H. and Robert M, C. (1993), "Metal Forming Mechanics and metallurgy", Prentice Hall, New Jersey, 62-65.

Woodward, R.L. (1977), "Communication: A note on the Determination of Accurate Flow Properties from Simple Compression Tests." Metallurgical and Materials Transactions A, Springer, Boston, 8, 1833-1834

Zhang, S., Hu, W., Berghammer, R., Gottstein, G. (2010), "Microstructure evolution and deformation behavior of ultrafine-grained Al–Zn–Mg alloys with fine η precipitates", Acta Materialia, 58, 6695–6705

Zhao, X, Frankel, G, S. (2006) "Effects of RH, Temper and Stress on Exfoliation Corrosion Kinetics of AA7178," Corrosion, 62, 256-266.

Zhao, X, Frankel, G, S. (2007), "Quantitative Study of Exfoliation Corrosion: Exfoliation of Slices in Humidity Technique", Corros. Sci., 49, 920-938.

Zienkiewicz, O, C. (1993), "The Finite Element Method", 3rd Edition. New York: McGraw Hill, 25-53

Zone-Ching Lina., Chang-Cheng Chenb, Hsin-Ho Wanga.(2009) "The determination of material strength coefficient and strain hardening constant by inverse method", journal of materials processing technology, 209, 2393–2401

APPENDIX I

MODEL CALCULATIONS

1. Theoretical punch pressure calculations for backward extrusion with a container of Al-5Zn-1Mg of 25 mm dia with 5mm punch depth.

$$263.55 [1 + (1/3 \times 0.31 \times 15/45)] + 263.55 [1 + 0.31 \times 45/5] = 1271.48 \text{ MPa}$$

Wherein $\sigma_{fm} = 263.55 \text{ MPa}$, $\mu = m = 0.31$, $d_p = 15 \text{ mm}$, $b = 45 \text{ mm}$, $s = 5 \text{ mm}$

2. Theoretical punch pressure calculations for Containerless backward extrusion of Al-5Zn-1Mg of 25 mm dia with 5mm punch depth.

$$263.55 [1 + (1/3 \times 0.31 \times 15/45)] = 272.63 \text{ MPa}$$

Wherein $\sigma_{fm} = 263.55 \text{ MPa}$, $\mu = m = 0.31$, $d_p = 15 \text{ mm}$, $b = 45 \text{ mm}$.

3. Flow stress calculations for Containerless backward extrusion of Al-5Zn-1Mg of 25 mm dia

$$[314 \times (0.45)^{0.1}] / (0.1 + 1) = 263.55$$

Wherein $K = 314 \text{ MPa}$, $\epsilon = 0.45$, $n = 0.1$

4. Extrusion strain calculation for Containerless backward extrusion of Al-5Zn-1Mg of 25 mm dia using a 15 mm punch

$$\epsilon = \ln (A_o/A_f)$$

$$\ln [25^2 / (25^2 - 15^2)] = 0.45$$

Wherein $d_o = 25 \text{ mm}$, $d_p = 15 \text{ mm}$

5.

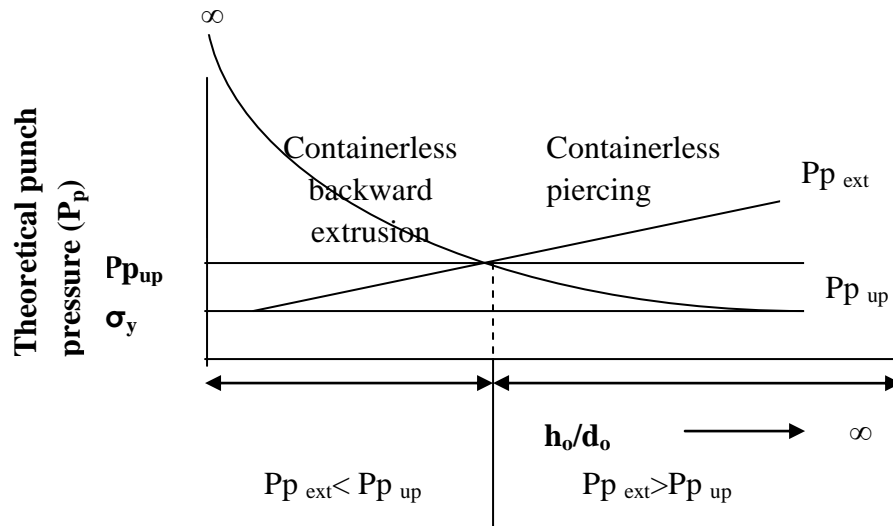


Fig.1 A plot of theoretical punch pressure against h_0/d_0 showing clear distinction between containerless backward extrusion and containerless piercing

APPENDIX II

EXPRESSION FOR STRAIN

d_o remains constant, h_o becomes h_f . for piercing with vertical displacement i.e. for extrusion to take place.

$$\text{Initial volume} = V_o = (\Pi d_o^2 h_o) / 4$$

$$\text{Final volume} = V_f = (\Pi d_o^2 h_f) / 4 - \Pi d_p^2 / 4 (h_f - b)$$

Volume constancy gives $V_f = V_o$

$$(h_f / h_o) (d_o^2 - d_p^2) + d_p^2 (b / h_o) = d_o^2$$

$$d_o^2 [1 - (h_f / h_o)] = d_p^2 [(b / h_o) - (h_f / h_o)]$$

$$d_o^2 [h_o - h_f] = d_p^2 [b - h_f]$$

$$\ln [d_o^2 / (d_o^2 - d_p^2)] = \ln[(h_f - b) / (h_o - b)]$$

where d_p = Diameter of punch

d_o = Diameter of billet

h_o = Initial height of billet

h_f = Final height of billet

b = Undeformed height below the punch

$$\ln [d_o^2 / (d_o^2 - d_p^2)] = \ln(d_o / (d_o - d_p)) + \ln(d_o / (d_o + d_p))$$

$$\text{since } d_o^2 - d_p^2 = (d_o - d_p) (d_o + d_p)$$

APPENDIX III

PUNCH PRESSURE

$$P_{\text{pext}} = \sigma_m \left(1 + \frac{1}{3} \mu \frac{d_p}{b} \right)$$

$$P_{\text{pup}} = \sigma_y \left[1 + 2\mu \frac{r_o}{h_o} \right]$$

$$r_o = (d_o/2)$$

For $h_o/d_o = 0.5$

$$P_{\text{pup}} = \sigma_y [1 + 2\mu]$$

For $h_o/d_o = 0.25$

$$P_{\text{pup}} = \sigma_y [1 + 4\mu]$$

As h_o/d_o decreases P_{pup} increases. For extrusion d_p/d_o should be small as possible. With increase in d_o and decrease in h_o upsetting is made difficult and extrusion is made easier. Increase in d_o with constant d_p means extrusion strain is decreasing.

LIST OF PUBLICATIONS
(BASED ON Ph.D. RESEARCH WORK)

International Journals

Rijesh M, A O Surendranathan (2011), “Deformation of Al-5Zn-1Mg in the temperature range of 303 – 673 K”, Int. J. Engg. Sc. & Mgmt, Vol. 1, Issue II, 18-22

Rijesh M , A O Surendranathan (2012), “Determination of friction factor by ring compression test for Al-5Zn-1Mg using graphite and MoS₂ lubricants”, Thammasat International Journal of Science and Technology, Vol. 17, No. 3, 13-19

Conference Proceedings and Presentations

Rijesh M, K Srinivasan (2007), “Warm working temperature range for Al-5Zn-1Mg alloy”, International Symposium on Energy - related Materials, 45th National Metallurgist Day & 61st Annual Technical Meeting of the Indian Institute of Metals, November 13-16, 51

Rijesh M, K Srinivasan (2007), “Determination of friction factor for Al-5Zn-1Mg at various temperatures”, International Symposium on Energy - related Materials, 45th National Metallurgist Day & 61st Annual Technical Meeting of the Indian Institute of Metals, November 13-16, 42

Rijesh M, K Srinivasan (2008), “Effect of temperature on the friction factor of Al-10Zn-1Mg alloy”, International Conference on, “Towards Global Leadership in Minerals and Metals”, 46th National Metallurgist Day & 62nd Annual Technical Meeting of the Indian Institute of Metals, November 13-16, 323

Rijesh M, K Srinivasan (2008), “Determination of working temperature range for Al-10Zn-1Mg alloy”, International Conference on “Towards Global Leadership in Minerals and Metals”, 46th National Metallurgist Day & 62nd Annual Technical Meeting of the Indian Institute of Metals, November 13-16, 205

Rijesh M, K Srinivasan (2009), “Determination of friction factor by ring compression test for Al-5Zn-1Mg using graphite and MoS₂ lubricants”, National Conference on, “Recent Trends in Advanced Materials [RTAM 2009]”, Department of Mechanical Engineering & Research Centre and Department of Chemistry & Research Centre, KVG College of Engineering, Sullia, December 18, 168

BIO-DATA

Name : Rijesh M

Date of Birth : 06-05-1979

Permanent address : Sai Kripa, Cherukurussi nilam road, Silent world
residential association, West Hill-Chungam, Calicut,
673005, India

E-mail : rijeshm@yahoo.com

Academic qualification

B.E : National Institute of Technology Karnataka, Surathkal,
(Metallurgical PO Srinivasanagar -575025, India
Engineering)

M.Tech : National Institute of Technology Karnataka, Surathkal,
(Materials PO Srinivasanagar -575025, India
Engineering)

Experience : 7 years of teaching and consultancy at Department of
Metallurgical and Materials Engineering, National
Institute of Technology Karnataka, Surathkal as an
Assistant Lecturer